Rapid Seismic Repair of Column to Footing Connections – Phase 2

Photo of Plastic Hinge Relocation Repair #6 taken by Taylor Brodbeck, October 2020

Prepared By:
Taylor J. Brodbeck, Ph.D. Student
Zachary A. Shurow, MS
Mervyn J. Kowalsky, Professor, Ph.D.
Rudolf Seracino, Professor, Ph.D.

Prepared For:
Alaska Department of Transportation & Public Facilities
Research, Development, and Technology Transfer
P.O. Box 112500
3132 Channel Drive
Juneau, Alaska 99811-2500

and

Federal Highway Administration
P.O. Box 21648
709 West 9th Street
Juneau, Alaska 99802-1648

REPORT DOCUMENTATION PAGE

Form approved OMB No.

1. AGENCY USE ONLY (LEAVE BLANK)	2. REPORT DATE	3. REPORT TYPE AND DATES COVERED
	May 31, 2022	FINAL REPORT, Jan. 2019 through May 2022

4. TITLE AND SUBTITLE
Rapid Seismic Repair of Column to Footing Connections – Phase 2

5. FUNDING NUMBERS

6. AUTHOR(S)
Taylor J. Brodbeck, Ph.D. Student
Zachary A. Shurow, MS
Mervyn J. Kowalsky, Professor, Ph.D.
Rudolf Seracino, Professor, Ph.D.

7. PERFORMING ORGANIZATION NAME(S) AND ADDRESS(ES)
Department of Civil, Construction, and Environmental Engineering
North Carolina State University
Raleigh, NC 27606

8. PERFORMING ORGANIZATION REPORT NUMBER
N/A

9. SPONSORING/MONITORING AGENCY NAME(S) AND ADDRESS(ES)
Alaska Department of Transportation and Public Facilities
Research, Development &Technology Transfer
3132 Channel Drive
Juneau, Alaska 99811-2500

10. SPONSORING/MONITORING AGENCY REPORT NUMBER
IRIS #: HFHWY00125
FHWA-AK-RD-4000(184)

11. SUPPLEMENTARY NOTES

12a. DISTRIBUTION / AVAILABILITY STATEMENT
Copies available online at http://www.dot.alaska.gov/stwddes/research/search_lib.shtml

12b. DISTRIBUTION CODE
N/A

13. ABSTRACT (Maximum 200 words)
Presented in this report is the development of a rapid seismic repair of column to footing connections. The use of plastic hinge relocation as a repair technique for extreme levels of damage in reinforced concrete bridge columns is investigated. Before the development of this repair, if a column was severely damaged (e.g. had fractured longitudinal bars) a complete replacement of the bridge was suggested. Prior studies have already shown the repair's ability to restore a damaged column's load and displacement capacities, and its potential for rapid deployment is favorable. This research aimed to improve the repair constructability by using a bolted connection and methods for simplified implementation. Another goal of this research was to improve repair performance by anchoring previously fractured bars to increase seismic resistance, and enhance the behavior of the relocated hinge when these bars are anchored.

14. KEYWORDS :
Reinforced concrete bridges, Repairing, Earthquake resistant design, Plastic hinge relocation, Buckled reinforcement, Fractured reinforcement

15. NUMBER OF PAGES
163

16. PRICE CODE
N/A

17. SECURITY CLASSIFICATION OF REPORT	18. SECURITY CLASSIFICATION OF THIS PAGE	19. SECURITY CLASSIFICATION OF ABSTRACT	20. LIMITATION OF ABSTRACT
Unclassified	Unclassified	Unclassified	None

Notice

This document is disseminated under the sponsorship of the U.S. Department of Transportation in the interest of information exchange. The U.S. Government assumes no liability for the use of the information contained in this document.

The U.S. Government does not endorse products or manufacturers. Trademarks or manufacturers' names appear in this report only because they are considered essential to the objective of the document.

Quality Assurance Statement

The Federal Highway Administration (FHWA) provides high-quality information to serve Government, industry, and the public in a manner that promotes public understanding. Standards and policies are used to ensure and maximize the quality, objectivity, utility, and integrity of its information. FHWA periodically reviews quality issues and adjusts its programs and processes to ensure continuous quality improvement.

Author's Disclaimer

Opinions and conclusions expressed or implied in the report are those of the author. They are not necessarily those of the Alaska DOT&PF or funding agencies

SI* (MODERN METRIC) CONVERSION FACTORS

APPROXIMATE CONVERSIONS TO SI UNITS

Symbol	When You Know	Multiply By	To Find	Symbol
		LENGTH		
in	inches	25.4	millimeters	mm
ft	feet	0.305	meters	m
yd	yards	0.914	meters	m
mi	miles	1.61	kilometers	km
		AREA		
in^2	square inches	645.2	square millimeters	mm^2
ft^2	square feet	0.093	square meters	m^2
yd^2	square yard	0.836	square meters	m^2
ac	acres	0.405	hectares	ha
mi^2	square miles	2.59	square kilometers	km^2
		VOLUME		
fl oz	fluid ounces	29.57	milliliters	mL
gal	gallons	3.785	liters	L
ft^3	cubic feet	0.028	cubic meters	m^3
yd^3	cubic yards	0.765	cubic meters	m^3
		NOTE: volumes greater than 1000 L shall be shown in m^3		
		MASS		
oz	ounces	28.35	grams	g
lb	pounds	0.454	kilograms	kg
T	short tons (2000 lb)	0.907	megagrams (or "metric ton")	Mg (or "t")
		TEMPERATURE (exact degrees)		
°F	Fahrenheit	5 (F-32)/9 or (F-32)/1.8	Celsius	°C
		ILLUMINATION		
fc	foot-candles	10.76	lux	lx
fl	foot-Lamberts	3.426	$candela/m^2$	cd/m^2
		FORCE and PRESSURE or STRESS		
lbf	poundforce	4.45	newtons	N
lbf/in^2	poundforce per square inch	6.89	kilopascals	kPa

APPROXIMATE CONVERSIONS FROM SI UNITS

Symbol	When You Know	Multiply By	To Find	Symbol
		LENGTH		
mm	millimeters	0.039	inches	in
m	meters	3.28	feet	ft
m	meters	1.09	yards	yd
km	kilometers	0.621	miles	mi
		AREA		
mm^2	square millimeters	0.0016	square inches	in^2
m^2	square meters	10.764	square feet	ft^2
m^2	square meters	1.195	square yards	yd^2
ha	hectares	2.47	acres	ac
km^2	square kilometers	0.386	square miles	mi^2
		VOLUME		
mL	milliliters	0.034	fluid ounces	fl oz
L	liters	0.264	gallons	gal
m^3	cubic meters	35.314	cubic feet	ft^3 m^3
	cubic meters	1.307	cubic yards	yd^3
		MASS		
g	grams	0.035	ounces	oz
kg	kilograms	2.202	pounds	lb
Mg (or "t")	megagrams (or "metric ton")	1.103	short tons (2000 lb)	T
		TEMPERATURE (exact degrees)		
°C	Celsius	1.8C+32	Fahrenheit	°F
		ILLUMINATION		
lx	lux	0.0929	foot-candles	fc
cd/m^2	$candela/m^2$	0.2919	foot-Lamberts	fl
		FORCE and PRESSURE or STRESS		
N	newtons	0.225	poundforce	lbf
kPa	kilopascals	0.145	poundforce per square inch	lbf/in^2

*SI is the symbol for the International System of Units. Appropriate rounding should be made to comply with Section 4 of ASTM E380.
(Revised March 2003)

TABLE OF CONTENTS

LIST OF FIGURES

LIST OF TABLES

NOTATION

A_b area of longitudinal bar

c concrete cover to longitudinal reinforcement

c neutral axis depth

c_b lesser of: (a) the distance from center of a bar or wire to nearest concrete surface, and (b) one-half the center-to-center spacing of bars or wires being developed, in.

d_b nominal diameter of bar, wire, or prestressing strand, in.

D diameter of circular column

D bolt diameter

D_j diameter of steel jacket

D' core diameter of circular column

E_{sj} elastic modulus of jacket steel

f_c' specified compressive strength of concrete, psi

f_{cc}' confined compressive strength of concrete

f_l lateral confining stress

f_s required transfer stress in reinforcement in lap-splice

f_y specified yield strength, psi

f_{yj} yield stress of jacket steel

f_{yl} yield stress of longitudinal reinforcement

H column height

H_{repair} height of repair

K dimensionless coefficient for bolt conditions

K_{tr} transverse reinforcement index, in.

l_d development length in tension of deformed bar, deformed wire, plain and deformed welded wire reinforcement, or pretensioned strand, in.

l_s length of splice or sleeve

L_{eff} effective length of column

L_p plastic hinge length

M_u ultimate moment capacity

n number of longitudinal bars

n_{bolts} number of bolts

p perimeter of crack surfaces around bar in lap splice failure

P pretension

t_j jacket thickness

t_{sleeve} thickness of sleeve

T torque

T_b minimum bolt pretension

V_{sj} shear strength enhancement provided to member by retrofit jacket

V^o overstrength shear demand

Δ_y yield displacement

Δ_u ultimate displacement

ε_c compression strain in concrete

ε_{cm} maximum concrete compression strain

ε_{cu} ultimate compression strain in concrete

ε_{sm} strain at maximum stress in confining jacket material

ε_{su} ultimate reinforcement strain

θ angle between inclined diagonal tension cracking and member axis

λ modification factor to reflect the reduced mechanical properties of lightweight concrete relative to normal weight concrete of the same compressive strength

μ coefficient of friction

ρ_{sj} volumetric ratio of confining steel

φ_y yield curvature

φ_u ultimate curvature

ψ_e factor used to modify development length based on reinforcement coating

ψ_s factor used to modify development length based on reinforcement size

ψ_t factor used to modify development length for casting location in tension

Executive Summary

Recent studies have shown that plastic hinge relocation is capable of repairing extreme damage levels. In this repair, the original plastic hinge is strengthened such that should another large earthquake occur, new damage will form above the repair in a previously undamaged section. This helps to ensure a predictable and ductile response, and experimental tests have shown its capabilities of restoring force and displacement capacities to that of the original column.

This research aims to improve the constructability and performance of the plastic hinge relocation repair approach. The study consists of an experimental investigation of ten reinforced concrete cantilever bridge columns which were damaged to extreme levels before being repaired and retested. The first four tests were used to develop a bolted connection which would simplify construction of the repair by eliminating the need for specialized workers. Additionally, these four tests allowed for improvements to the repair performance by determining how to anchor previously fractured bars within the repair, leading to greater energy dissipation and seismic resistance. The next three tests focused on more improvements to constructability through the use of embedded couplers to reduce the time of construction and an epoxy grout to allow for this repair method to be used in underwater applications. These construction simplifications resulted in similar performance to the original repair.

The tradeoff for improving the seismic resistance and force capacity by anchoring the previously fractured bars within the repair is a reduction in displacement capacity. The final three tests investigated methods to achieve the same displacement capacity as the original column. One option for increasing the displacement capacity is to decrease the height of the repair. Alternatively, a CFRP wrap was used to increase the curvature capacity of the relocated hinge and therefore the displacement capacity of the repaired column. While using CFRP would require specialized workers, it is not essential to be done at the same time as the hinge relocation and can be delayed with minimal risk. All these repair strategies can be used independently or together to tailor the repair to the specific needs of any damaged column.

Chapter 1: Introduction

1.1 Background

In recent decades, the seismic performance of reinforced concrete bridges has been notably improved through the development of performance-based design (Paulay & Priestley, 1992; Priestley et al., 1996). In performance-based design, structures are designed by prescribing multiple limit states and the corresponding hazard under which those limit states should be achieved. An example of this would be to specify that a structure will suffer minimal damage for an earthquake with a 50 year return period, while in the case of a 1000 year return period, extensive damage is accepted as long as the structure does not collapse. While there has been extensive research in the repair of structures with mild damage, more extreme damage, such as buckling or rupture of reinforcing bars, was considered unrepairable and requiring complete replacement of the bridge (Rutledge et al., 2014). Depending on the bridge, constructing a replacement could take years. This would not only be costly in terms of material and labor costs, but also the economic losses associated with the interruption of service. However, since seismic damage will be concentrated in the plastic hinges, recent research has shown that requiring complete replacement of the bridge may not be necessary.

While replacing the entire column could be an option, this too would take a long time, be costly, and again, the damage is concentrated in plastic hinges. Although these plastic hinges have suffered permanent damage and restoring them to their original condition is difficult, the section of the column just above the plastic hinge remains largely undamaged. This has led researchers to investigate a repair technique, called plastic hinge relocation, where a repair is placed around the damaged column's plastic hinge in such a way that should another earthquake happen, new damage will occur above the repair in a previously undamaged section (Krish, 2018; Lehman et al., 2001; Pantelides et al., 2014; Parks et al., 2016; Rutledge et al., 2014; Wu & Pantelides, 2017). Figure 1.1 illustrates this plastic hinge relocation from the original column to the repaired column, and experimental tests have shown it can effectively restore the columns load and displacement capacities.

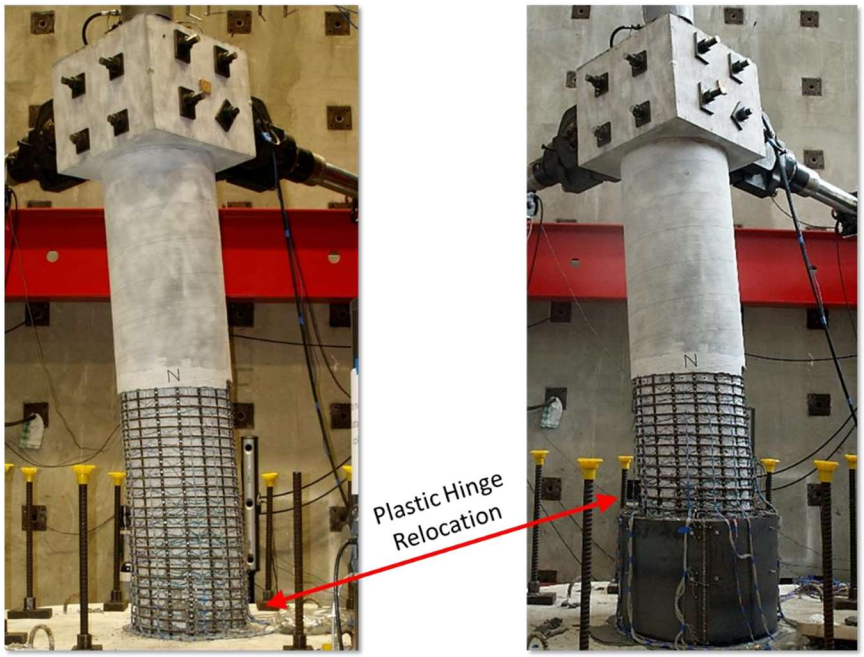

Figure 1.1: Plastic Hinge Relocation Repair - Courtesy of Dr. Krish.

A major advantage of this repair technique is that it can be rapidly deployed, and construction completed in only a couple of days (Krish, 2018; Pantelides et al., 2014; Parks et al., 2016; Rutledge et al., 2014; Wu & Pantelides, 2017). The typical construction process involves embedding reinforcing bars into the connecting member, then placing a concrete filled jacket around the bars. In most studies, the jacket is formed from a CFRP wrap; however, a welded steel sleeve has also been used. While both methods have been successful, actual installation in the field could be difficult depending on weather and accessibility of the column and each requires specialized workers that may not be readily available should an extreme earthquake occur and cause this damage. For these reasons, an alternative repair solution that does not have these limitations is desirable. The research in this report aims to provide this by investigating the use of a steel sleeve with a mechanically bolted connection.

Aside from providing this alternative, much of this report is focused on understanding and improving the behavior of fractured reinforcing bars inside the repair. While this repair technique is intended for extreme damage levels where longitudinal bars will have fractured, experimental tests using the repair have shown that these bars often debond in the repair tests which weakens the repair's performance. To understand this behavior, the left side of Figure 1.2 presents a typical configuration for a column-footing connection showing only two longitudinal bars. To ensure that the bar is anchored into the footing, there is a requirement on how long the

bars must be embedded inside of the footing (i.e. the development length). This length is often larger than the height of the footing, so 90° bends are used to meet this requirement and the bar can extend as far as needed.

If a large earthquake occurs that fractures these bars and this repair technique is used, that length of the bar inside the footing no longer anchors the bar; instead, anchorage of these fractured bars comes from their embedment length into the repair, shown on the right of Figure 1.2. In past research studies (Krish, 2018; Parks et al., 2016; Wu & Pantelides, 2017), this embedment length alone has often not been enough to anchor the bars inside the repair, so at large displacements these bars debond and can no longer carry load. Since not all the longitudinal bars will be fractured, this does not cause failure of the repaired column because the load can be transferred to the other bars; however, this weakens the repaired column's performance, so prevention of this behavior is preferred.

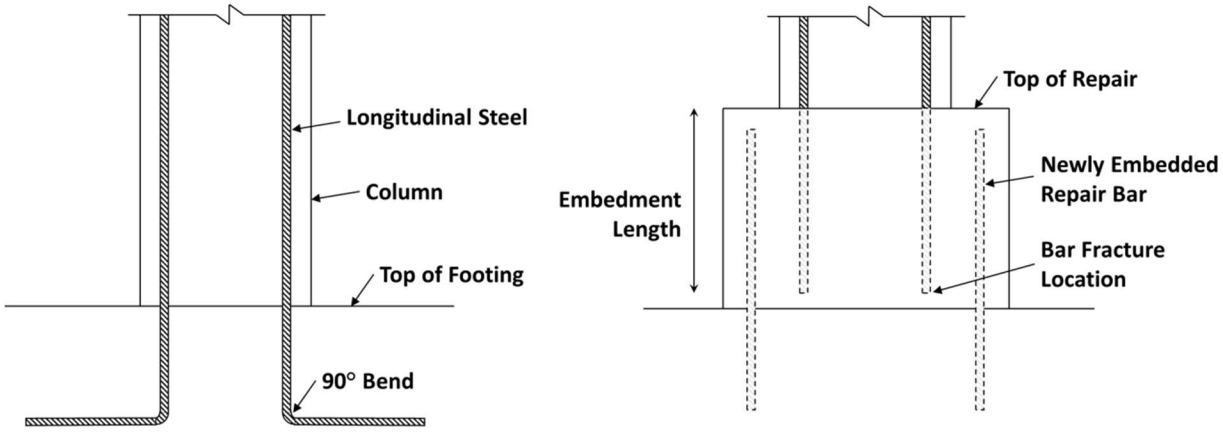

Figure 1.2: Anchorage of Longitudinal Bars Before (left) and After (right) Repair.

1.2 Research Objectives

The previous section presented a few research needs which will be addressed in this report. Firstly, while repairing extreme damage states through plastic hinge relocation has potential, research using this technique has been limited and more studies are needed. In this project ten damaged reinforced concrete columns were repaired with this technique, then retested to compare their behavior with undamaged columns. Aside from increasing the number of studies with this repair configuration, there were two primary objectives presented in the following sections.

1.2.1 Improve Repair Constructability

To provide an alternative repair solution with an easier construction, a mechanically bolted steel sleeve was used for each of the repairs in this project. Given that both CFRP wraps and welded steel sleeves require specialized workers for construction, a more constructible option could be useful. With this repair configuration, rapid construction is still possible and would no longer be limited to the availability of those specialized workers. To reduce construction time further, coupled bars were placed in the footings of two of the repairs in this project. These coupled bars would eliminate the effort and time associated with drilling holes to place additional reinforcement. Additionally, many column to footing connections are underwater where casting grout becomes cumbersome. As an alternative, an epoxy grout which can be placed more easily at these connections was utilized and studied in one of the repairs in this project. Implementation of different materials would allow for an expanded use of this repair method.

1.2.2 Improve Repair Performance

While research using this plastic hinge relocation repair method has been capable of restoring the load and displacement capacities of the column, bars that were fractured in the original plastic hinge have been shown to lose their bond inside the repair which weakens the repair's response during subsequent seismic events. It is hypothesized that if this behavior can be prevented, by improving the anchorage of these bars, the repair's strength will not degrade. Although labor intensive methods exist that could accomplish this (e.g. splicing and headed studs), these are not ideal as they would lead to longer repair times.

When the bars are fully anchored within the repair, the displacement capacity is reduced. This project aimed to determine if the behavior of the repaired column can be improved to match the original column by using additional confinement at the relocated hinge which will allow for greater deformation capacity.

1.3 Report Contents

Chapter 1: Introduction – This chapter began by presenting a brief background on plastic hinge relocation repair and how modern design principles have led to its effectiveness. With this understanding, the research objectives for this project are defined. Mainly, this project seeks to develop a more constructible repair solution and improve its performance through better anchorage of fractured bars. Lastly this chapter provides a brief description of each of the chapters in this report.

Chapter 2: Background and Motivation – In this chapter, previous experimental repair tests using plastic hinge relocation are presented. Each column repaired was severely damaged, and it is shown that if a bar is fractured during the initial test it tended to debond during the repair test which led to a weakened repair performance. Later in this chapter, the various factors that influence the anchorage of these bars is discussed, and it will be seen that improving bond and confinement will improve the anchorage of the bars. A method of improving the bond is discussed, followed by a thorough description of a steel jacket retrofit designed which was mimicked for the repair configuration used in this report and aims to provide enough confinement to fully anchor the fractured bars inside the repair.

Chapter 3: Experimental Setup – This chapter will briefly describe the laboratory setup used for the column tests, as well as the methods of loading and loading protocol. Next, each of the materials used in the repair are described, along with material properties when relevant. This leads into a detailed step-by-step explanation of the repair construction process, followed by information about the various instruments used for the experimental tests.

Chapter 4: Test Summaries – Here, the ten experimental repair tests will each be thoroughly discussed. Since each repair aimed to improve the performance compared to the last test, this chapter is presented in a fairly chronological order. It begins by describing the objective for Repair #1, followed by a description of the test and the results of data analysis. Using this, conclusions are then drawn that lead into a new objective for Repair #2 and the process is repeated. After the ten tests have been described, the final section of the chapter compares their results to further demonstrate the improvements and effectiveness of each repair.

Chapter 5: Repair and Steel Sleeve Designs – In this chapter, the design processes for the implementation of the repair presented in this research will be discussed. The first section will outline the results when following Krish's plastic hinge relocation design for each of the repairs in this project. The next section will propose additional requirements to the required sleeve thickness based off the experimental tests in Chapter 4. The proposed design requires a much thicker sleeve thickness which aims to provide enough confinement to prevent fractured bars from debonding inside the repair. The next two sections of this chapter

then present the design assumptions used for the bolts and their pre-tensioning for the experimental tests in this project.

Chapter 6: Conclusions – This chapter presents the key findings and conclusions of the work in this report relating to the two objectives presented in Section 1.2. Through experimental tests, the use of a steel jacket with a pre-tensioned bolted connection was shown to be an effective alternative to a welded connection or CFRP wrap. It was also shown that improving the bond and confinement for fractured bars inside the repair can fully anchor them, which improves the repaired column's performance.

Chapter 2: Background and Motivation

While much research has been done on the repair of reinforced concrete bridge columns, extreme damage states such as fractured longitudinal bars have received little attention. Such damage levels have long been considered un-repairable and requiring replacement; however, recently multiple studies have shown that plastic hinge relocation can be used to effectively restore the load and displacement capacity of the damaged column to that of the original column. In addition, many repair techniques have a very short deployment time, making it ideal for rapid repairs.

This chapter aims to provide background, context, and motivation for the work presented in this report. Presented are three examples of plastic hinge relocation repair of extremely damaged columns containing fractured bars. It will be shown that these fractured bars often do not have sufficient anchorage inside the repair, which leads to the bar debonding and consequently a loss of load carrying capability. This is followed by a softened and pinched behavior in the global response, which likely indicates reduced seismic resistance. To improve this repair, this project aims to fully anchor the fractured bars inside of the repair, which is expected to eliminate the pinching and softening of the global response.

This debonding behavior is akin to a reinforcing bar having a shorter embedment length than its development length, which leads to a pullout or splitting failure instead of bar fracture. Unfortunately, increasing the embedment length of the fractured bars in this repair requires an increase in the repair height, which is undesirable as this also increases the shear demand to other components of the bridge that may not be capable of sustaining the increased load. Furthermore, a higher repair height increases the moment demand into the adjacent footing and decreases the displacement capacity of the column since the distance from the plastic hinge to column top shortens. Because of this, it is advantageous to improve the anchorage of these bars through other avenues besides increasing embedment length, thus keeping the relocated hinge as close to footing as possible. To understand how this could be done, the second section of this literature review discusses the various factors that affect the anchorage of embedded bars. It will be shown that confinement and bond conditions both play an important role in the anchorage of the fractured bars and increasing these may completely anchor these bars.

This leads to the third section, where a retrofit design with a similar geometric configuration as the repairs in this project is presented. This design aims to ensure ample confinement is provided by a steel jacket so that a lap-spliced column can sustain large inelastic deformations without failure. This methodology was

adapted for the repair technique in this project and is the foundation of the sleeve thickness design of Section 5.2.

2.1 Plastic Hinge Relocation Repair

This research is the third in a series of studies on plastic hinge relocation (Krish, 2018; Rutledge et al., 2014). Given its relevance to the study at hand, a thorough review of the study by Krish (2018) is recounted first in this section followed by two other similar repair projects. Of the four tests by Krish with fractured bars, every bar that was fractured during the original column test debonded during the repair test except for one where a headed stud was attached. The headed stud was not pursued further in this project because it is labor intensive to install. In the next study by Parks et al. (2016) all four columns were connected to the support through a grouted splice sleeve (GSS) connection and contained either one fractured bar or had multiple GSS pullouts. In one test, a fractured bar was completely anchored and re-fractured above the plastic hinge. The debonding behavior discussed earlier was explicitly stated as the failure mechanism for one of the repair tests, however the other two tests each had one fractured bar that did not refracture in the repair test and could have debonded, though this was not stated. In the final paper by Wu & Pantelides (2017), two additional repair tests were conducted with a CFRP shell designed using FEM. While this shell performed well and was not damaged during the repair test, the fractured longitudinal bars still debonded during the repair tests. This indicates that confinement alone may not be enough to ensure anchorage of the fractured bars, and that bond between the repair and damaged column must be considered.

2.1.1 Krish (2018)

In the study by Krish (2018), six reinforced concrete columns were repaired using plastic hinge relocation on columns with varying levels of damage, from all longitudinal bars being buckled to having 6 of 16 bars fractured. The emphasis of this study was to develop a rapid repair for modern, well-designed bridge columns with severe seismic damage. Prior to this, little research had been done on the repair of columns containing fractured bars, and a rapid repair for them was considered impractical. This consideration was challenged by Krish where a repair with an estimated 48-hour instillation time was developed that only used conventional materials that are typically readily available. The construction process of this repair was similar to what was done in this report, with a complete description given in Section 3.3.2. Since Krish's research is the

foundation for the research in this report, a description of each of the six tests is provided below. An emphasis is placed on Repair #1, 2, and 5 as they are the most relevant to the research described in this report.

Repair #1

The first column contained only buckled bars and was considered the lower bound of damage where this repair would be logical. For this repair, holes were drilled into the footing where steel reinforcing bars were later placed and bonded using a two-part epoxy. Next a steel sleeve was placed around the bars and welded together which acted as a stay in place form while also providing shear strength and confinement. Lastly the steel sleeve was backfilled with grout to bond with the dowels.

The repair successfully relocated the plastic hinge and restored the strength and displacement capacities of the column. The global force-displacement response of the column in both the X and Y direction are shown below in Figure 2.1 where Load Path Test 4 refers to an original column test with the same steel detailing and loading (Goodnight et al., 2017). Of particular interest, is that Repair #1 showed no sign of strength degradation or pinching which was observed in every other test by Krish that contained fractured bars.

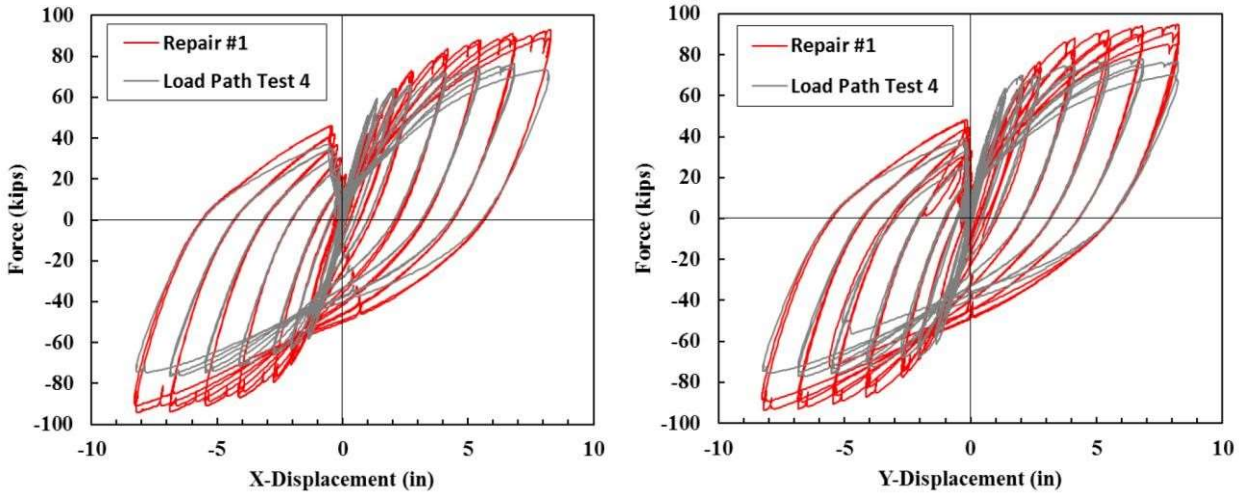

Figure 2.1: Repair #1 Global Response in the X (left) and Y (right) Directions (Krish, 2018).

Repair #2

With Repair #1 as a baseline for this repair technique, Repair #2 sought to see the effects of repairing a column with fractured bars. This was done by repairing a similar column exactly the same as Repair #1, but with 6 of the 16 longitudinal bars fractured from the initial testing. While most other studies on column repairs

with fractured bars used patching or splicing, this is not practical for a rapid repair and the fractured bars were left unchanged, aside from removal of loose concrete.

The repair performed similarly to the first column, and successfully relocated the plastic hinge and restored the strength and displacement capacities. The global response is shown below in Figure 2.2, again with Load Path Test 4 for comparison. The biggest difference between this repair and Repair #1 can be seen in the Y-direction, which had the 3 extreme bars in each loading direction fracture during the initial test. The softening and pinching behaviors are both indicative of a weakened repair response due to the fractured bars. Post-processing showed that all 6 fractured bars debonded and no longer contributed to the column's response, which is evident from the strain history of the bar in Figure 2.3. Where tensile strains in the bars typically increase with larger displacements, after a peak strain around 0.01 the bars debonded and its anchorage inside the repair rapidly degraded, leading to the bar being incapable of sustaining load. This debonding behavior is the primary topic of study for the research in this report and is hypothesized to result in the softened and pinched response of the column.

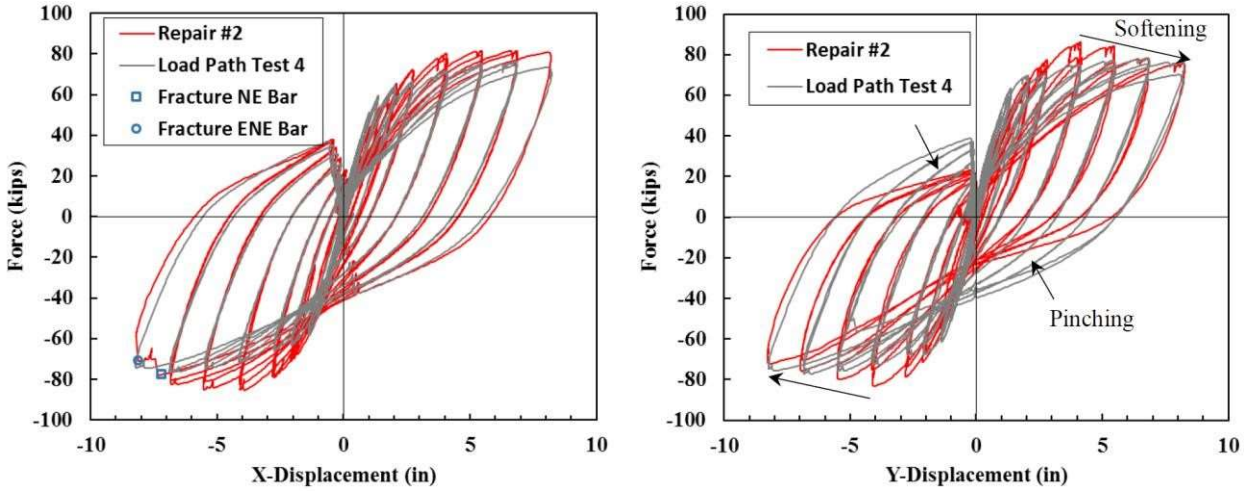

Figure 2.2: Repair #2 Global Response in the X (left) and Y (right) Directions (Krish, 2018).

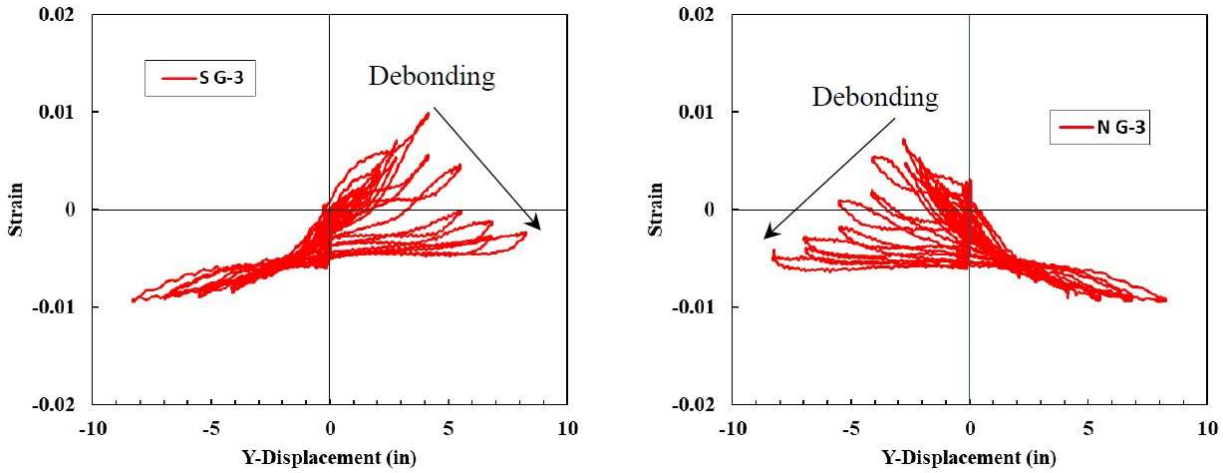

Figure 2.3: Repair #2 Strain vs. Displacement of the extreme south (left) and north (right) bars (Krish, 2018).

Repair #3

The Repair #3 aimed to address capacity design concerns from the previous tests. Especially in the first repair, the repaired column had a larger strength capacity due to the shorter effective height of the repaired column. If the column's footing does not have sufficient strength, it would be possible for the increased demand from the column plastic hinge to lead to failure in the footing which is clearly undesirable. A potential solution was to cut 4 of the longitudinal bars above the repair to purposely weaken the relocated plastic hinge to match the strength of the original column. While this was successful, it reduced the column's displacement capacity and should not be done unless the footing is incapable of supporting the increased demand.

Repair #4

The fourth repair test used a traditional reinforced concrete repair to provide an alternative solution. Instead of the welded steel sleeve, rebar hoops were tied around the repair bars, and instead of grout a flowable concrete pump mix was used. The column also only contained one fractured bar to determine if reducing the number of fractured bars effects their anchorage. While this repair successfully relocated the plastic hinge along with restoring the strength and displacement capacities, the only fractured bar still debonded around the same peak strain of 0.01.

Repair #5

For the fifth repair, two methods of anchoring the fractured bars inside the repair were investigated. On one fractured bar, the concrete surrounding it was completely chipped out so that when the repair concrete was poured it surrounded the fractured bars throughout the entire height of the repair. This was based on the recommendation in the ACI Guide to Concrete Repair (ACI Committee 546, 2014) and was expected to improve the bond conditions of the bar. On a separate fractured bar, a mechanically fastened headed stud was applied to the base. The purpose of the stud was to provide a bearing surface which provides additional anchorage for the bar, however attaching it required a significant amount of work to clear out the concrete and cut both the buckled section of the bar and transverse steel. These two additions to the repair are shown in Figure 2.4.

Figure 2.4: New Anchorage Mechanisms in Repair #5 (Krish, 2018).

While this test started off well, the repair suffered an early failure due to rupture of the weld in the steel sleeve, which is shown in Figure 2.5. This failure led to conclusions that the use of a welded connection requires careful cutting and surface preparations for the thin sleeve. This was one reason that a mechanically bolted connection was investigated in this project. Despite the weld rupture, which was initiated during ductility 3, an analysis of the repair was conducted up to that point. For the two new anchorage mechanisms, the bar with the headed stud showed no signs of debonding. Although it was believed that this would have continued if the weld had not ruptured, the headed stud required so much labor for installation it was recommended only if complete bar anchorage was absolutely necessary. As for the bars that had the surrounding concrete removed,

the strain histories were similar to the other fractured bars that debonded with only a slight improvement in peak strain and it was concluded that this alone had little improvement on anchorage of the bar.

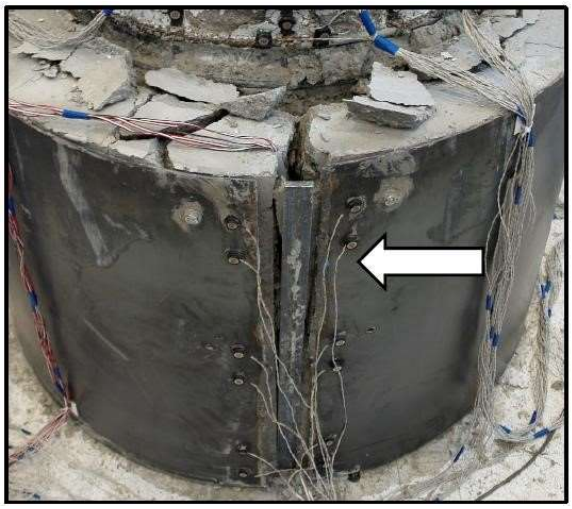

Figure 2.5: Weld Failure during Repair #5 (Krish, 2018).

Repair #6

The final repair also aimed to fully anchor fractured bars inside the repair, this time by placing a corrugated pipe inside the repair to act as a shear key and improve the bond conditions inside the repair. It was believed that this would lead to a flexural response of the repair instead of the column-socket like action that had been observed so far. This only slightly improved the anchorage of the bar, and ultimately the fractured bars still debonded inside the repair.

2.1.2 Parks et al. (2016)

In this paper, four hexagonal columns with GSS connections were repaired using plastic hinge relocation. Three of the damaged columns had 1 of 6 longitudinal bars fractured, and the final column suffered GSS pullout of multiple bars. The repair was similar to Krish's except that a CFRP shell was used instead of the steel sleeve, and the repair bars were headed to ensure sufficient development. Additionally, 2 of the repairs used expansive concrete to provide active confinement to the repair. It was not mentioned if this was done to better anchor the fractured bars.

Both repairs with normal concrete performed well, completely or closely restoring force and displacement capacities to the original column test and ending with longitudinal bar fracture in the relocated plastic hinge. In

one case, a bar which fractured during the original column test fractured again above the repair indicating that the bar was fully anchored inside the repair and did not debond.

Neither repair tests that used the expansive concrete ended with failure in the relocated plastic hinge. One column suffering an early fracture of the extreme west longitudinal bar due to embrittlement from a welded instrument; however, it still performed well in the other direction of loading throughout the remainder of the test. It is not mentioned if the extreme east bar, which was fractured during the original test, showed any evidence of debonding. Failure of the other column was due to the longitudinal bars that pulled out of the GSS connection in the original test debonding in the repair test, followed by rupture of the CFRP shell. This failure was attributed to a shorter plastic hinge in the GSS pullout and stronger material properties of this column causing more demand on the repair.

The authors conclude that the repair can restore displacement and load capacities to the original column, along with their energy dissipation and stiffness. They also indicated that the expansive concrete provides active confinement to the repair, which increased the tensile capacity of the concrete and reduced the demand to the repair bars, but too much expansion will reduce the capacity of the CFRP shell.

2.1.3 Wu & Pantelides (2017)

Wu built on the research by Parks, performing two additional repair tests, this time with a more typical connection to the footing and cap beam and only using normal concrete. Additionally, a finite element analysis was used to design the CFRP shell to prevent rupture. Both original column tests led to 2 of the 6 longitudinal bar fractures, one on each side. While both repairs succeeded in restoring the load and displacement capacities, they exhibited softening and pinching in the global response and ended with concrete crushing and no additional bar fractures. During the tests, a gap was noticed between the column and repair which was attributed to the weak bond due to the previously fractured bars. It was concluded that bond between the repair and the damaged column is essential and that methods of doing this need to be studied, however no suggestions of how to do this were given. This separation of repair and column was also observed in the tests by Krish and is believed to be evidence that the fractured bars have debonded. A method of improving the bond between the repair and column is investigated in Repair #3 of this report.

Of interest for the research in this project, was that neither repairs' CFRP shells exhibited any signs of damage or excessive loading. This would imply that the shell provided continuous and large confining pressures

inside the repair and it is unlikely that additional confinement would have sufficiently anchored the fractured longitudinal bars.

2.2 Factors that Influence Rebar Anchorage

One of the goals of this study was to provide enough anchorage for any fractured longitudinal bars so that that they will re-fracture during the repair test. For new designs, this could be done by increasing the anchorage length of the bar or by adding bends or hooks to meet the required development length. Most development length equations take similar forms with bar size, concrete strength, and rebar strength being the primary variables. As an example, ACI 318-08 defines the development length using Equation 2.1 (ACI Committee 318, 2008), where the ψ factors account for different bond conditions based off location, coating, and size of the reinforcement, and $(c_b + K_{tr})/d_b$ accounts for the amount of confinement provided and is limited to 2.5. This limit of 2.5 illustrates that when enough confinement is provided, the bar will suffer a pullout failure instead of a splitting failure. At this point, additional confining pressures will not increase the bond strength of concrete to reinforcing bars. This development length is often required to be increased for lap splices, which the repair bars and fractured longitudinal bars form; however, lap splices are typically not permitted in or near a plastic hinge, which is unavoidable in this repair.

$$l_d = \left(\frac{3}{40} \frac{f_y}{\lambda \sqrt{f'_c}} \frac{\psi_t \psi_e \psi_s}{\left(\frac{c_b + K_{tr}}{d_b}\right)} \right) d_b \qquad \textbf{Equation 2.1}$$

The limitation of no lap splices in the plastic hinge is precisely because of the debonding behavior that has been observed in the repair tests. Despite this, the development length equation still serves to show how anchorage can be improved for the fractured bars. Given that the bars are already in place, the size and yield strength of the fractured bars cannot be adjusted, and that concrete strength may be limited in rapid deployments, bond and confinement are the remaining variables that will affect anchorage.

A method of improving the bond of the fractured bars was investigated in Repair #3 of the research described in this report, which involved removing the concrete surrounding the bar within the height of the repair. This concrete was then replaced by the repair grout when the repair was cast. This was done because even though a majority of the damage in the original column was concentrated in the plastic hinge, small flexural cracks still form throughout the entire height of the column. In a study by Desnerck et al. (2015), the bond behavior of reinforcing bars in cracked concrete was investigated, and from experimental tests the authors showed that the bond strength can be reduced by more than 50% in cracked concrete, even when the cracks are less than 0.04 mm. By replacing the cracked column concrete with a fresh, uncracked repair grout the bond strength is therefore expected to be improved. If enough confinement is provided, there should only be minimal new cracks forming during the repair test, which will maintain the high bond strength to anchor the bars. This is precisely what Priestley et al. (1996) aimed to accomplish using the design process discussed in the following section.

2.3 Sleeve Thickness Requirements

Since the Priestley et al. (1996) retrofit design process became the foundation for the sleeve thickness design in this repair (presented in Section 5.2) the philosophy will be thoroughly described here. Much of the work in Priestley et al. (1996) stems from the fact that most columns built before the 1970s were inadequately designed in terms of flexural ductility, shear capacity, and confinement. This led Priestley et al. (1996) to include the retrofit design process developed by Chai et al. (1991) for columns using steel jackets. An example of when this retrofit was needed due to a lap splice in the plastic hinge is shown in Figure 2.6. Priestley stated that lap splices should not be placed in plastic hinge regions because insufficiently confined lap splices were shown to be progressively damaged by cyclic loading which led to a rapid loss in load capacity. It is believed that this is the mechanism that caused debonding of the fractured bars in the repair tests, though it does not cause failure of the column since other longitudinal bars are still intact.

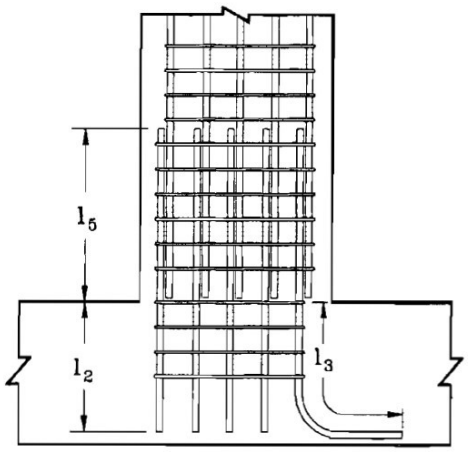

Figure 2.6: Deficient Column Construction Requiring Retrofit (Priestley et al., 1996).

The configuration in the Figure 2.6 will be used to illustrate the retrofit design. In this example, the footing would have been cast with starter bars extending out of the footing, which would have then been tied to the column cage and the column cast. With the maximum moment occurring at the base of a cantilever column, this could be the location of the plastic hinge, and would likely require retrofit due to insufficient confinement. In this retrofit, instead of relocating the plastic hinge above the lap splice, a steel jacket that is slightly bigger than the column would be placed around the column along the splice. To ensure proper behavior of the retrofitted column, three potential failure mechanisms are discussed in the following sections.

2.3.1 Confinement to Prevent Lap-Splice Failure

The first check described here aims to prevent the lap-splice failure by providing enough confinement to prohibit large splitting cracks from forming. To perform this design, the crack shape is estimated, and the tensile capacity of the concrete along that crack is compared with the load applied to the bar. If the load on the bar is greater than the capacity of the concrete, then lap splice failure is expected to occur. For the above configuration, Priestley presents two potential crack shapes, shown in Figure 2.7, which lead to perimeter lengths given by Equation 2.2. With this assumed crack shape extending along the height of the splice, the confining stress expected to prevent lap splice failure, f_l is found assuming a simple static friction relationship, given by Equation 2.3.

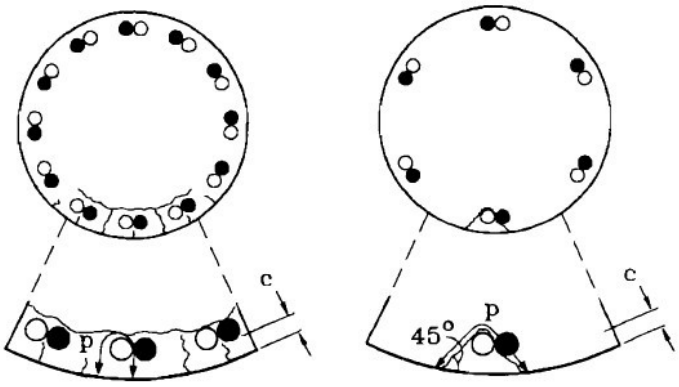

Figure 2.7: Assumed Crack Shape in Circular Columns (Priestley et al., 1996).

$$p = \frac{\pi D'}{2n} + 2(d_b + c) \leq 2\sqrt{2}(c + d_b) \qquad \textbf{Equation 2.2}$$

$$\mu f_l p l_s = A_b f_s \qquad \textbf{Equation 2.3}$$

For a circular jacket, the confining pressure can be found using Equation 2.4 where f_{sj} cannot be larger than the stress at a strain of 0.0015. This dilation strain limitation is used to ensure that cracking within the concrete is kept to a minimum, which ensures high bond stresses where the coefficient of friction, μ, can be assumed to be 1.4. By combining Equation 2.3 with Equation 2.4 and assuming that $f_s = 1.7 * f_{yl}$ and $\mu = 1.4$, Priestley formulated Equation 2.5 to determine the required volumetric ratio of confining steel, which relates to the required jacket thickness through Equation 2.6.

$$f_l = 0.5\rho_{sj} f_{sj} \qquad \textbf{Equation 2.4}$$

$$\rho_{sj} = \frac{2.42 A_b f_{yl}}{p l_s (0.0015 E_{sj})} \leq \frac{2.42 A_b f_{yl}}{p l_s f_{yj}} \qquad \textbf{Equation 2.5}$$

$$\rho_{sj} = \frac{4t_j}{D} \qquad \textbf{Equation 2.6}$$

2.3.2 Confinement for Ductility

Since inadequately confined columns are incapable of sustaining large flexural deformations, the next design consideration in this retrofit aims to increase the ductility capacity of the column. To do this, the strain-energy capacity relationship shown in Equation 2.7 is used to ensure that the confining steel can withstand the

large compressive strains required to reach higher ductilities. When insufficient confinement is provided, the ultimate compressive strain will be limited by yielding of the transverse steel, which also limits the deformation capacity of the column. By substituting Equation 2.6 into Equation 2.7, Priestley formulated Equation 2.8 to determine the required jacket thickness to reach the desired ductility. While Priestley developed charts that could be used to avoid calculation of f'_{cc} given that it is dependent on the confining steel, the approach suggested for the designs in this repair use conservative values to eliminate this (as will be shown later), so that process is not discussed here.

$$\varepsilon_{cu} = 0.004 + \frac{1.4\rho_{sj} f_{yh} \varepsilon_{su}}{f'_{cc}} \qquad \textbf{Equation 2.7}$$

$$t_j = \frac{0.18(\varepsilon_{cm} - 0.004) D f'_{cc}}{f_{yj} \varepsilon_{sm}} \qquad \textbf{Equation 2.8}$$

2.3.3 Shear Capacity

The final design consideration in this retrofit is regarding the shear capacity. The columns requiring this retrofit had very little transverse steel, which may lead to shear failures. The steel jacket retrofit was useful to increase the shear strength of the column and ensure a flexural failure. In the retrofit, the shear force of the concrete and existing transverse steel was calculated and subtracted from the overstrength shear demand to determine the additional required shear resistance. With this, Equation 2.9 would be used to determine an acceptable jacket geometry. By assuming θ is 35° and solving for the jacket thickness, Equation 2.10 can then be used to determine the required jacket thickness for a given shear force. This equation shows that even a thin steel jacket can resist very large shear forces.

$$V_{sj} = \frac{\pi}{2} t_j f_{yj} D \cot\theta \qquad \textbf{Equation 2.9}$$

$$t_j = \frac{V_{sj}}{2.24 f_{yj} D} \qquad \textbf{Equation 2.10}$$

2.4 Combined Confinement with CFRP

Relocating the plastic hinge results in a reduction of displacement capacity due to an increased stiffness of the system. One goal of this project was to design a repair which restores the column to its original force and displacement capacities. In order to increase the displacement capacity, a carbon fiber reinforced polymer

(CFRP) wrap was placed around the relocated hinge. CFRP is often used for confinement around columns with insufficient transverse steel detailing, such as large spiral spacing. In these cases, the effect of the existing steel on the confinement of the core can generally be neglected. The columns in this study were well designed with sufficient transverse steel for the required ductility of the original column. Consequently, the transverse steel would work with the CFRP to create a combined confinement effect within the core of the column. Several models exist which consider this combined confinement (Pellegrino and Modena, 2010; Hu and Seracino, 2013). By including the confinement of both the CFRP and steel spirals, the ultimate strain of the concrete can be increased. This increase in ultimate strain is advantageous because it allows for the same section to reach a larger curvature, and thus a larger displacement. The design used for the repairs in this report was the model by Hu and Seracino (2013), which considers the relative stiffness in the contribution from both the steel and CFRP to determine the relationship between axial and lateral stresses. This relationship can be utilized to determine the full stress-strain relationship of the confined concrete.

Chapter 3: Experimental Setup

For the large-scale laboratory tests in this research, circular reinforced concrete columns were repaired using the plastic hinge relocation method developed by (Krish, 2018). The damaged columns were obtained from a separate ongoing research study at the NC State Constructed Facilities Laboratory that is investigating the use of high-strength (Grade 80) steel in seismic design (Manhard, 2019). This project was a continuation of the work by Barcley & Kowalsky (2020) and aims to evaluate if Grade 80 reinforcing steel can be reliably used in the plastic hinge region of reinforced concrete columns. Because the repairs were done on existing damaged columns, the level and extent of previous damage was not identical. The test matrix of the repair parameters is included in Table 3.1.

Table 3.1: Test Matrix

Repair	Sleeve Thickness	Bolt Pretension	Removal of Loose Concrete	Column Height	Column Diameter	Sleeve Height	Grout	CFRP Layers
1	10-ga	No	No	8’	24”	0.9D	Cementitious	--
2	10-ga	Yes	No	8’	24”	0.9D	Cementitious	--
3	0.25”	Yes	On one side	8’	24”	0.9D	Cementitious	--
4	0.25”	Yes	Yes	8’	24”	0.9D	Cementitious	--
5	0.25”	Yes	Yes	8’	18”	0.9D	Cementitious	--
6	0.25”	Yes	Yes	13’	18”	1.2D	Cementitious	--
7	0.25”	Yes	Yes	13’	18”	1.2D	Epoxy	--
8	0.25”	Yes	Yes	8’	18”	0.75D	Cementitious	--
9	0.25”	Yes	Yes	8’	18”	0.75D	Cementitious	3
10	0.25”	Yes	Yes	8’	18”	0.9D	Cementitious	2

3.1 Laboratory Setup

The experimental tests were conducted using the same laboratory setup as Manhard (2019). Figure 3.1 and Figure 3.2 show the conceptual and actual laboratory setup that was used for the original and repaired column tests. This section summarizes the application of the lateral and axial loading along with the loading protocol; however, a complete description of the setup is given by Manhard (2019).

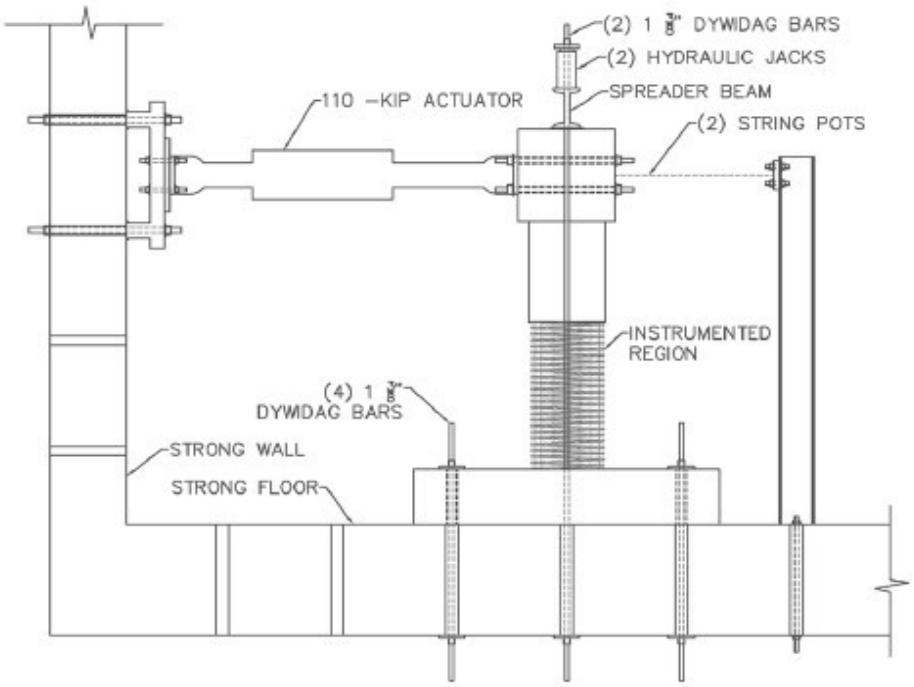

Figure 3.1: Laboratory Setup (Manhard, 2019).

Figure 3.2: Actual Laboratory Setup.

3.1.1 Loading Application

On the left-hand side of Figure 3.1 and Figure 3.2, the 110-kip actuator that applied the lateral loading for the first four repairs can be seen. This displacement-controlled actuator has a 20-inch stroke and was connected to the column from the strong wall. For the last six repairs, a 220-kip actuator with a 40-inch stroke was used. While the lateral force applied to the column was measured by the actuator, the lateral displacement of the column was directly measured by two string pots on the opposite side.

The axial force was applied by two hydraulic jacks connected with a spreader beam across the cap of the column. Because these jacks are not capable of maintaining a constant load on the column as it is displaced, the two jacks were connected to a third jack that was placed in an MTS machine. With all three jacks connected in a closed loop, it was possible to apply a specific force on the jack in the MTS machine which would in-turn apply the same load to each of the jacks. The MTS machine was then capable of maintaining a constant axial force on the column even as it was subjected to lateral displacements.

3.1.2 Lateral Loading Protocol

Each of the columns were originally subjected to the loading history shown in Figure 3.3. For the early stages of the tests, the loading was based upon the analytical first yield force (Fy'). For this, the column was subjected to one cycle of positive and negative forces at ¼ Fy', ½ Fy', ¾ Fy', and Fy'. The average of the absolute displacements at Fy' was then deemed the first yield displacement (Δy'). The equivalent yield was then obtained by: $\Delta_y = M_n \times \Delta'_y / M_y'$, where M_n is the analytical nominal moment capacity. Following first yield, the three-cycle set loading began at displacement ductility (μ_Δ) levels 1, 1.5, 2, 3, 4, and so on until failure.

In order to evaluate the effectiveness of the repair, a comparison with original column data is desirable. All the repairs followed the same load history as an original comparison column with nominally identical detailing and axial load ratios. This meant that rather than using an analytical first yield force for the first cycles, quarter-increments of the original column's Δ_y' was used, followed by the three-cycle set at the same ductility levels as the original test.

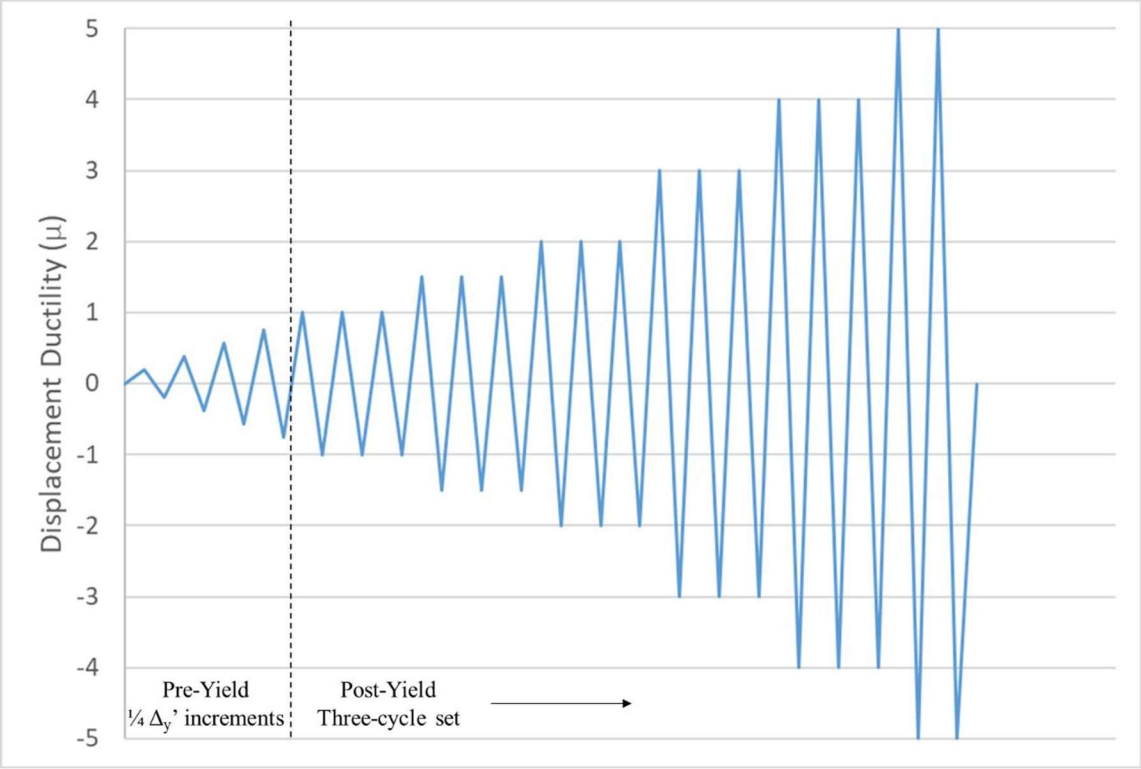

Figure 3.3: Lateral Loading Protocol.

3.1.3 Axial Loading Protocol

For the axial load, the initial plan was to use the same axial load as the original column tests, however while preparing for the first repair test there were concerns that the axial load bars could have yielded when using 10% axial load ratio (ALR). Since these bars could not be easily switched out, it was decided to use 5% axial load. Although this limits the comparison between the original and repaired columns, other column test data is available with the same steel detailing and axial load ratio (Barcley & Kowalsky, 2020).

Table 3.2 clarifies the following parameters for each of the repairs: which damaged column was repaired, the lateral load path that was repeated, and which of the available column data serves as the best comparison between the original and repaired columns. To reiterate, the columns for Repairs #1 & 2 were originally tested at 10% ALR, however 5% ALR was used for the repair tests, thus Barcley's Column #1 with the same steel detailing and ALR serves as a better comparison. In contrast, the column for Repair #3 was tested at 5% axial load ratio for both the original and repaired tests, thus it serves as the optimum comparison column. For Repairs #5 through #10, the column diameter was smaller, so using an axial load ratio of 10% resulted in a smaller axial load which would not yield the axial load bars. An axial load of 10% was used for both the original and repair tests.

Table 3.2: Repair and comparison columns.

Repair Number	Column Repaired	Displacement Path Used	Axial Load Ratio	Comparison Column
1	Manhard #4	Manhard #4	5%	Barcley #1
2	Manhard #3	Manhard #4	5%	Barcley #1
3	Manhard #1	Manhard #1	5%	Manhard #1
4	Manhard #2	Manhard #2	5%	Manhard #2

Initially it may seem improper to use the same displacement path loading for the repair test when the applied axial load is different; however, it is well established that the yield curvature of a concrete section is proportional to the yield strain of the longitudinal steel and diameter of the section (Priestley et al., 2007). This means that a change in axial load will have little effect on the yield displacement (Δy). Since the displacements for the three-cycle set loading are displacement ductilities, which are multiples of Δy, it can be concluded that even if the original column test was done at 5% axial load ratio the load path would have been approximately the same.

3.2 Materials

The following sections describe the materials used to construct the plastic hinge relocation repair developed by Krish (2018). To aid in keeping this repair suitable for rapid application, only conventional materials that are likely to be readily accessible are used for the repair. A complete explanation on how each of these materials were chosen can be found in Krish (2018).

3.2.1 Longitudinal Repair Bars

Relocating the plastic hinge above the column-footing interface increases the flexural demand in the column. To account for this, additional longitudinal reinforcement is needed within the repair that must be connected to the footing. This was done using steel reinforcing bars as they are readily accessible and have well known structural properties.

For Repairs #1 – 4, No. 8 ASTM A706 Grade 80 steel reinforcing bars were used. Repairs #5, 6, 7, and 10 used No. 6 ASTM A706 Grade 80 steel reinforcing bars, and Repairs #8 and 9 used No. 5 bars due to the shorter development length in those repairs. It is worth noting that while Grade 80 steel has been used for all the repair bars by Krish as well, any grade steel or other material could be used as long as it can be designed to remain elastic. This is necessary to ensure capacity protection of the repaired portion of the specimen. Measured material properties for the #8 bars used in this project are shown in Table 3.3.

Table 3.3: Longitudinal Repair Bar Mechanical Properties.

Sample	Yield Stress (ksi)	Yield Strain (με)	Elastic Modulus (ksi)
1	84.2	3572	23578
2	84.1	4001	21016
3	83.7	3006	27854
4	83.6	3549	23556
5	83.6	3909	21392
6	84.5	3266	25860
Average:	84.0	3551	23876

3.2.2 Bonded Anchor

The longitudinal bars need to be anchored into the footing in order to contribute to the flexural capacity of the repair. This is done by hammer drilling holes into the footing and then anchoring the bars with grout or epoxy.

Krish (2018) found that grouting would require larger holes and have a longer set time, so epoxy was used. ITW Redhead Acrylic 7 epoxy was selected as it is compatible with rebar, has a quick set time, and has acceptable temperature bounds for curing in the Alaskan climate.

3.2.3 Steel Sleeve

Encasing the longitudinal bars in grout requires transverse steel to achieve the required confinement. In all of Krish's (2018) tests (expect for Repair #4 which used rebar hoops) this was achieved by cold rolling an 11-gauge A36 steel sheet into two semi-circles which were welded together around the column. For the repairs in this report, the weld has been replaced with a mechanically bolted connection. To do this, the steel sheet was

cut to be slightly larger than a semi-circle. Consequently, when the two pieces were placed around the column they overlapped on both ends, leaving room for the pieces to be bolted together.

To aide in decreasing the likelihood of a bearing failure at the bolts, a slightly thicker 10-gauge steel sheet was used for the first two repairs in this project, which is the largest thickness that could be cold rolled by the NC State machine shop. For the third test, the sleeve thickness was increased to ¼ inch. A discussion on why this was done can be found in Section 4.2.6.

3.2.4 Structural Bolts

A new technique deployed in the research described in this project was the use of structural bolts to mechanically fasten the two steel sheets together. For Repair #1, ½" diameter ASTM A325 bolts were used which is the smallest size of that standard and was felt to be most appropriate for the thin steel sleeve. For the remaining repairs, 5/8" diameter ASTM A490 bolts were used instead to allow for a greater pre-tensioning force. An explanation for why this was done can be found in Section 4.1.6. Additionally, recommendations for the design of this bolted connection can be found in Sections 5.3 and 5.4.

3.2.5 Backfill Grout

The last step of the repair is to backfill the steel sleeve to restore the original column's cross section and allow forces to transfer from the column to the repair bars. In the previous research by Krish (2018), this was primarily done with a high-strength grout, although a flowable pea gravel concrete mix was also used to investigate a more cost-effective alternative. For the tests in this research, the same high strength grout (BASF Masterflow® 928) was used as it has worked well for various experiments at NC State for the Alaska DOT.

The grout was poured in three lifts using five 55 lb bags for each lift. Per the grout manufacturer's directions, approximately 9.5 lbs of water per bag were placed into a gas powered drum mixer. The grout was not extended with pea gravel. The grout was then slowly added into the mixer and left to mix until a "milkshake-like" consistency was obtained.

The previous research by Krish found that testing 2x2 cubes per ASTM C109 gave inconsistent material strengths versus using a 4x8 cylinder tested per ASTM C39. Because of this, only cylinder samples were taken from the grout mixes in this project. Three cylinders from each lift were tested on the day of the column test.

For Repair #7, a commercially available epoxy grout, Denso SeaShield550, was used. The grout was mixed in batches corresponding to the kits of epoxy, and poured into the repair consecutively. The grout was poured in five lifts using two 50 lb bags for each lift. Because of the fast mix time and consistent material properties, there were no concerns of a cold joint forming between the layers and cylinders were taken from one of the batches. This grout can be used with coarse aggregate to reduce cost, however in this repair no coarse aggregate was used as it decreases workability. The grout was poured into the repair to create a level surface with the top of the steel sleeve. As the grout hardened it did shrink and developed one radial crack. This crack was later filled with epoxy to prohibit any adverse effects to the repair's performance. A summary of the grout compressive strength on the day of the test for each repair is given in Table 3.4.

Table 3.4: Grout Material Properties.

Repair	1	2	3	4	5	6	7	8	9	10
Test day strength (ksi)	7.93	8.82	9.33	7.93	7.41	6.24	9.28	5.48	7.50	7.62

3.2.6 Carbon Fiber Reinforced Polymer

For the final two repairs, a Carbon FRP wrap was applied to the relocated hinge to increase the confinement and improve the displacement capacity of the repaired column. Although it is a less conventional material, the CFRP wrap could be beneficial in scenarios where the steel jacket can be deployed rapidly, which allows for the bridge to return to service and the CFRP could be applied later to improve the seismic performance. The CFRP used in these repairs was the Structural Technologies V-Wrap C200H. The fabric was saturated with epoxy following the manufacturer instructions, and the average cured laminate properties are shown in Table 3.5.

Table 3.5: CFRP Laminate Properties.

Tensile Strength	180,000 psi
Modulus of Elasticity	10.7×10^6 psi
Elongation at Break	1.7%
Thickness	0.04 inches
Strength per Unit Width	7,200 lbs/in

3.3 Construction

3.3.1 Original Column Construction

As mentioned at the beginning of this chapter, the damaged columns were obtained from a separate research study on the use of high-strength (Grade 80) steel in seismic design (Manhard, 2019). These columns were constructed at the Constructed Facilities Lab at NC State, and a complete description of this process can be found in Manhard (2019). To aide in instrumentation, the bottom 4 feet of the column was cast with no cover concrete so that both the longitudinal and transverse steel was exposed and Optotrak sensors (discussed in Section 3.4.1) could be placed directly onto the steel.

3.3.2 Repair Construction

The plastic hinge relocation repair used in this project was developed by Krish (2018) and the construction process remains largely the same. The repair is intended to be rapid, capable of being done within a few days. As such, only conventional materials which are likely readily available are used. This section will give a complete description of the recommended repair construction based off the new findings from this research.

Step 1: Straighten Column

In the work by Krish (2018), the column's residual drift was determined to be the best indicator of reparability of the structure. Using the fragility curves he developed, the engineer should first determine if the column's residual drift is within acceptable limits. If not, the column should be straightened as upright as possible. Exact methods for accomplishing this have not been studied in this project and would likely be dependent on what heavy equipment is available to push or pull the bridge system.

Step 2: Remove Damaged Concrete

The plastic hinge region of the column will likely have substantial damage to the cover and core concrete, and any loose concrete should be removed through a hammer drill or other less destructive methods. Additionally, if the damaged column has any fractured bars, the concrete around these bars

within the height of the repair should be removed. This ensures that the fresh repair grout will completely surround the fractured bar and is a necessity to fully anchor the bar within the repair. An example before and after of this step is shown in Figure 3.4. On the left, the damaged column is shown with large cracks near the base being evidence of the loose concrete that needs to be removed. For this column, the three frontmost bars were fractured during the original test, so within the height of the repair the concrete around the bars was removed, which can be seen on the right. Although the exact depth for concrete removal around the fractured bars has not been studied in this project, it is recommended to remove at least a the nominal maximum aggregate size around the bar (shown in Figure 3.5).

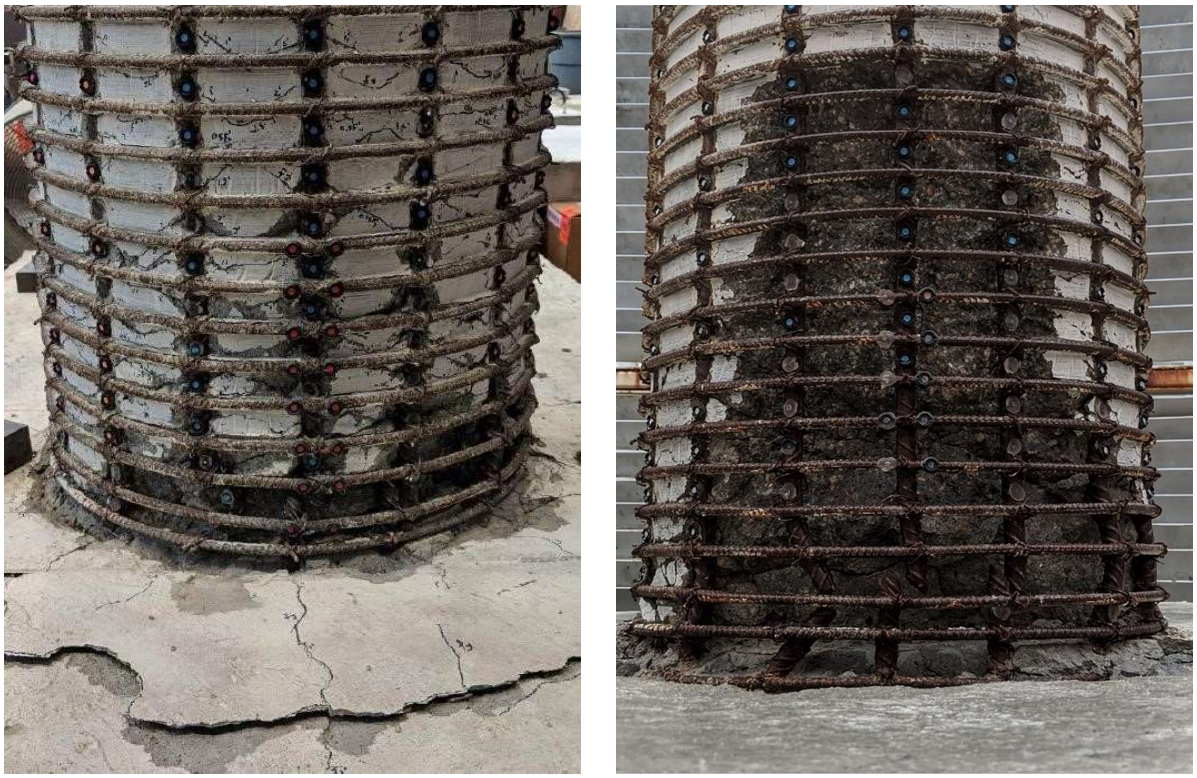

Figure 3.4: Before and After Removal of Damaged Concrete.

Figure 3.5: Removal of Concrete Around the Perimeter of Fractured Bars.

Step 3: Drill Holes into Footing

The repair design will determine the number, size, and approximate locations of the new longitudinal repair bars. The first step in placing these bars is to drill holes into the footing. This should be done according to the manufacturer's specifications of the grout or epoxy used to anchor the bars (Step 4). For the repairs in this project, the No. 8 bars required a 1-1/8" drill bit, and the drilling depth was limited to 15 inches due to the footing being 18 inches deep. This step is shown in Figure 3.6.

As a note, finding locations where the holes can be drilled can be difficult depending on how congested the footing reinforcement is. For this project, the exact locations of reinforcing bars in the footing were measured prior to casting of the footing, which aided in determining where bars could be placed. Even with these measurements, drilling into the footing did not always go smoothly and sometimes required removal of the cover concrete above the top mat of the footing in order to find a spot where the holes could be drilled.

Figure 3.6: Drilling Holes into Footing for Repair Bars.

Step 4: Embed Longitudinal Repair Bars into Footing

Next, the bars should be anchored to the footing through epoxy or grout. For this project, epoxy has been used because it has been shown to have a shorter set time and require a smaller hole size (Burtz, 2003). To start, the drilled holes typically need to be prepped for the epoxy to sufficiently bond with the footing concrete. For the Redhead A7+ epoxy used in this project, the holes should be sprayed twice with compressed air, then a wire brush is used to roughen the surface, followed by another two bursts of compressed air. In the lab, a vacuum was also used before the compressed air to limit the amount of airborne dust.

Once the holes have been prepped, the next step is to partially fill the holes with the epoxy. The bar is then slowly pushed into the hole while being twisted to prevent air bubbles and provide the best bond for the epoxy. For this project, nothing needed to be done to ensure the bars stayed vertical while the epoxy set due to a small hole tolerance and a viscous epoxy. Injection of the epoxy into the hole, as well as a completed bar is shown in Figure 3.7.

Figure 3.7: Anchorage of Repair Bars in Footing via Epoxy.

Step 5: Level Footing Surface (if needed)

For a column plastic hinge to form the extreme level of damage this repair is intended for, there will possibly be some amount of surface damage to the footing concrete near the joint. This damage can make it difficult to create a seal at the bottom of the sleeve and leveling may be needed. With the bars now in place and the epoxy set, any rapid set grout or concrete can be poured to create a level surface of the footing. Figure 3.8 shows an example of this step before (left) and after (right) levelling.

Figure 3.8: Use of Grout to Provide a Level Base for the Steel Sleeve.

Step 6: Place Steel Sleeve around Column

Once the grout used to level the footing has sufficiently set, the steel sleeve can then be placed around the column. For a repair, this cannot be done using a complete circular ring as there would be no way to get it around the column (i.e. a circular pipe could not be placed around a column). Instead, the sleeve must be comprised of two pieces, which are placed around the column and connected. It has been shown that this could be done through a welded (Krish, 2018) or a mechanically bolted connection (this research). Each method is discussed below:

Welded Connection:

For this connection, the steel sleeve is comprised of two semi-circular plates. These plates are placed around the column, then tack welded in place with a backer bar to align the connection. Once this is done, the entire height of the sleeve is butt welded, essentially creating a continuous ring around the column. This process was thoroughly studied by Krish (2018) and is shown in Figure 3.9.

Figure 3.9: Use of Tack Welds (left) then Butt Weld (right) for Welded Connection (Krish, 2018).

Mechanically Bolted Connection:

As previously discussed, the replacement of the welded connection with a bolted connection was the primary objective in the early stages of this research. For this connection, the steel sheet is cut to be slightly larger than a semi-circle. Consequently, when the two pieces are placed around the column they overlap on both ends, leaving room for the pieces to be bolted together. From the experimental tests, using this connection necessitates the use of pretensioned bolts to prevent slip at the plates. In the lab, this was done using a calibrated torque wrench, however any reliable method of bolt pre-tensioning can be used as long as slip of the plates can be prevented. The use of the calibrated torque wrench to tighten the bolts is shown in Figure 3.10, and the design for the sleeve, bolts and pre-tensioning can be found in Chapter 5.

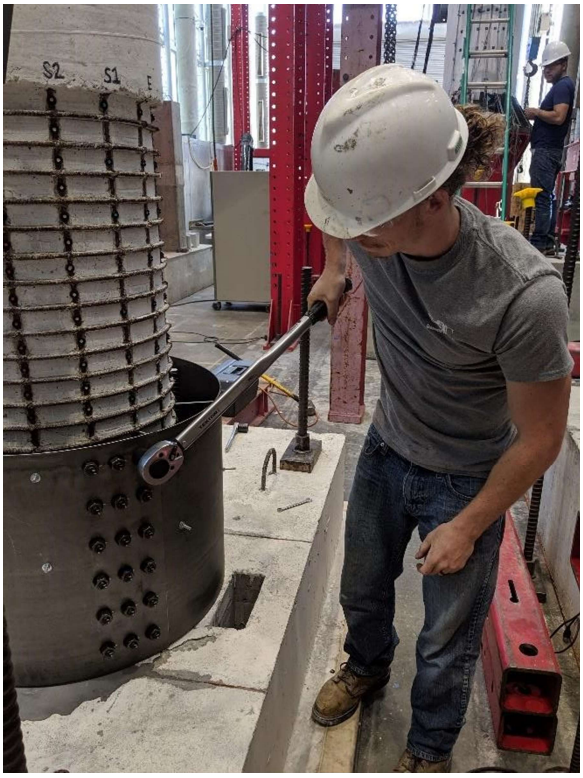

Figure 3.10: Pre-tensioning of Bolts via Calibrated Torque Wrench.

Step 7: Center Sleeve around Column

Regardless of the connection type used, the next step is to center the sleeve around the column. In the lab, this was done by using 2x4s cut to the same length and placed around the column to act as spacers. With the sleeve now centered, ¼" diameter threaded rods were extended through the sleeve to

the column. Using nuts and washers, the length of the rod could be adjusted so that the sleeve was secured to the column, then the 2x4s were removed. Both the 2x4 spacers and ¼" threaded rods can be seen in Figure 3.11. It should be noted that there are likely other methods of accomplishing this, but regardless of the process the sleeve should be uniformly spaced and secured so that it will not shift throughout the remainder of the construction process.

Figure 3.11: Centering of Steel Sleeve around the Column.

Step 8: Seal the Base of the Sleeve

Before grout can be poured into the repair, it is recommended that a water-tight seal be made at the base of the sleeve to prevent leakage. This is easily done in the lab using a silicone sealant caulk, however in the field any method that prevents severe leakage of the repair grout should be sufficient. The white silicone sealant caulk used for this project can be seen at the base of the sleeve in Figure 3.12.

Figure 3.12: Silicone Sealant (White) shown at the Base of the Sleeve.

Step 9: Pour Grout

The final step in this repair is to fill the annular space between the column and the steel sleeve with grout or concrete. This should be done using an appropriate nonshrink grout or concrete following manufacturer's instructions. For the large-scale laboratory tests in this report, the grout was poured in three lifts using five 55 lb bags for each lift. Per the grout manufacturer's directions, 9.5 lbs of water per bag were initially placed into a gas-powered drum mixer (Figure 3.13). The grout was then slowly added into the mixer and left to mix until a "milkshake-like" consistency was obtained. After all the grout was added to the mix, a small (less than 1 lb) amount of water was added, if needed, to reach the desired flowability. Once completely mixed, the grout was transferred into buckets then poured into the repair (Figure 3.14). Once this grout has set, the repair is complete and can be seen in Figure 3.15.

Figure 3.13: Gas-Powered Mixer used for Grout.

Figure 3.14: Pouring Grout into Repair.

Figure 3.15: Completed Repair.

Optional Step: Couplers

In the repairs using pre-embedded couplers in the footing, the bottom portion of the repair bars are placed in the footing at the time of initial construction. Unlike the repairs using drilled holes and epoxy, the development of the embedded coupled bar relies on the bond between the footing concrete and the bar. In case there was any damage to the footing concrete during the initial loading which would reduce the bond, steel plates were attached to the bottom of the bar to provide additional anchorage. Tack welds were used to keep the couplers in place while the footing concrete was being poured. The portion of the repair embedded in the footing is shown in Figure 3.16. The location of the couplers and formwork for casting are shown in Figure 3.17. At the time of the repair, the upper portion of the repair bars were threaded into the couplers and the repair process followed the same as previous repairs.

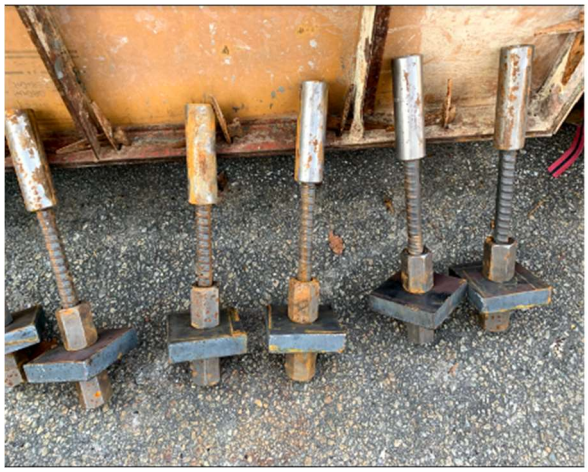

Figure 3.16: Embedded Portion of Repair Bars.

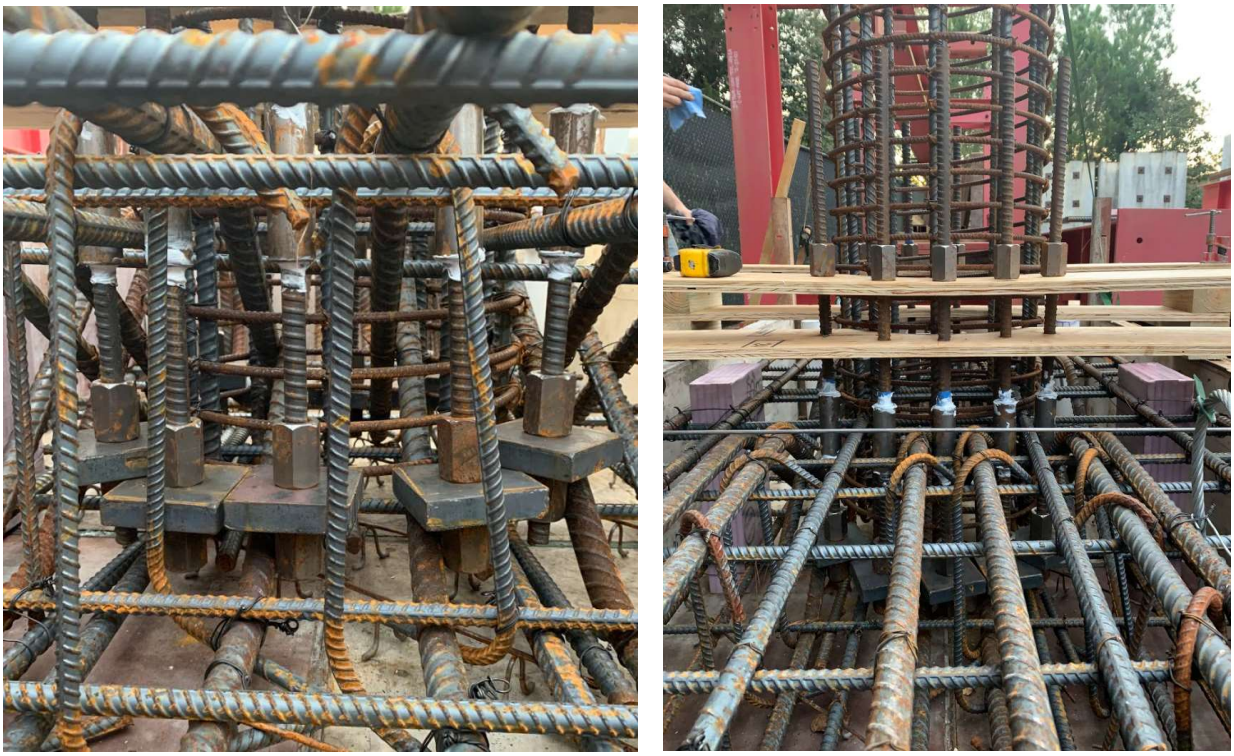

Figure 3.17: Repair Reinforcement Placed in Footing (left) and Formwork (right).

Alternative: Embedded Threaded Bars in Footing

One alternative method for integrating the possibility of repair into initial construction is to embed threaded bars that protrude above the surface of the footing. These bars serve as anchor points to connect the steel sleeve to the footing via a flange or leg, shown in Figure 3.18. This repair method was

intended to be used for two of the columns in this project; however, the damage from the initial test exceeded the damage anticipated at the time of construction. This level of damage resulted in demands on the repair that were greater than what it was designed for, and would lead to premature failure. The design remains a feasible alternative, given that the bars are appropriately sized and flange thickness can be accommodated.

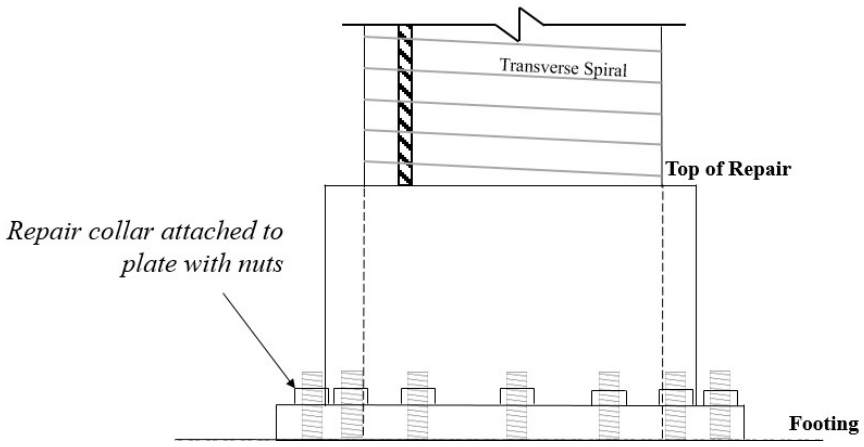

Figure 3.18: Schematic of Possible Repair Connection.

Optional Step: CFRP application

The original columns are constructed with the cover blocked out such that the longitudinal and transverse reinforcement can be instrumented. Before applying the CFRP wrap, the cover was restored. A sonotube was cut along the length, wrapped around the column, and sealed with silicone. The same high strength grout which filled the annular gap of the steel jacket was used to restore the circular section because of its ability to flow into the small gap between the sonotube and original column. After the grout hardened, the sonotube was removed. This step of casting additional cover would not be required in an actual repair application, but any damage to the concrete cover at the location of the new hinge should be patched before applying the CFRP.

Figures 3.19 through 3.22 show the application process of the CFRP wrap. The surface of the column was prepped using a needle scaler to remove any sharp edges which may cause stress concentrations within the CFRP. Following manufacturer instructions, the correct ratios of a two-part epoxy were measured into buckets and mixed. A thin layer was applied directly to the column. A portion of the mixed epoxy was separated into another container where it was mixed with fumed silica to create

a thickened epoxy. This thickened epoxy was used to fill any gaps and voids in the cover concrete and create a smooth and level surface for the CFRP. The CFRP fabric was measured and cut to the circumference of the column plus approximately 6 inches of overlap. The fabric was placed on a flat surface and paint rollers were used to spread the epoxy in a thin layer to saturate the fibers. Epoxy was spread on both sides of the fabric before placing it on the column. The CFRP was wrapped around the column and air bubbles were eliminated by smoothing over the fabric and using a rib roller. The CFRP was permitted to set between layers to reduce the possibility of sagging. The locations of the overlaps were staggered.

Figure 3.19: Needle-scaled Cover Concrete with Applied Primer Layer (left) and Thickened Epoxy (right).

Figure 3.20: Application of CFRP Wrap.

Figure 3.21: Removal of Air Voids from CFRP Wrap.

Figure 3.22: Completed CFRP Application.

3.4 Instrumentation

3.4.1 Optotrak

The Optotrak Certus HD 3D position sensor system produced by Northern Digital, Inc. has been reliably used to measure strains of longitudinal and transverse steel since 2007 at NC State's Constructed Facilities Lab. This system uses small LED markers and a calibrated camera to obtain precise three-dimensional positions of the markers. For column tests like this, three cameras are place around the column so that all sides can be seen. For each of the experimental tests in this project around 360 LED markers were placed directly on the steel sleeve, longitudinal steel and transverse steel, which can be seen in Figure 3.23.

With the three-dimensional position of each marker, it is possible to calculate an initial length between two markers and then monitor how the length changes as the test progresses. This information is used to calculate the strain between any two markers throughout the entirety of the test.

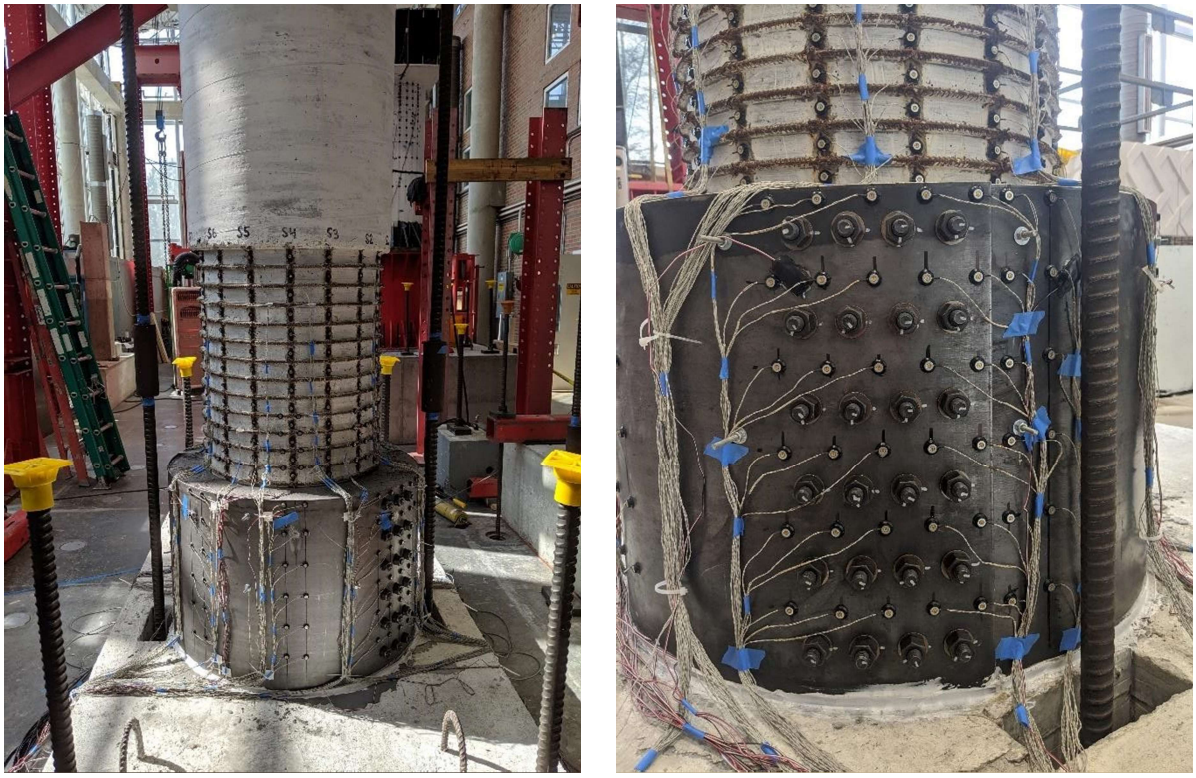

Figure 3.23: Optotrak LEDs Placed on Specimen.

3.4.2 Strain Gauges

For steel that is not viewable from outside (i.e. within the concrete), it is impossible to use the Optotrak system. Instead electrical resistance strain gauges must be used to measure steel rebar strains within the repair. Previous research (Krish, 2018) showed that strain gauges applied to the original column bars within the repair rarely provided useful data. This was primarily due to the bar strains exceeding the capacity of the gauges because the gauges are typically only reliable until yielding which was exceeded early in the test. Because of this, strain gauges were only applied to the longitudinal repair bars and the steel sleeve, which have a much lower strain demand. Examples of the locations of these gauges are shown in Figure 3.24, highlighted by red arrows.

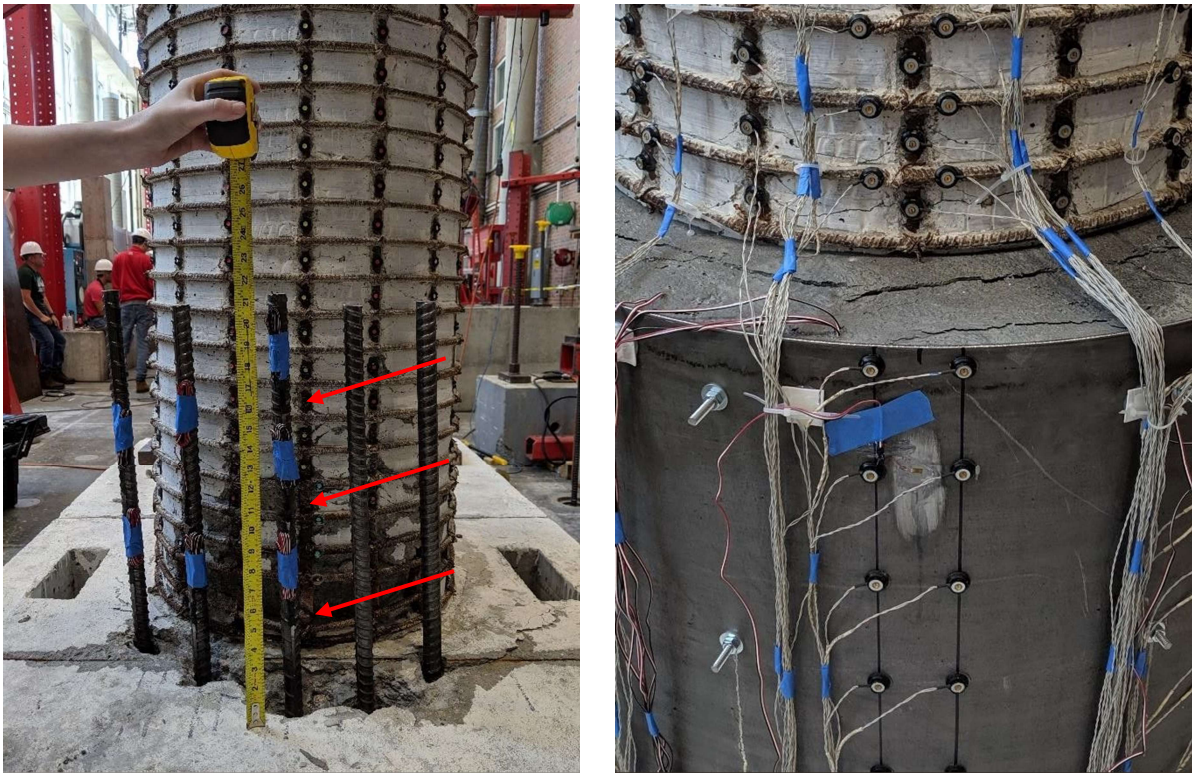

Figure 3.24: Location of Strain Gauges on Repair Bars (left) and Steel Sleeve (right).

3.4.3 String Pots

String potentiometers were used to measure the column displacement at the center of lateral loading. One was attached to the center and served as the primary recorder of column displacement, and a second was attached to the corner of the cap beam to check that the column was not twisting due to any torsional effects. This was not found to be significant in any of the tests.

Chapter 4: Test Summaries

In this chapter the experimental repair tests will each be thoroughly discussed. Since each repair aimed to improve the performance compared to the previous test, this chapter is presented in chronological order. Each repair's section begins with an explanation of the objectives for that repair, followed by a description of the damaged column and the repair. Next the progression of the repair test is recounted, after which the global and local responses of the repair are analyzed and conclusions drawn. After the tests are described, the final section compares their results to demonstrate the improvements and effectiveness of each repair.

4.1 Repair #1

4.1.1 Primary objective

As already mentioned, the previous research by Krish (2018) used a welded connection for the steel sleeve in the repair. This was done using two semi-circular steel sheets, which were cold rolled to the appropriate diameter, placed around the column, and then welded together. This method worked well for 4 of the 5 tests but resulted in an early failure of test #5 due to the sleeve rupturing around the weld before the column reached its desired displacement capacity. This led to restrictions on how the sleeve should be cut and how the edges should be prepared before welding can be done. A combination of this, and the recognition that welding the two steel sleeves together may not always be an option in the field (due to weather or accessibility) led to the realization that mechanically fastening the steel sleeve may be a more reliable method of connecting the two steel sheets. Because of this, the objective for this repair was to replace the welded connection of the sleeve with a mechanically bolted connection.

4.1.2 Damaged Column and Repair

The use of a bolted connection is in-line with the repair philosophy of only using conventional materials that are readily available and serves to keep this a rapid repair. While designing this connection, it was realized that the force demand for the sleeve was not known, so a conservative design was chosen to inhibit a connection failure. To do this, it was assumed that the sleeve would yield up the entire height, which is easily equated to a concentric point load at the center of the sleeve height. This allowed for a connection design to be found where bolt bearing, bolt shear, and sleeve rupture would have a higher capacity than sleeve yielding. This design led to the use of 6 rows and 3 columns of ½" diameter ASTM F3125 Grade A325 bolts (which can be seen in Figure

4.2). The holes for these bolts were inadvertently oversized and drilled to 5/8” instead of 9/16”. As a note, the conservative design for this repair was later refined, and the updated design is described in Section 5.3.

The column repaired in this test was severely damaged, having 7 longitudinal bar fractures along with a substantial loss in core concrete. The repair was designed following the steps described in Section 5.1. The damaged state of the column is shown in Figure 4.1, and the repaired cross section and bolt configuration are shown in Figure 4.2. The properties for the original column, comparison column, and repair are summarized in Table 4.1.

Figure 4.1: Damaged Column for Repair #1 on the North (left) and South (right) sides.

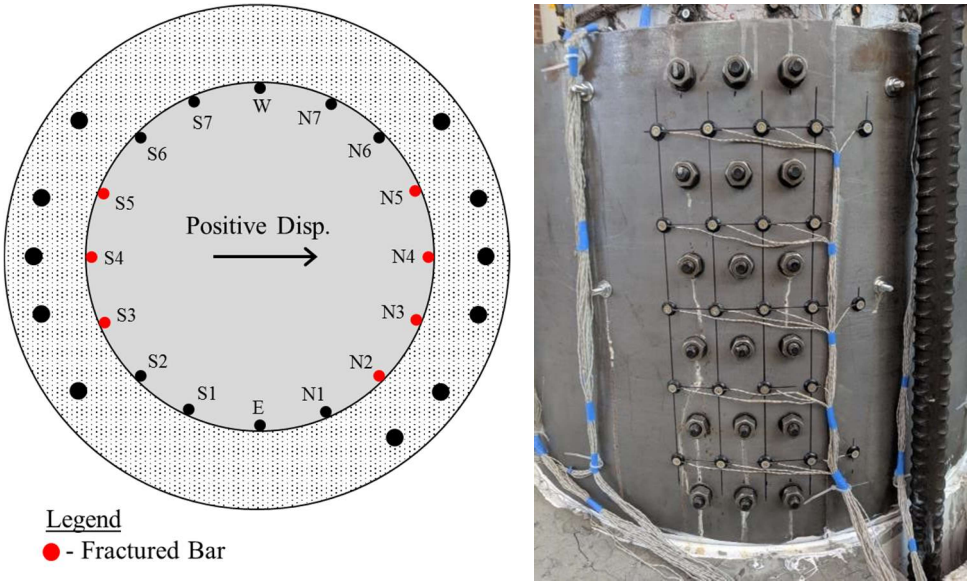

Figure 4.2: Repair Cross Section and Bolt Configuration for Repair #1.

Table 4.1: Column and Repair Properties for Repair #1.

	Original Column	**Comparison Column**	**Repair**
Column	Manhard Test 4	Barcley Test 1	Repair #1
Geometry	Height = 8 ft Diameter = 24 inches	Height = 8 ft Diameter = 24 inches	Height = 22 inches Diameter = 32 inches
Longitudinal Steel	16 #6 (ρ_l = 1.6%) f_y = 84.8 ksi ε_y = 0.37% f_u = 106.0 ksi ε_u = 9.6%	16 #6 (ρ_l = 1.6%) f_y = 83 ksi ε_y = 0.29% f_u = 110 ksi ε_u = 10.4%	11 #8 bars f_y = 84.0 ksi ε_y = 0.35%
Transverse Steel	#3 Spirals @ 2.0" (ρ_s = 1%) f_y = 79 ksi ε_y = 0.48% f_u = 117 ksi ε_u = 7.6%	#3 Spirals @ 2.0" (ρ_s = 1%) f_y = 79 ksi ε_y = 0.48% f_u = 117 ksi ε_u = 7.6%	10-gauge A36 Steel Connected by 18 ASTM A325 bolts with ½" diameter
Concrete/Grout Strength	f'_c = 6.51 ksi	f'_c = 5.77 ksi	f'_c = 7.85 ksi
Axial Load	ALR = 10.5% P = 311 kips	ALR = 5% P = 130 kips	ALR = 5% P = 147 kips
Load Path	Δy' = 1.025 inches Δy = 1.34 inches	Δy' = 0.78 inches Δy = 1.05 inches	Δy' = 1.025 inches Δy = 1.34 inches
Bar Fractures	N2, N3, N4, N5, S3, S4, and S5	N3, N4, N5, S3, S4, and S5	S6

4.1.3 Test progression

For this test, the column was subjected to the same displacement history as the original column test where Δy'= 1.026 in. and Δy = 1.34 in. Cracking of the grout at the top of the repair was initiated at the very first cycle (1/4 Fy') as shown in Figure 4.3.a. When first yield (Fy') was reached, this crack had already become larger than the crack width ruler (>0.060 inches) (Figure 4.3.b). More cracks formed and all continued to widen, with minimal to no damage visible on the column above the repair on both sides of the column (Figure 4.4.a). At the end of the cycles at ductility 2, the loose grout was removed from the top of the repair (Figure 4.4.b). Since the three most extreme bars on each side were fractured, and likely debonded by now, there was still only minimal cracking or crushing of the concrete around these bars. However, during the first cycles at ductility 4, concrete crushing and cracking was found at the most extreme nonfractured bars (S2, S6, N1, and N6) which can be seen in Figure 4.5. Notably, the crushing and cracking primarily occurred just below the top of the repair,

as opposed to above the repair as expected. By the final cycles at ductility 4, buckling was observed for the S2, S6, N1, and N6 bars. In the 1st of the ductility 5 cycles, each of these bars were further buckled, and on the 2nd cycle, S6 fractured during the positive displacement, and N6 fractured on the negative displacement. At this point, the test was concluded. Figure 4.6 shows the repaired column's maximum displacement.

During the test, it was observed that the plates were slipping relative to each other. This was most noticeable at the base where the silicone was used to seal the sleeve and by the end of the test a visible gap had formed which is shown in Figure 4.7.

(a) (b)

Figure 4.3: Cracking of the Top of Repair Grout at (a) ¼ F_y' and (b) F_y'.

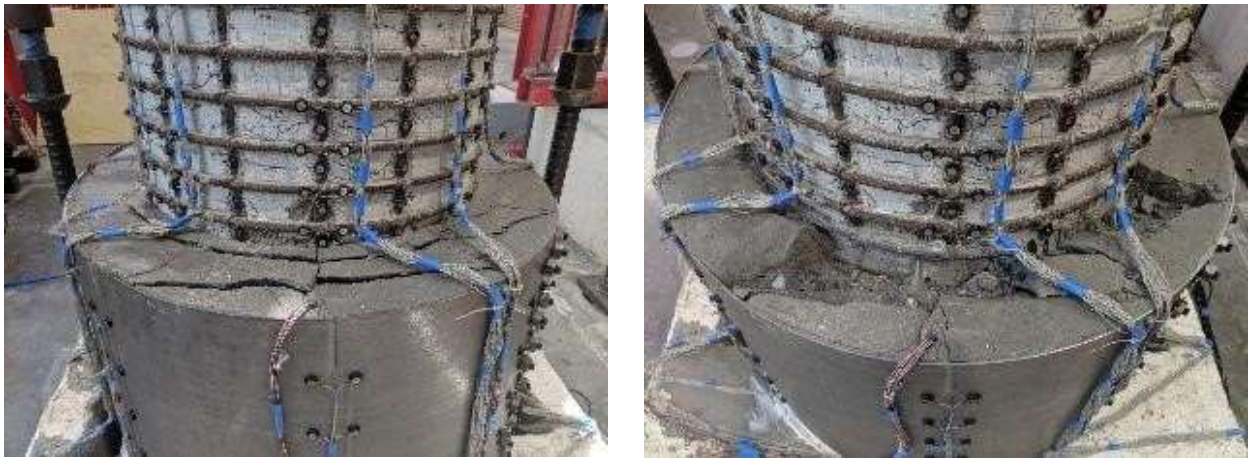

(a) (b)

Figure 4.4: Cracking of the Top of Repair Grout (a) Before Removal of Loose Grout and (b) After.

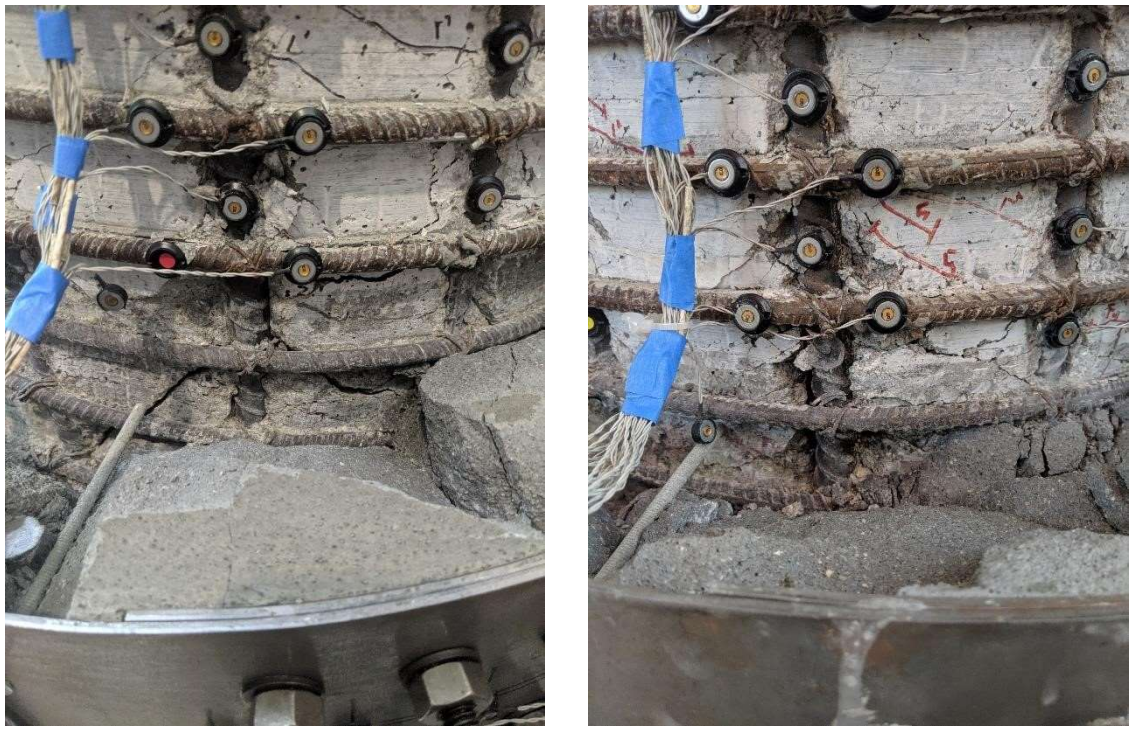

(a) (b)

Figure 4.5: Concrete (a) cracking and (b) crushing visible during the 1st cycle at ductility 4.

Figure 4.6: Maximum displacement and final cycle of test.

Figure 4.7: View of silicone sealant where gap formed due to plates slipping.

4.1.4 Global response

Although the repair test was forced to use a smaller axial load than the original column test (discussed in Section 3.1.3), data from a column with the same axial load and detailing was available for comparison. In Figure 4.8, the global response of Repair #1 is compared with the equivalent column. From Figure 4.8, it can be seen that the repaired column was capable of reaching the same displacement as the comparison column, but the repaired column exhibits a softening behavior after a displacement of 4 inches, which is not seen in the original column test. This behavior has been observed in previous research using this repair technique and is attributed to debonding of fractured bars within the repair.

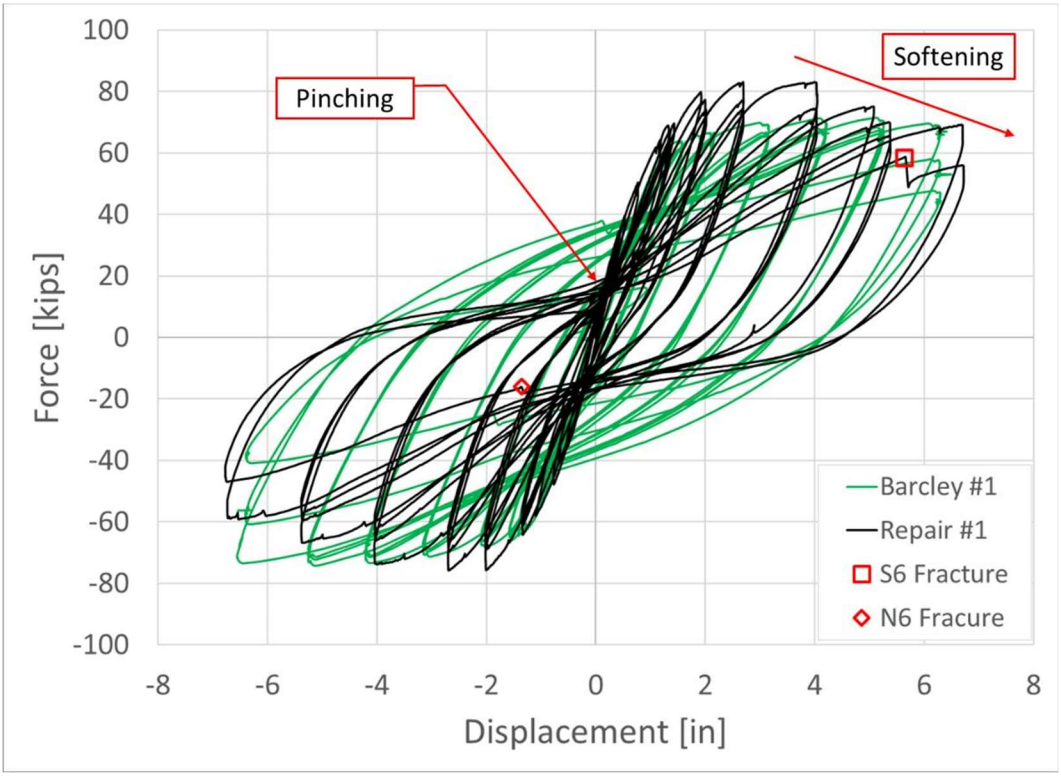

Figure 4.8: Force vs. Displacement Response of Repair #1.

Aside from the softened response, another difference in the repaired response is the pinching behavior near zero displacement. While this too was observed in prior repair tests containing fractured bars, this repair appears to be significantly more pinched than what was seen using a welded connection for the steel sleeve. This is concerning because it implies that the repaired column dissipates less energy which would indicate that it has less seismic resistance. Since bar debonding and column-socket action are attributed to causing the

pinched response, it can be implied that the anchorage of the fractured bars was weaker in this repair. This can be attributed to the slipping of the plates at the bolted connection, as this would limit the confining stressed developed.

4.1.5 Local Response

Using Optotrak data from LEDs on separate plates at the connection, plate slip can be monitored throughout the duration of the test. An example of two of these LEDs is shown on the left of Figure 4.9, and on the right is a plot of the length change between the two markers vs. the top displacement of the column. This data shows that the first push of the early cycles would cause the plates to slip, and there was almost no rebound. Eventually (at around 3 inches of displacement), enough of the bolts began to bear on the holes and there is minimal subsequent increase in slip. While some amount of this change in length would be due to the strain in the sleeve, it is believed that this would be minimal until the bolts were bearing on the holes. With no strain developing in the sleeve, the confining stresses from the sleeve would be minimal, which would diminish the anchorage effect of the fractured bars within the repair. While the oversized holes would have worsened this behavior, prevention of plate slip completely would theoretically lead to a behavior similar to a welded connection where there would be no slip.

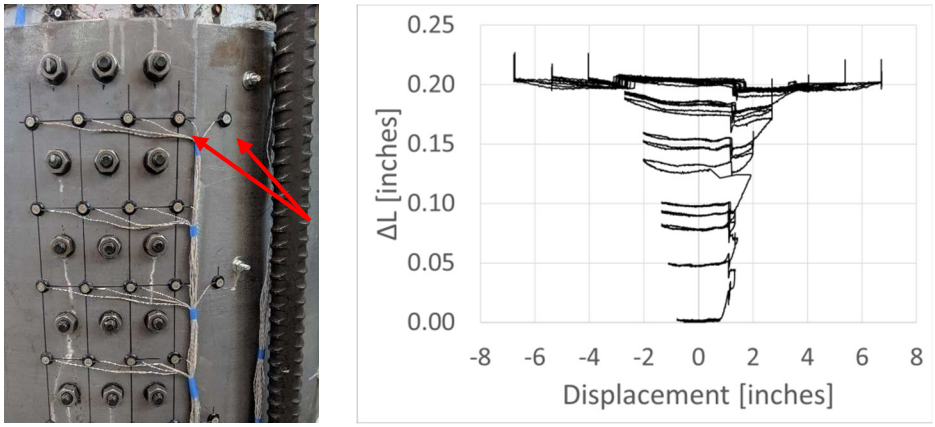

Figure 4.9: Slip of Plates in Repair #1.

The longitudinal bars of the column were also instrumented with LEDs and can measure strains throughout the test. To better understand the use of this, the strains of the S6 bars are analyzed first. This bar was not fractured during the original column test and was one of the next most extreme bars in the repair test when ignoring bars that would have debonded. As before, the left side of Figure 4.10 shows the two LEDs used, and this time the right side displays the strain in the bar vs top column displacement. As a note, the bottom LED was not used because it was hidden from the camera in the middle of the test and did not record any data. The

strain vs. displacement response of S6 exhibits the behavior typical for a longitudinal column bar that is well anchored, with increasing displacement corresponding to an increase in strains until buckling occurs when the bar is in compression. As the bar continues to buckle further and further, eventually it ruptures in tension, highlighted by the red x.

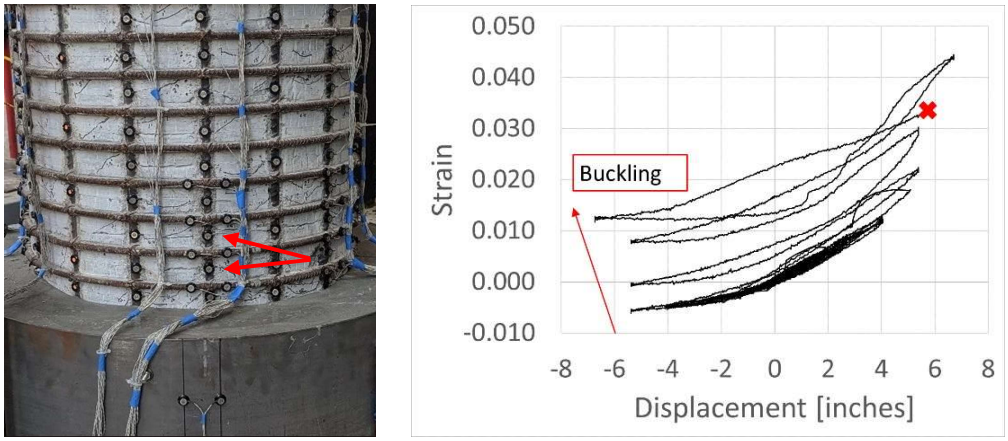

Figure 4.10: Strain in Longitudinal Bar S6.

With an understanding of what the strain history in a longitudinal bar typically looks like, the strains in the N4 and S4 bars will now be analyzed. These are the most extreme bars on each side and were expected to debond during the repair test because they had fractured during the original column test. From Figure 4.11 it can be seen that the initial behavior of the bars is similar to the well anchored bar analyzed previously, but once the column reaches a displacement of around 2 inches, the strains begin to drop off. This indicates that the bar has debonded and is no longer sustaining any load or contributing to the repaired column's response. While this was expected, the reduction in confinement from slip of the plates is believed to have worsened this, causing the bars to debond earlier and at a lower strain than if the plates had not slipped.

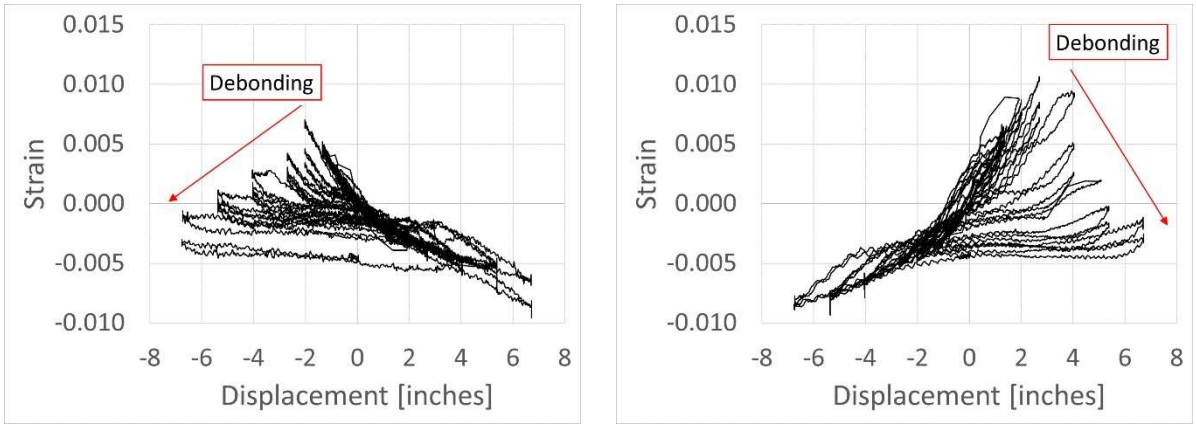

Figure 4.11: Strain in Longitudinal Bars N4 (left) and S4 (right).

4.1.6 Conclusions

From this test, it appears that a bolted connection of the two steel sleeves is a viable option instead of welding. The repair successfully relocated the plastic hinge and restored the column's load and displacement capacity; however, the pinched response of the column could indicate a lowered seismic resistance. With the pinching behavior being largely attributed to longitudinal bars debonding, better anchorage for these bars is desirable. It is believed that the slipping of the plates would hinder the confining stresses of the sleeve from developing until the bolts were bearing on the bolt holes. If slip could be prevented, anchorage of the fractured bars should be improved, which would in turn improve the repaired column's response. To further investigate this, the next repair test will aim to prevent slip via a pre-tensioned bolted connection. If successful, the repair is expected to behave more like a welded sleeve connection, which would improve the pinching behavior in the repaired column's global response.

4.2 Repair #2

4.2.1 Primary objective

As mentioned, the objective of this repair was to prevent slip at the bolted connection through a pre-tensioned bolt connection. Through pre-tensioned bolts, the two plates will be clamped together which will develop a frictional force between them that serves to resist slip. If slip can be completely prevented, the sleeve will be capable of providing more confinement to the repair than the previous test and should behave as if the sleeve was welded together. A comparison between this repair and Repair #1 can be done to determine the effectiveness and necessity of the pre-tensioned connection.

4.2.2 Damaged Column and Repair

A calibrated torque wrench was used to apply the pre-tension of 250 ft-lbs to the bolts. Although it is known that this is not the most reliable method of pre-tensioning, due to the relationship between torque and pre-tension being heavily dependent on friction of the bolts, it was deemed acceptable because any amount of pre-tensioning would be an improvement compared to the previous repair. The method used for determining the size and number of bolts to prevent slip is given in Section 5.4. Following this, it was found that keeping the same pattern of 6 rows and 3 columns of bolts but using larger 5/8" diameter ASTM F3125 Grade A490 bolts should prevent plate slip.

The column repaired for this test was nominally identical to the previous column aside from the longitudinal bars coming from a different steel mill. The original column test resulted in 5 bars being fractured and a significant amount of concrete spalled off. Although Repair #1 contained 7 fractured bars, the south sides of the columns from both tests contained 3 fractured bars and had 5 repair bars. This gives an optimal location for comparison of local strains between the two tests. The damaged state of the column prior to repair as well as the repaired cross section are shown in the following Figures 4.12 and 4.13. The properties for the original column, comparison column, and repair are summarized in Table 4.2.

Figure 4.12: Damaged column for Repair #2 on the North (left) and South (right) sides.

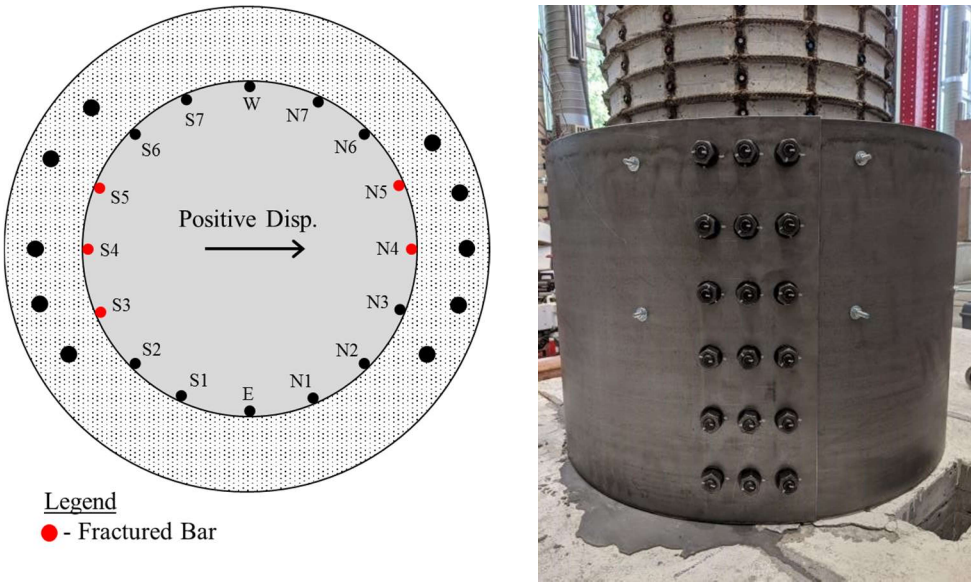

Figure 4.13: Repair cross section and bolt configuration for Repair #2.

Table 4.2: Column and Repair Properties for Repair #2.

	Original Column	**Comparison Column**	**Repair**
Column	Manhard Test 3	Barcley Test 1	Repair #2
Geometry	Height = 8 ft Diameter = 24 inches	Height = 8 ft Diameter = 24 inches	Height = 22 inches Diameter = 32 inches
Longitudinal Steel	16 #6 (ρ_l = 1.6%) f_y = 85.9 ksi ε_y = 0.38% f_u = 113.5 ksi ε_u = 10.3%	16 #6 (ρ_l = 1.6%) f_y = 83 ksi ε_y = 0.29% f_u = 110 ksi ε_u = 10.4%	10 #8 bars f_y = 84.0 ksi ε_y = 0.35%
Transverse Steel	#3 Spirals @ 2.0" (ρ_s = 1%) f_y = 79 ksi ε_y = 0.48% f_u = 117 ksi ε_u = 7.6%	#3 Spirals @ 2.0" (ρ_s = 1%) f_y = 79 ksi ε_y = 0.48% f_u = 117 ksi ε_u = 7.6%	10-gauge A36 Steel Connected by 18 pretensioned ASTM A490 bolts with 5/8" diameter
Concrete/Grout Strength	f'_c = 6.87 ksi	f'_c = 5.77 ksi	f'_c = 8.82 ksi
Axial Load	ALR = 10.0% P = 311 kips	ALR = 5% P = 130 kips	ALR = 5% P = 147 kips
Load Path	Δ_y' = 1.065 inches Δ_y = 1.35 inches	Δ_y' = 0.78 inches Δ_y = 1.05 inches	Δ_y' = 1.025 inches Δ_y = 1.34 inches
Bar Fractures	N4, N5, S3, S4, and S5	N3, N4, N5, S3, S4, and S5	N2, N3, N6, S2, S6

4.2.3 Test progression

This repair was subjected to the same displacement history as Repair #1. Cracking on the top of the repair again occurred very early in the test, with a separation of the column from the repair grout being noticed at half of first yield (1/2 Fy') which can be seen in Figure 4.14.a. More cracks formed and widened throughout the early ductility cycles, growing to larger than a tenth of an inch after the first cycle at ductility 1 (Figure 4.14.b). During the cycles at ductility 1.5, tension cracks were clearly visible on the column (Figure 4.15.a) which was not observed during the first repair test. Keeping consistent with Repair #1, after the conclusion of the ductility 2 cycles, loose concrete was removed from the top of the repair, which is shown in Figure 4.15.b.

Nearing the end of the test, the north side of the column had a large amount of concrete crushing, while the south side had fairly little. A comparison of the concrete crushing on the two sides is shown in Figure 4.16.

This is likely due to the north side having less initial damage than the south (2 fractured bars vs 3). Buckling was first observed in N3 during the final cycle at ductility 4. On the first push cycle of ductility 5, N2 and N6 also buckled. When pulling back in the opposite direction N3 fractured and S2 and S6 buckled. In the second cycle at ductility 5 each of the buckled bars were further buckled but did not fracture. For the third cycle S2, N2, and N6 fractured. Though the column had completed all three cycles at ductility 5, the column was pushed one more time to fracture S6. At a displacement of 7.45 inches, S6 fractured and the test was concluded. A progression of buckling to fracture is shown in Figure 4.17 for N6, with other bars showing similar damage progression. Lastly, Figure 4.18 shows the column's displacement during the final cycle of ductility 5.

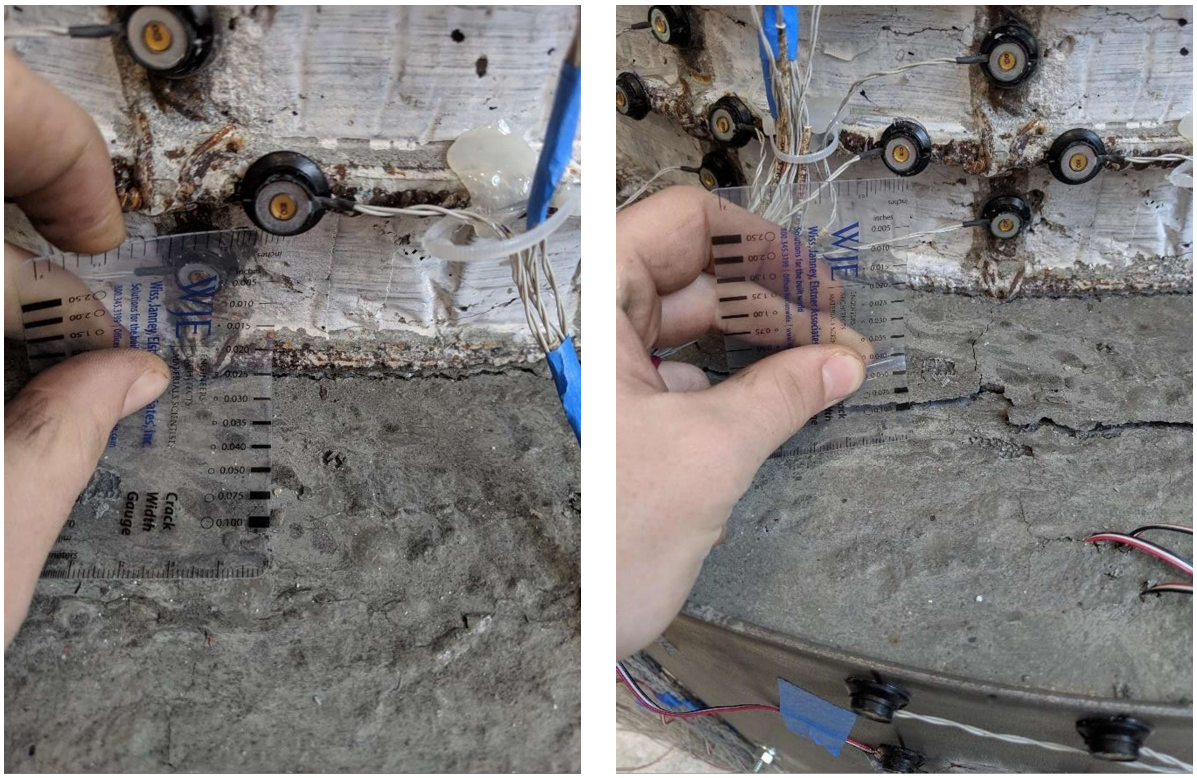

(a) (b)

Figure 4.14: Cracking of the top of repair grout at (a) ½ F_y' and (b) ductility 1.

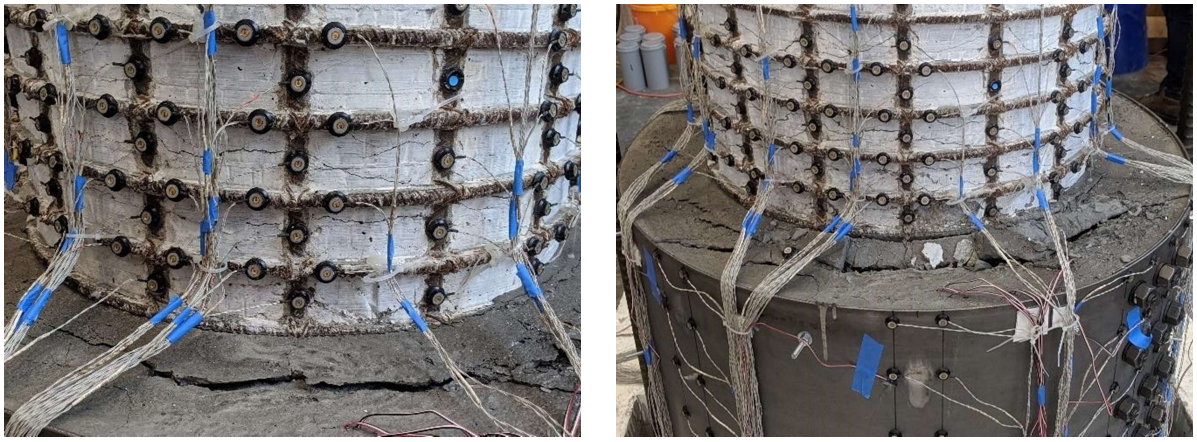

(a) (b)

Figure 4.15: (a) cracking on column and (b) removal of loose grout.

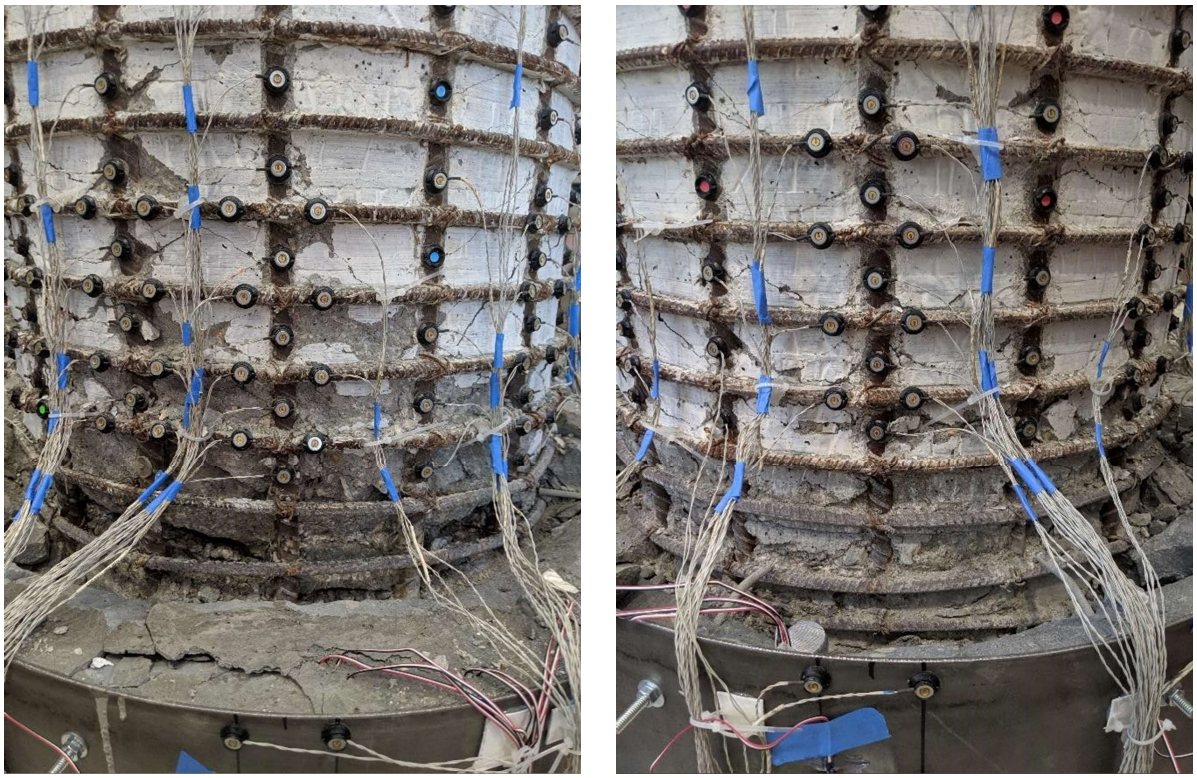

(a) (b)

Figure 4.16: Damage comparison during ductility 5 on the North (left) and South (right) sides.

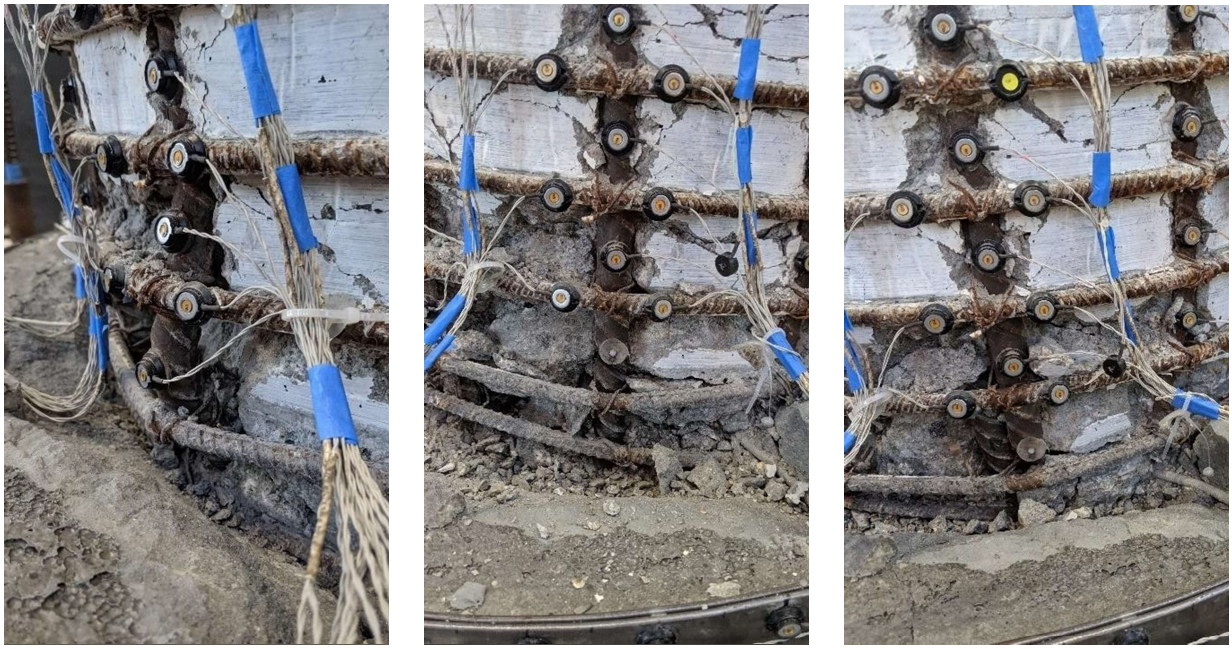

Figure 4.17: Final cycles of N6 showing (left) buckling, (middle) fracture, and (right) next compression cycle.

Figure 4.18: Column displacement during final cycle of ductility 5.

4.2.4 Global response

In Figure 4.19, the global response of Repair #2 is compared with the response of an original column test. Although the repaired column still exhibits the pinching behavior, this appears to be more consistent with the level of pinching observed in previous research using a welded steel connection.

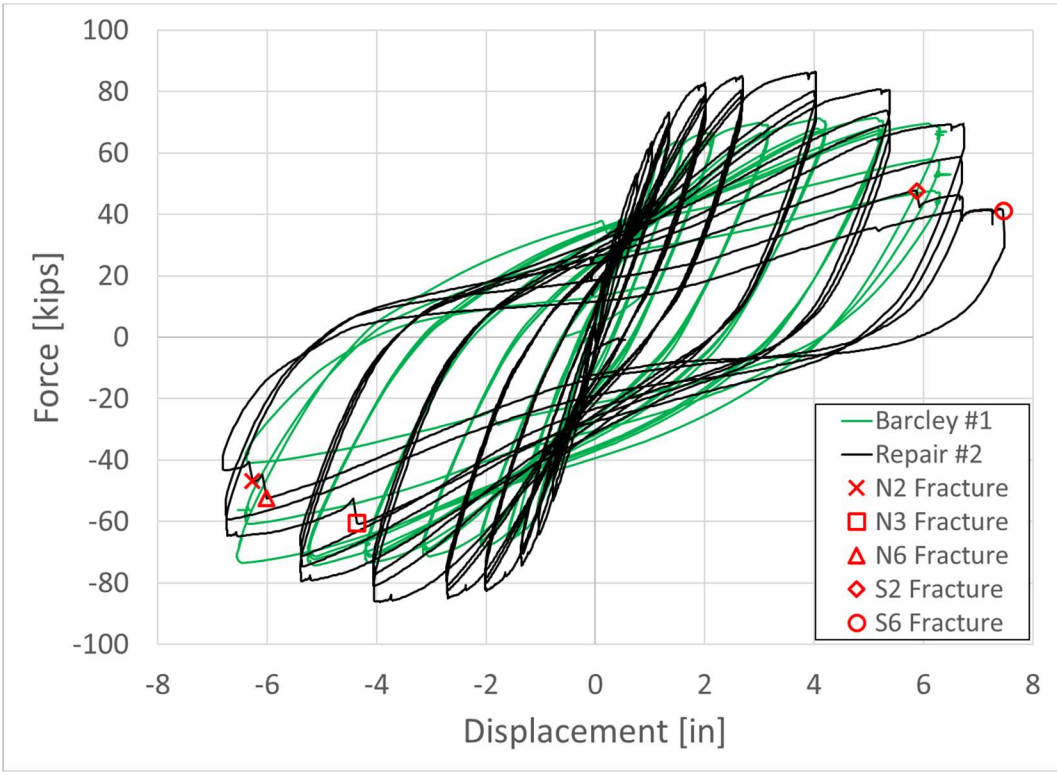

Figure 4.19: Force vs. Displacement Response of Repair #2.

To evaluate the effectiveness of the pre-stressed bolts, Figure 4.20 compares the response of Repair #1 to Repair #2. It is clear from Figure 4.20, especially at the early ductilities that the pinching behavior has been improved.

Looking at the response of the columns in the negative direction, there is a large difference in force which is attributed to the Repair #1's North side having more damage than Repair #2's North side. As previously mentioned, both Repair #1 and Repair #2 contained 3 fractured bars and was repaired with 5 bars on the south side, so this side serves as the optimal side to compare the two repairs and evaluate the effectiveness of the pre-stressed bolts.

Focusing on the positive displacements, when the South side would be in tension, it is clear that Repair #2 was slightly stiffer than Repair #1 up to the first cycle at 5.4 inches, however after this the response is almost

identical. This difference in the beginning is believed to be due to the better confinement provided to the repair from the pre-tensioned bolts preventing slip in the plates. By the end of the test though, the fractured bars would have debonded which would lead to the responses becoming similar. This hints that while confinement can improve the anchorage of fractured bars, it has little effect once the bar has debonded and is no longer sustaining any load.

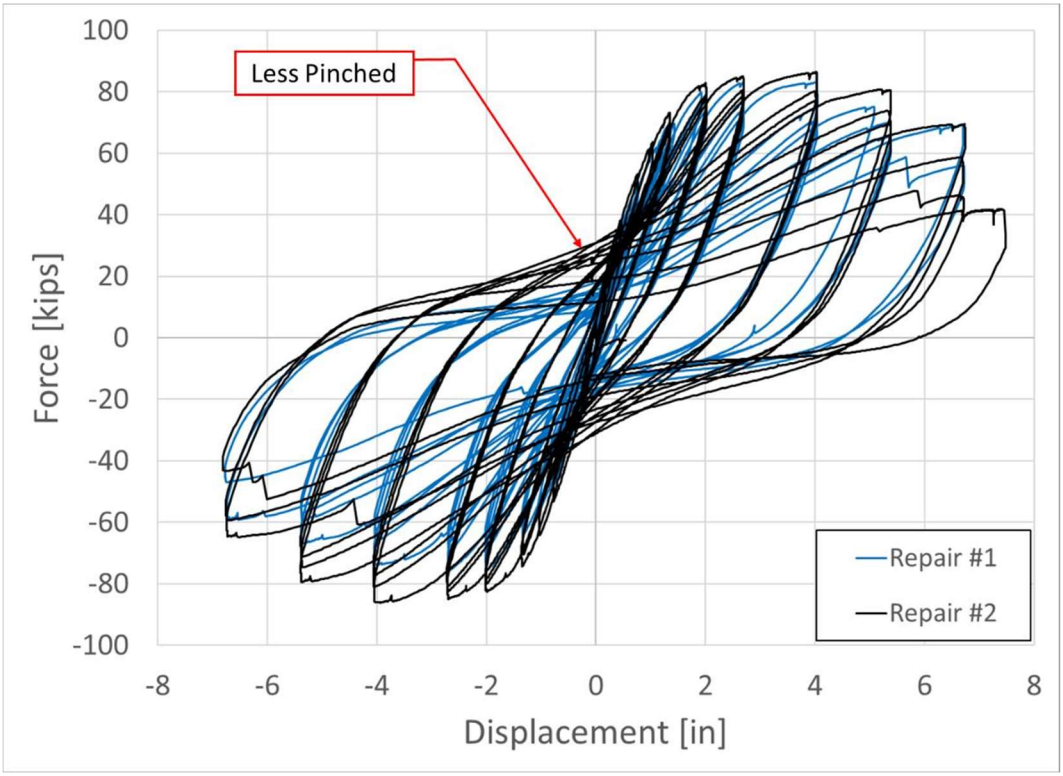

Figure 4.20: Comparison of Global Response in Repair #1 and Repair #2.

4.2.5 Local Response

Using the same process as Repair #1, slip of the steel plates can be monitored using Optotrak LEDs on the two plates. Figure 4.21 shows that the maximum change in length of the two markers was around 0.01 inches. For comparison, Repair #1 had a maximum change in length of 0.20 inches. With this information, we can conclude that the pretensioned bolts succeeded in minimizing the plate slip. It is worth reiterating that the values above are the change in length of the two LEDS. For this reason, the values are not a direct measure of slip because strain within the sleeve would also contribute to the change in length. In other words, a change in length of 0.01 inches does not imply that the plate slipped 0.01 inches, because steel strain would also be

included in this. Further analysis would need to be done to determine actual slip length, but it must be less than 0.010 inches which is negligible.

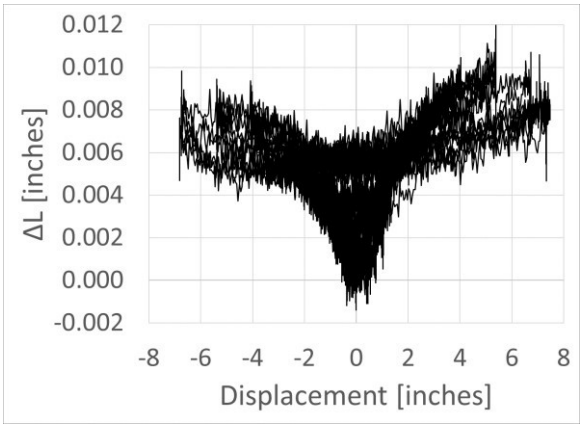

Figure 4.21: Slip of Plates in Repair #2.

Knowing that the pre-tensioned bolts succeeded in preventing slip of the plates, the next step is to compare the behavior of the fractured longitudinal bars that were expected to debond during this test. It was hypothesized that during Repair #1, lower confining forces led to poor anchorage and early debonding of the fractured bars. With the plate slip essentially eliminated, a direct comparison of the strains in the two repairs can be done to verify this hypothesis. Since the south side of both columns contained 3 fractured bars and had 5 repair bars, it gives an ideal location for comparison. Figure 4.22 shows the strain history of the S4 longitudinal bar for both Repair #1 and #2, with the peak strains pointed out.

From Figure 4.22, it is clear that the bar in this repair performed substantially better than the first repair. Not only was the peak strain in the bar increased from 0.01 to nearly 0.03, but the column displacement at which debonding began was delayed an entire ductility cycle. The strains in S3 and S5 show similar improvements. With the primary difference between the two repairs being the pre-tensioned bolts, this is evidence that slipping of the plates led to the fractured bars in Repair #1 debonding earlier than expected.

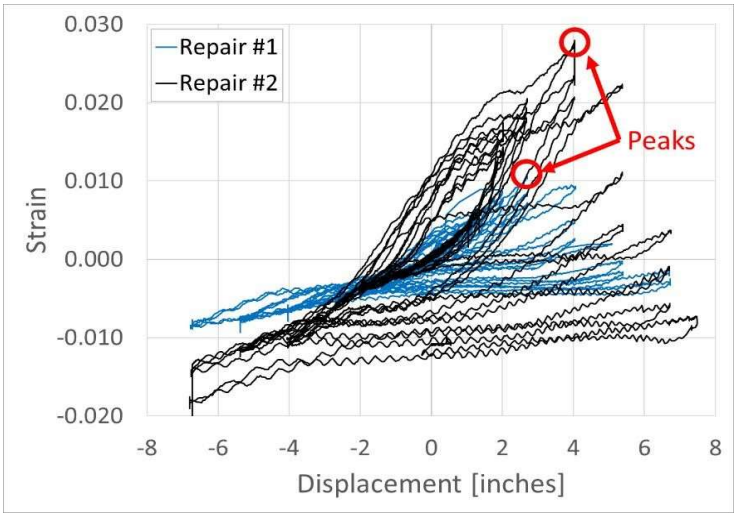

Figure 4.22: Comparison of Strain History of S4 in Repair #1 and #2.

In this repair, strain gauges were applied to the steel sleeve approximately 3.5 inches from the top of the sleeve which is shown on the left of Figure 4.23. Although the sleeve was instrumented with Optotrak markers, the data from these markers tends to show a lot of scatter at strains below 2000 με. To illustrate this, the right side of Figure 4.23 compares the strains obtained from Optotrak and a strain gauge on the extreme North side of the repair. While there appears to be an agreement between the two, the scatter from Optotrak makes it impractical to use. Although the data from Optotrak is not always this scattered, the strain gauges consistently give reliable data with minimal scatter at lower strains.

Focusing on the strain gauge data in Figure 4.23, the peak measured strain in the steel sleeve was 2934 με at a displacement of 5.38 inches. With the A36 steel used in this repair having an expected yield strain of 1500 με, the sleeve yielded during this repair test. This is concerning because yielding of the sleeve leads to plastic deformation. Similar to how plate slip reduced the confining pressure in Repair #1 at smaller displacements, plastic deformation at higher displacements would limit the confining pressure that can be developed. Although yielding of the sleeve was observed in the previous research using the welded connection for the sleeve, it was not considered to be detrimental to the repair's response.

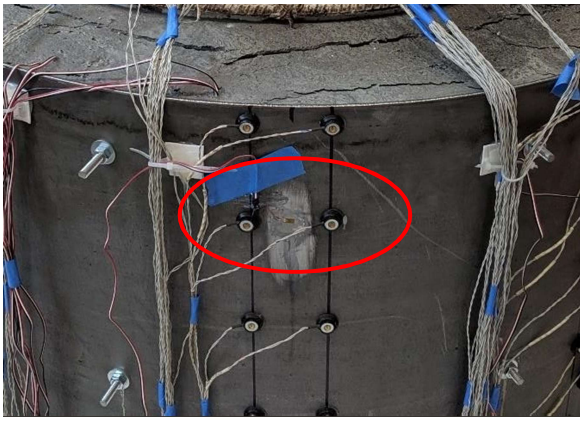

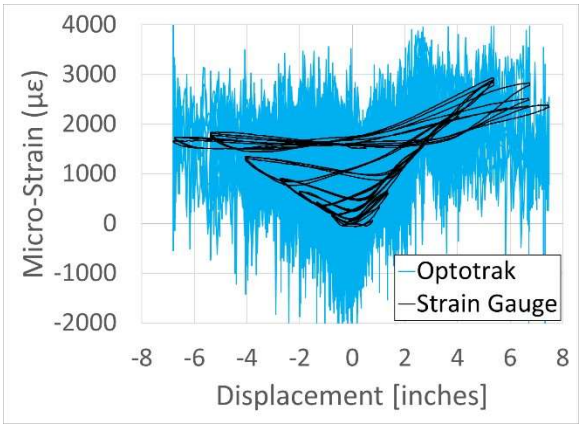

Figure 4.23: Location (left) and comparison of strains on the North side of the steel sleeve (right).

4.2.6 Conclusions

In this repair, slippage of the plates was successfully mitigated by using pre-tensioned bolts. The results of this test show substantial improvements to the column's seismic resistance, evident by the reduction in pinching in the global response of the column. Additionally, the fractured bars within the repair reached a higher peak strain and did not debond until much later in the test at larger column displacements. Knowing this, it can be concluded that the bolted connection with pre-tensioned bolts that prevent slip leads to a similar performance as when the welded connection was used.

This test highlighted the importance role that confinement plays in the anchorage of fractured bars within the repair. If the confining pressures can be further increased, it could be possible to fully anchor the bars throughout the entire duration of the test. If successful, this could eliminate the pinching behavior observed in the global response, which would maximize the repair's resistance to seismic loading.

4.3 Repair #3

4.3.1 Primary Objective

With Repair #2 showing that the welded connection of the steel sleeve could be replaced with a pre-tensioned bolted connection, the emphasis of Repair #3 was to further improve the global response of the repaired column. One clear shortcoming of this repair method thus far has been that if a bar was fractured during the original column test, it would eventually debond inside the repair and consequently not contribute to the repaired column's response. If these bars were sufficiently anchored, the strains would continue to increase

with larger column displacements and would be capable of exhibiting bar buckling and fracturing like what is seen in the original column tests.

The previous two tests highlighted the important role that confinement plays in the anchorage of these fractured bars. Although yielding of the sleeve has not been considered detrimental to the repaired column's response, it would limit the confining pressure that the sleeve can provide. For this reason, the objective of Repair #3 was to use a thicker steel sleeve with the aim of avoiding yielding and providing additional confinement to the repair. Furthermore, a method of improving the bond of these fractured bars was re-investigated to evaluate its effectiveness.

4.3.2 Damaged Column and Repair

The steel sleeve in the previous repairs was cold-rolled from a 10-gauge plate with a thickness of 0.1345 inches, which was the maximum thickness that could be rolled by the NC State machine shop. Although increasing the sleeve thickness required this work to be done elsewhere, there was now no reasonable limit to the sleeve thickness. Following the design process in Section 5.2, it was believed that a thickness of 0.25 inches would conservatively prevent yielding of the sleeve. Since doing this has the potential to increase the demand to the bolted connection, a 4th column of bolts was added to ensure that slip of the plates would be prevented. Using the Optotrak data from Repair #2, the assumed stress distribution along the height of the connection was determined to be triangular, reducing the assumed forces on the sleeve by 2.

In contrast with the previous two repairs, the column repaired in this test had transverse reinforcement of #3 spirals spaced at 1½ inches instead of 2 inches. The original column test resulted in three bars fracturing on each side of the column and a significant amount of concrete spalled off. This symmetrical damage state gave an ideal opportunity to investigate a method of improving the anchorage of the fractured bars.

In the previous work by Krish (2018), one method of doing this was removing the concrete around the perimeter of the fractured bars within the height of the repair. This concrete is likely damaged from the original column test and bar fracture, so removing it makes it so that the repair grout will completely surround the bars which should improve their anchorage. When this was done by Krish (2018), it was found to slightly improve the peak strain that a bar could sustain before it would debond, but ultimately the bar still debonded; so in the interest of keeping the repair rapid the technique was not recommended. With the larger sleeve thickness expecting to improve the anchorage of the bars, the effectiveness of this technique was re-evaluated by chipping the concrete out on the North side and leaving the South side as it was. The damage after the original column test is shown in Figure 4.24. A comparison of the two sides after chipping is included Figure 4.25, and the

repaired section along with the completed repair is shown in Figure 4.26. The properties for the original column and repair are summarized in Table 4.3. Further, to improve the accuracy in comparing the response of the North and South sides, the damaged column was straightened to eliminate any effects from residual drift.

Figure 4.24: Damaged column for Repair #3 on the North (left) and South (right) sides.

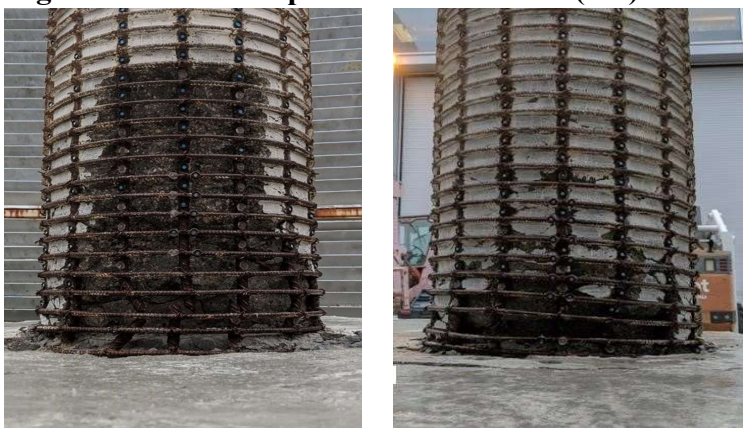

Figure 4.25: Repair conditions for the North (left) and South (right) sides.

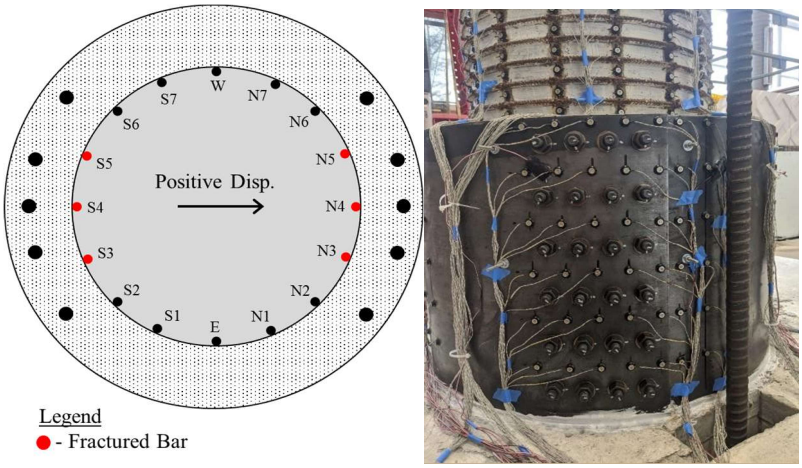

Figure 4.26: Repair cross section and bolt configuration for Repair #3.

Table 4.3: Column and Repair Properties for Repair #3.

	Original & Comparison Column	**Repair**
Column	Manhard Test 1	Repair #3
Geometry	Height = 8 ft Diameter = 24 inches	Height = 22 inches Diameter = 32 inches
Longitudinal Steel	16 #6 (ρ_l = 1.6%) f_y = 84.8 ksi ε_y = 0.37% f_u = 106.0 ksi ε_u = 9.6%	10 #8 bars f_y = 84.0 ksi ε_y = 0.35%
Transverse Steel	#3 Spirals @ 1.5" (ρ_s = 1.3%) f_y = 79 ksi ε_y = 0.48% f_u = 117 ksi ε_u = 7.6%	¼" A36 Steel Connected by 24 pretensioned ASTM A490 bolts with 5/8" diameter
Concrete/Grout Strength	f'_c = 5.62 ksi	f'_c = 9.33 ksi
Axial Load	ALR = 5% P = 127 kips	ALR = 5% P = 127 kips
Load Path	Δ_y' = 0.975 inches Δ_y = 1.29 inches	Δ_y' = 0.975 inches Δ_y = 1.29 inches
Bar Fractures	N3, N4, N5, S3, S4, and S5	N3, N4, N5, S2, and S6

4.3.3 Test progression

As with the two previous tests, cracking on the top of the repair occurred very early in the test, with a circumferential crack forming around the column at half of first yield (1/2 Fy') which can be seen in Figure 4.27. During the cycles at ductility 1, minor flaking was observed on both sides of the column and it became clear that there was substantially more cracking on the south side of the column when compared to the north side. Figure 4.28 gives a comparison of the two sides while they are in tension and the cracks are most visible. As the test progressed, typical tension cracking and concrete crushing was seen in the column above the repair.

Because there was a clear difference in damage for the two sides, comparison pictures were taken of the damage progression, beginning after ductility 1.5 (Figure 4.29) until the end of the test (Figure 4.34). For all of

these pictures, the left side shows the North side and the right side shows the South side. Additionally, these pictures were taken at the end of the ductility cycle when the column was brought to zero displacement unless otherwise noted.

In the second cycle of ductility 4, buckling was observed in the 3 extreme bars (N3 to N5) on the north side. On the next cycle the 2 next extreme bars (N2 & N6) buckled, but there was still no visible buckling on the south side (though it is possible it buckled below the top of the repair grout). For the very first pull at ductility 5, N3 fractured followed shortly by N4.During the next pull cycle, N5 fractured and for the first time buckling was observed in S2 and S6. It was at this point that the large crack seen on the left of Figure 4.33 was noted. After this, one more push cycle was completed which fractured S2 and S6, the column was brought back to zero displacement and the test was complete.

In summary, the south side performed similarly to what was seen in the previous test, but with slightly less damage. The three previously fractured bars (S3-S5) debonded, making the S2 and S6 the extreme bars that fractured in the repair test. The north side performance, however, was significantly different. For the first time ever, bars that had been fractured in the original tests (N3-N5) were fully anchored which led to them being re-fractured in the repair's relocated plastic hinge. It is worth emphasizing that not only did the North side have less damage to the repair, the relocated plastic hinge also formed completely above the top of the repair. For the previous two tests and the South side of this test, the relocated plastic hinge has appeared to be at or just below the top of the repair. It is believed that relocating the hinge above the repair is the ideal result for both capacity design and post-earthquake inspections.

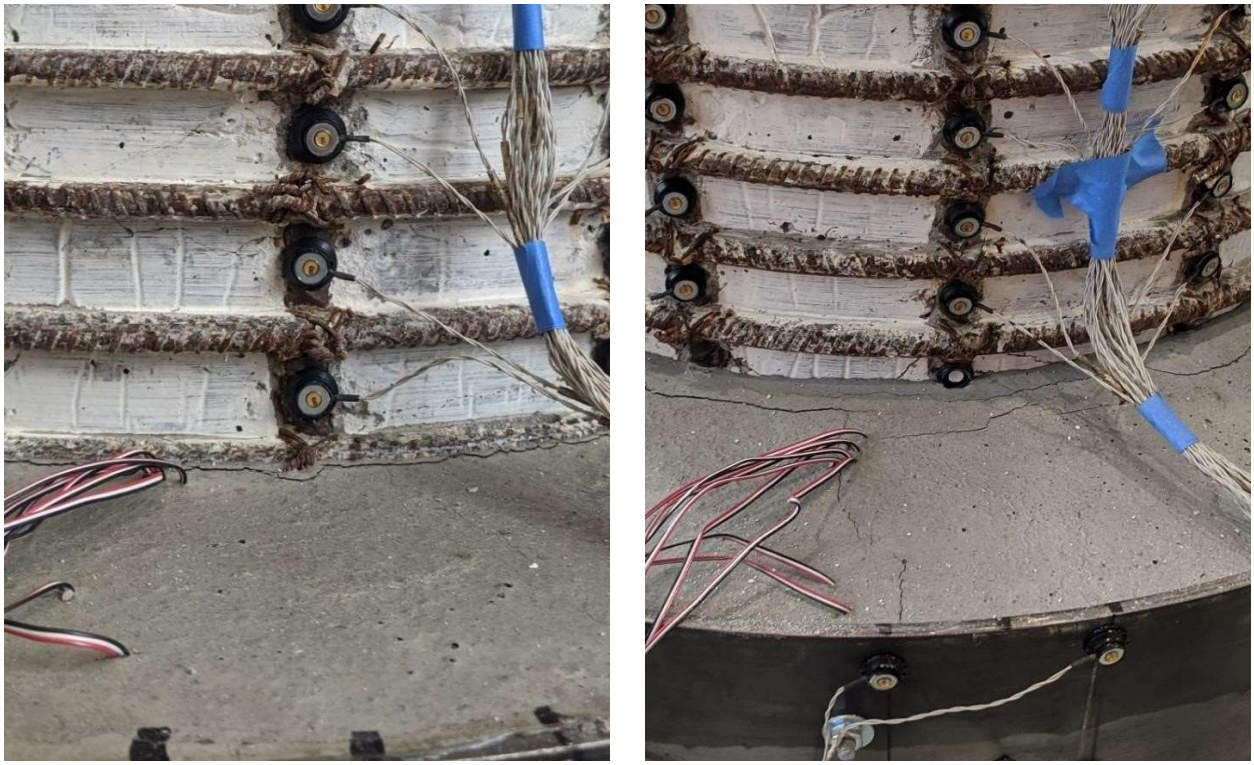

Figure 4.27: Circumferential cracks in grout at ½ F_y' for the North (left) and South (right).

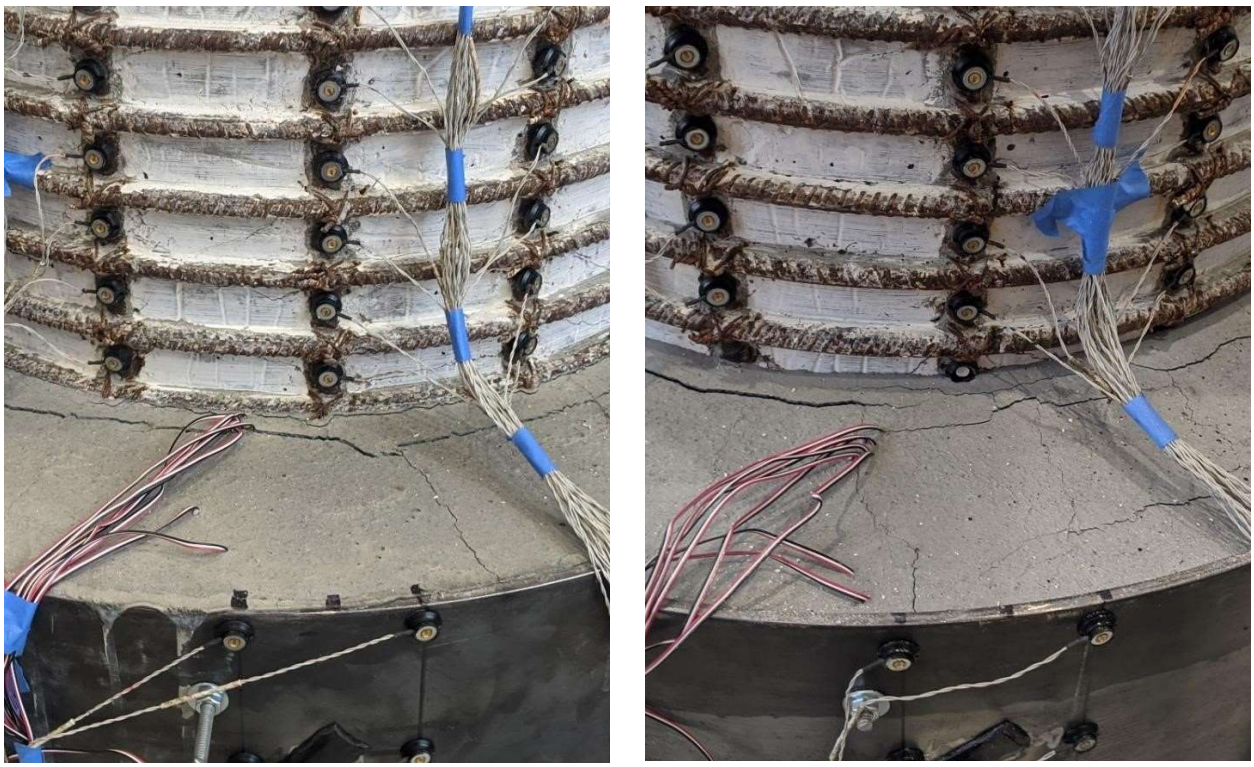

Figure 4.28: Comparison of cracking during ductility 1 for the North (left) and South (right).

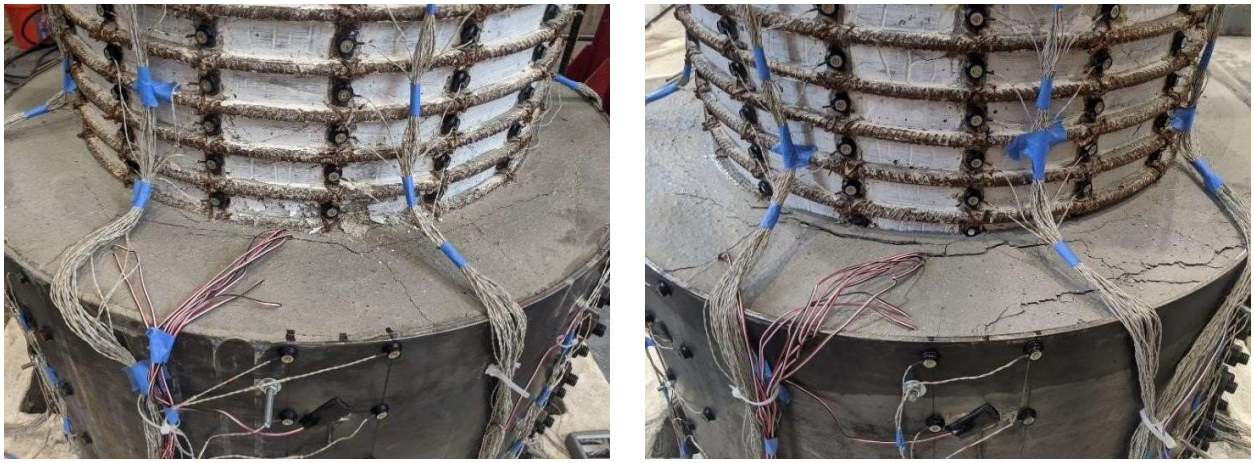

Figure 4.29: Damage Comparison after ductility 1.5 of the North (left) and South (right) sides.

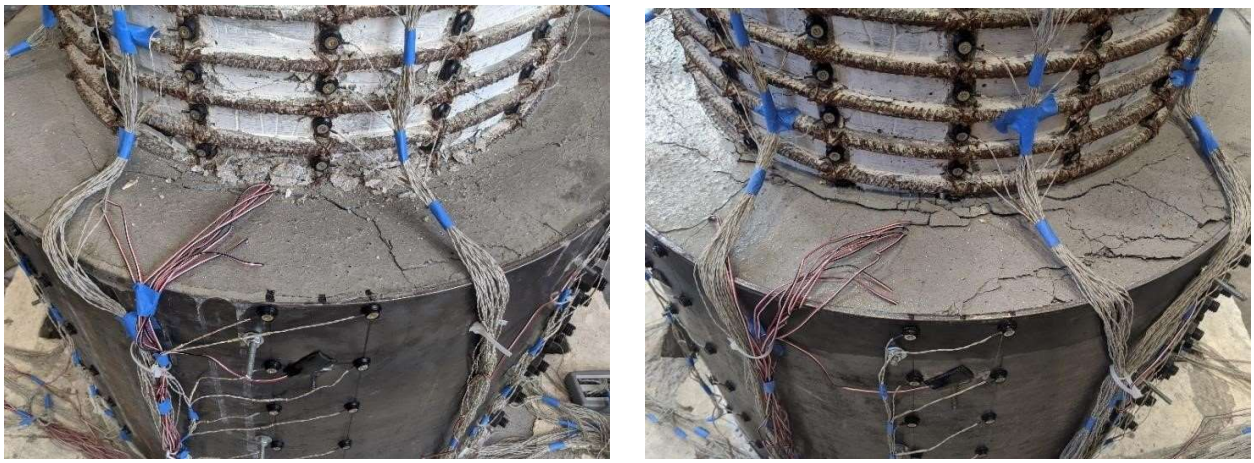

Figure 4.30: Damage Comparison after Ductility 2.

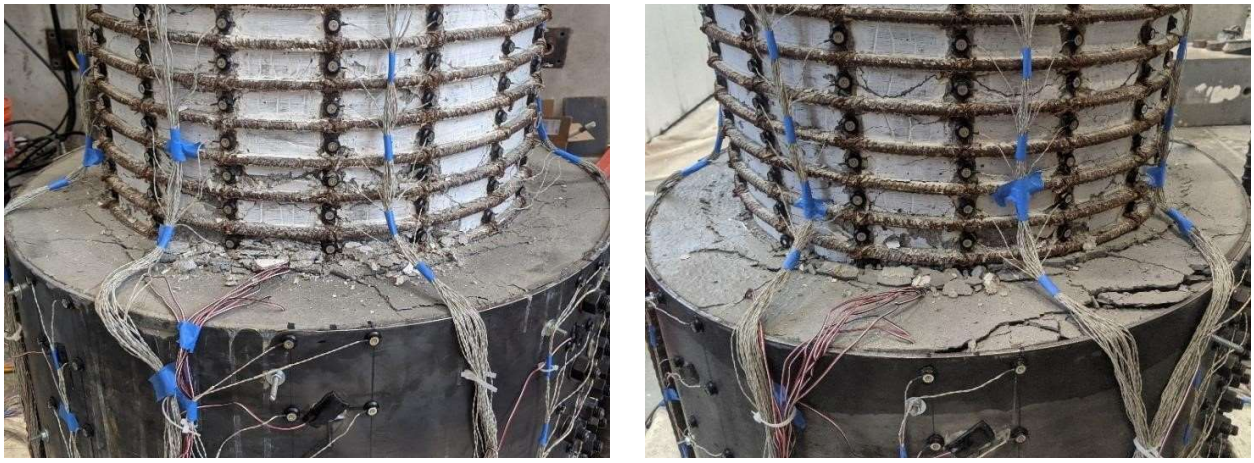

Figure 4.31: Damage Comparison after Ductility 3.

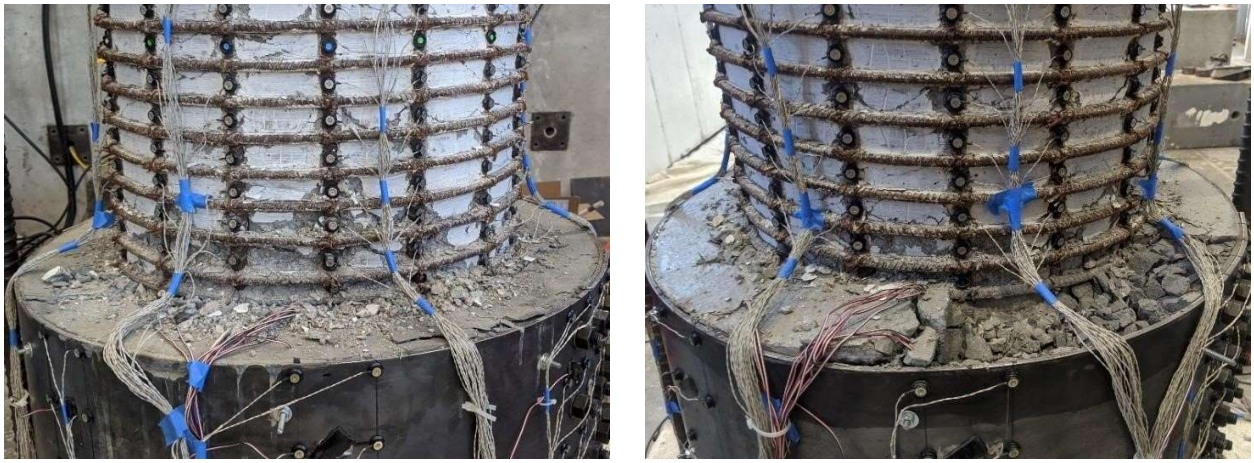

Figure 4.32: Damage Comparison after Ductility 4.

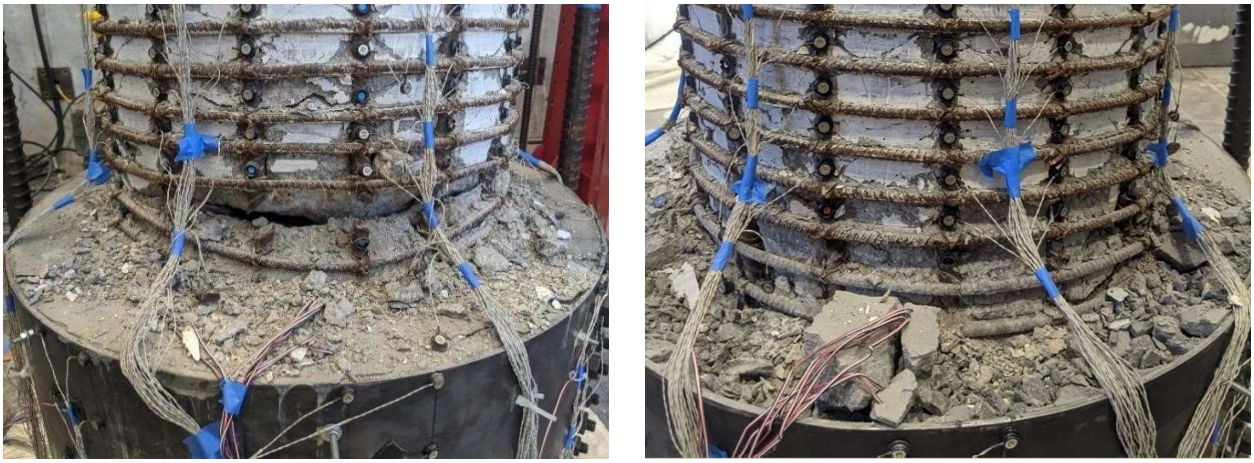

Figure 4.33: Damage Comparison during the final cycle of Ductility 5.

Figure 4.34: Damage Comparison after the test with loose grout removed.

4.3.4 Global response

Figure 4.35 compares the Force vs. Displacement response of the repaired column with the original column, from which a few observations can be made. Firstly, we can see that the repaired column did not reach the same ductility cycle as the original. The repaired column test ended after 2 cycles at ductility 5 (6.44 inches), whereas the original test completed all 3 cycles at ductility 5 and then one cycle at ductility 6. This is attributed to the repaired column having a shorter effective height, which is further discussed later in this section.

Secondly, it is clear that the repaired column does not exhibit the pinching behavior discussed in Chapter 2 until very late in the test. This is consistent with the results of Repair #2 and is again credited to the pre-tensioned bolts preventing slip of the plates. Especially during the lower ductility cycles, the repaired response follows a similar unloading and reloading curve which is ideal for the repair and indicates high seismic resistance. The primary difference in the curves is that the repaired column is much stiffer, which leads to the next observation.

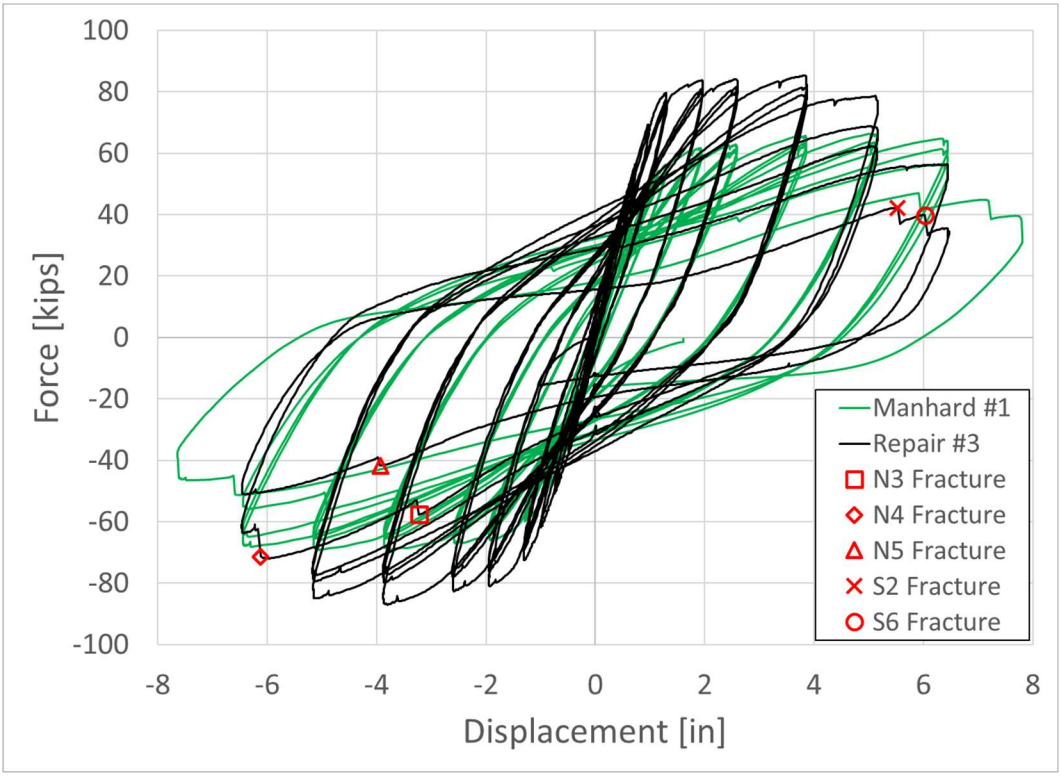

Figure 4.35: Force vs. Displacement Response of Repair #3.

When comparing the forces required to reach each displacement, it is obvious that the repair was much stronger up until bar fracture. This is primarily due to the repaired column having a shorter effective height. To illustrate this, a comparison of the moments in the plastic hinge vs displacement is shown in Figure 4.36. For the original column, the distance between the applied load and the top of the footing was 8 feet (96 inches). In the repaired column, the plastic hinge forms above the repair, which has a height of 22 inches and makes the effective height 74 inches. For this graph, the forces are multiplied by the effective heights of each column (96 and 74 inches for the original and repaired column, respectively). Theoretically, the main difference between these two are the boundary conditions at the base of the column with the original column connecting directly to the footing and the repaired column connecting to the repair. Ductility 5 is omitted from Figure 4.36 for clarity.

Figure 4.36 shows that the performance of the repaired column is very similar to that of the original column. Looking first at the positive displacement, we see that the response is almost identical until a displacement of 5.15 inches (ductility 4). This softening at 5.15 inches is attributed to the fractured bars having debonded and is further discussed in the following Section. In contrast, the negative displacement shows almost no softening, and the small amount is likely due to the socket-like anchorage of the repair being slightly weaker than a column-to-footing connection in the original test. Regardless, this curve still matches very well with the original column. It is worth noting that the original column test shows asymmetrical results with the negative displacement having higher strengths. A comparison of the positive moments of the original test and the negative moments of the repair test do not show the original column being stronger than the repaired column.

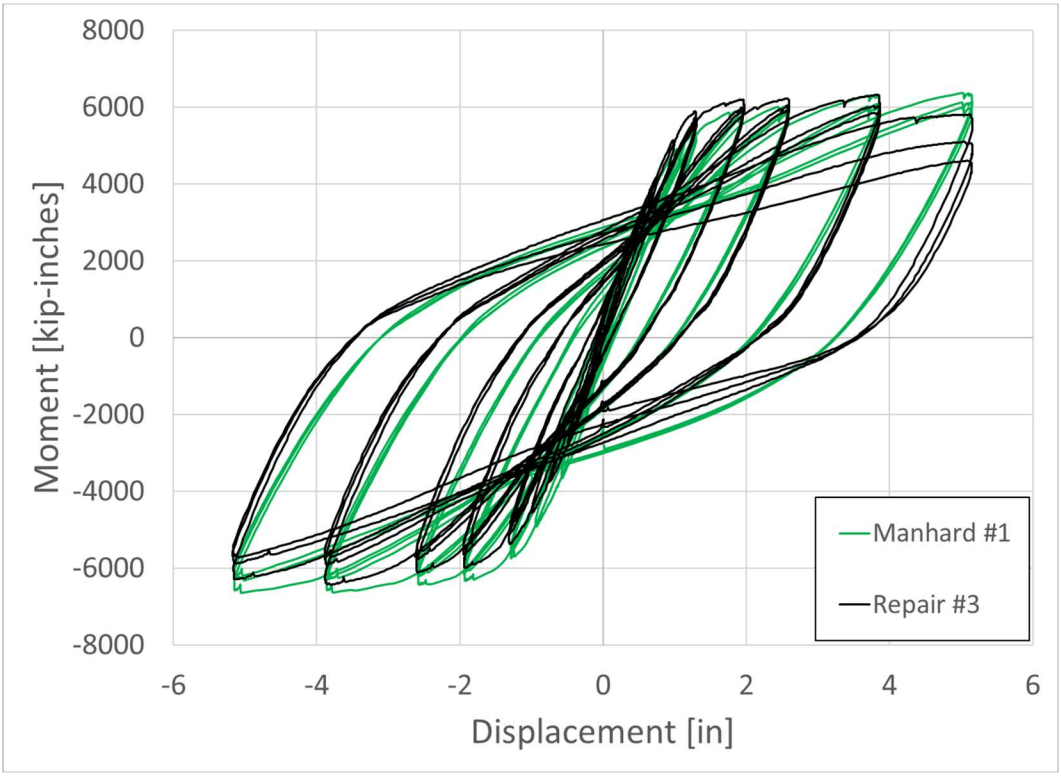

Figure 4.36: Moment in plastic hinge vs displacement for Repair #3.

4.3.5 Local Response

Since the objective of this repair was to prevent yielding of the sleeve, this data from the strain gauges on the sleeve are shown in Figure 4.37. These strain gauges were in the same location as the ones in Repair #2; 3.5 inches from the top of the sleeve and on the extreme North and South sides. As before, the yield strain of this steel is expected to be around 1500 με, so yielding was successfully prevented.

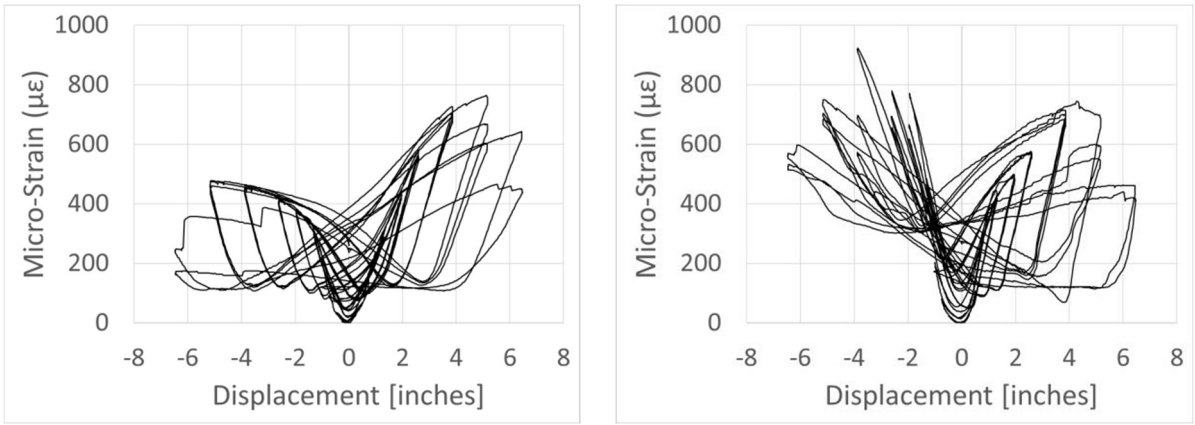

Figure 4.37: Strains in steel sleeve on North (left) and South (right) sides of the column.

Knowing this, the analysis of the south side of the column will be presented first since the primary difference between this side and the previous repair is the thicker sleeve. Based off the observations made during the experimental test, this side of the column showed a similar behavior as Repair #2. Since the S2 and S6 bars were the bars that fractured in this test, the three bars between them bars must have debonded and the strain data shown in Figure 4.38 confirms this. Although the peak strain that the bar sustained increased from around 0.03 in Repair #2 to 0.04 in this repair, the bars ultimately debonded after the first cycle at ductility 3 (3.86 inches). Given this increase, it appears unlikely that further increase in passive confinement alone would be capable of fully anchoring these bars within the repair.

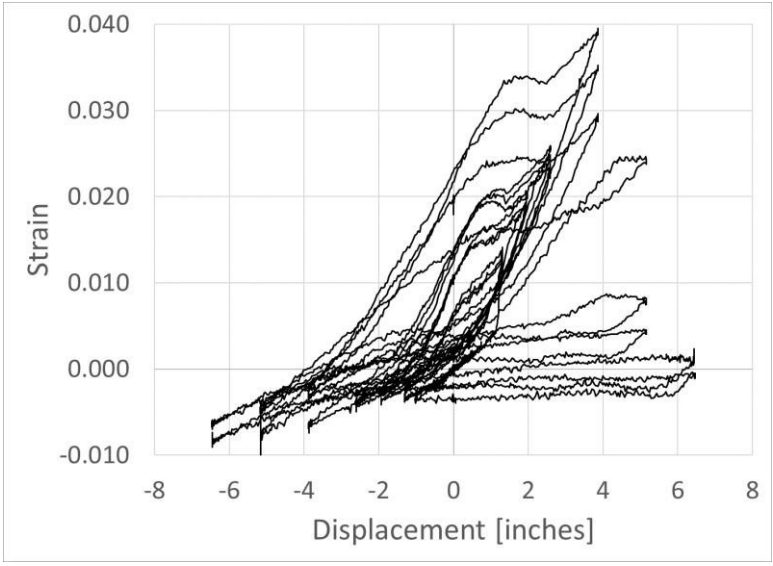

Figure 4.38: Strain History of S4 in Repair #3.

For the North side of the column, the combination of using the thicker steel sleeve and removing the concrete around the fractured bars was sufficient to fully anchor the bars within the repair. From Figure 4.39, the typical response of a well anchored longitudinal bar described earlier is seen, with increasing displacements corresponding to an increase in strains until buckling occurs when the bar is in compression. As the bar continues to buckle further, it eventually ruptures in tension, highlighted by the red x.

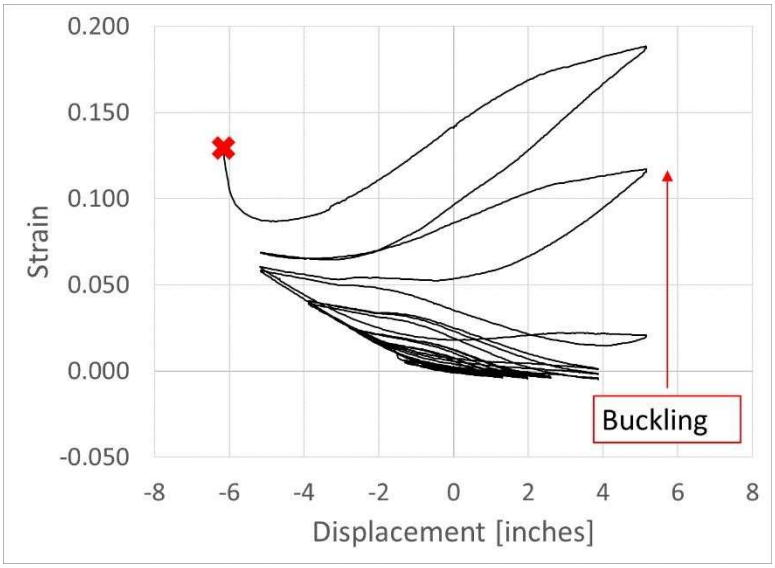

Figure 4.39: Strain History of N4 in Repair #3.

4.3.6 Conclusions

For this repair, a thicker steel sleeve was used to maximize the passive confinement provided to the repair. Additionally, the symmetric damage state gave an ideal situation to investigate a method of improving the bond of fractured bars within the repair. Based on the results of this test, the following conclusions can be inferred.

- The chipping of perimeter concrete can improve the bond of the bars with the repair. With thinner steel sleeves that yield, this difference is fairly small, but if a larger thickness is used which does not yield, the difference is significant.
- A combination of using a sleeve thick enough to avoid yielding and chipping of perimeter concrete around fractured bars can be capable of fully anchoring fractured bars within the repair.
- When the fractured bars are fully anchored, the response of the repaired column is similar to that of an original column test with a shorter effective height due to the plastic hinge being relocated.

4.4 Repair #4

4.4.1 Primary Objective

Repair #3 showed a difference in behavior on each side due to the bond conditions in the repair. In that repair, the previously fractured bars debonded on the side without concrete chipping, and were fully anchored on the side where the damaged concrete was removed around the perimeter of the bar. In order to demonstrate the repair's ability to anchor a fractured bar for more than one half of one test, the same design was used for Repair #4. Additionally, on one side of the column, the perimeter concrete was also chipped around the nonfractured bars to determine if that would impact the column's response.

4.4.2 Damaged Column and Repair

The initial damage condition of this column was 3 fractured bars on each side. The repaired column was subjected to the same axial load and displacement history as the original column. This repair maintained the use of the thicker steel sleeve from Repair #3, with the focus of evaluating the impact of chipping perimeter concrete around both fractured and unfractured bars. To accomplish this, the perimeter concrete was chipped around the fractured bars on the South side and concrete was chipped around all of the bars on the North side. Figure 4.40 shows the damage conditions prior to chipping perimeter concrete. The column after the concrete was chipped is shown in Figure 4.41. The properties for the original column and repair are summarized in Table 4.4.

Figure 4.40: Repair conditions for the North (left) and South (right) sides.

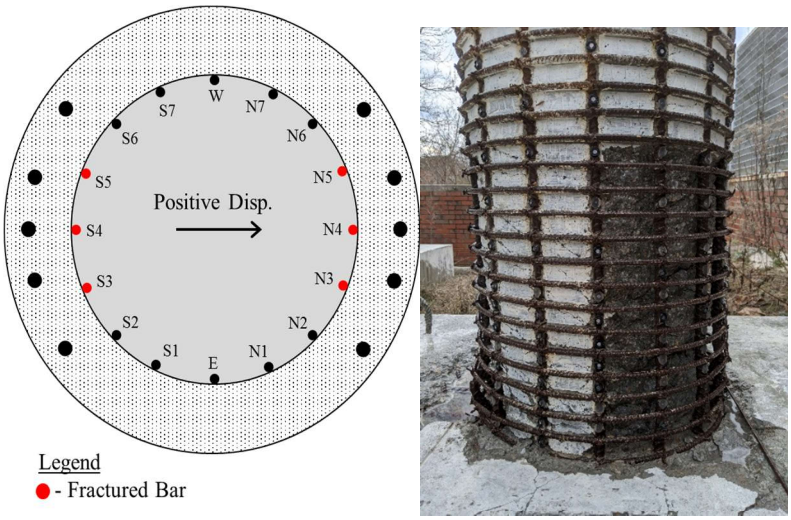

Figure 4.41: Repair cross section and conditions of chipped concrete for Repair #4.

Table 4.4: Column and Repair Properties for Repair #4.

	Original & Comparison Column	**Repair**
Column	Manhard Test 2	Repair #4
Geometry	Height = 8 ft Diameter = 24 inches	Height = 22 inches Diameter = 32 inches
Longitudinal Steel	16 #6 (ρ_l = 1.6%) f_y = 85.9 ksi ε_y = 0.38% f_u = 113.5 ksi ε_u = 10.3%	10 #8 bars f_y = 84.0 ksi ε_y = 0.35%
Transverse Steel	#3 Spirals @ 1.5" (ρ_s = 1.3%) f_y = 79 ksi ε_y = 0.48% f_u = 117 ksi ε_u = 7.6%	¼" A36 Steel Connected by 24 pre-tensioned ASTM A490 bolts with 5/8" diameter
Concrete/Grout Strength	f'_c = 5.62 ksi	f'_c = 7.93 ksi
Axial Load	ALR = 5% P = 139 kips	ALR = 5% P = 139 kips
Load Path	Δ_y' = 0.975 inches Δ_y = 1.29 inches	Δ_y' = 0.975 inches Δ_y = 1.29 inches
Bar Fractures	N3, N4, N5, S3, S4, and S5	N4, S3, S4, and S5

4.4.3 Test progression

Similar to the previous repair tests, circumferential cracks at the top of the repair grout formed around the column soon after the test began. Minor flaking was observed during the cycles of ductility 1.5. On both sides of the column, tension cracking and concrete crushing was observed in the column above the repair, similar to how they would occur in a typical column test.

To assess the potential differences in damage for the two sides, pictures were taken of each side after each ductility. The damage progression is shown in Figures 4.42 to 4.48. The North face of the column is shown in the photos on the left, and the South face is shown on the right. Unless otherwise noted, the photos were taken at the completion of the ductility cycle, when the column was brought to zero displacement. Cracks in the repair grout closed in compression on the North and South side throughout the test. Starting in ductility 4, loose concrete and grout was removed. By the end of the test, about ¼" of loose grout had been removed from the South side while the North side grout remained intact.

Buckling was observed during ductility 4 for the extreme bars on both sides of the column. On the South side, bars S4 and S5 buckled during the second cycle. On the North side, bars N4 and N5 buckled during the third cycle. The most extreme bars fractured on both sides of the column. S4 fractured on the South side during the third push of ductility 4, and N4 fractured on the first pull of ductility 5. Additionally, bars S3, S5, and S6 fractured in the cycles following the fracture of S4.

In summary, this repair showed full anchorage of previously fractured bars on both sides of the column. The chipping of weak concrete around fractured bars seems to be necessary to provide conditions in which the previously fractured bars do not debond. The similarity in damage to the top of the repair grout on each side indicates that chipping around bars that were not previously fractured does not provide additional benefits.

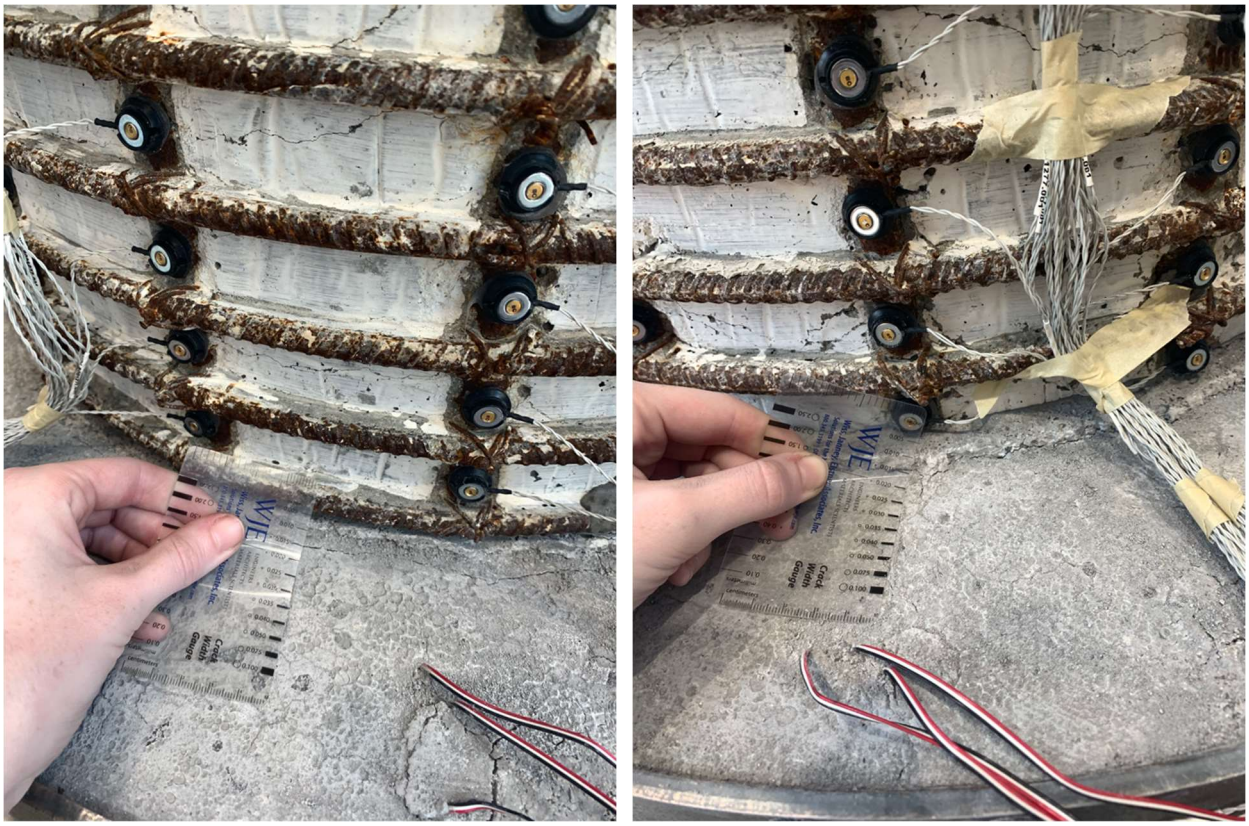

Figure 4.42: Circumferential cracks in the top of repair grout at ½ F_y' for the North (left) and South (right) sides.

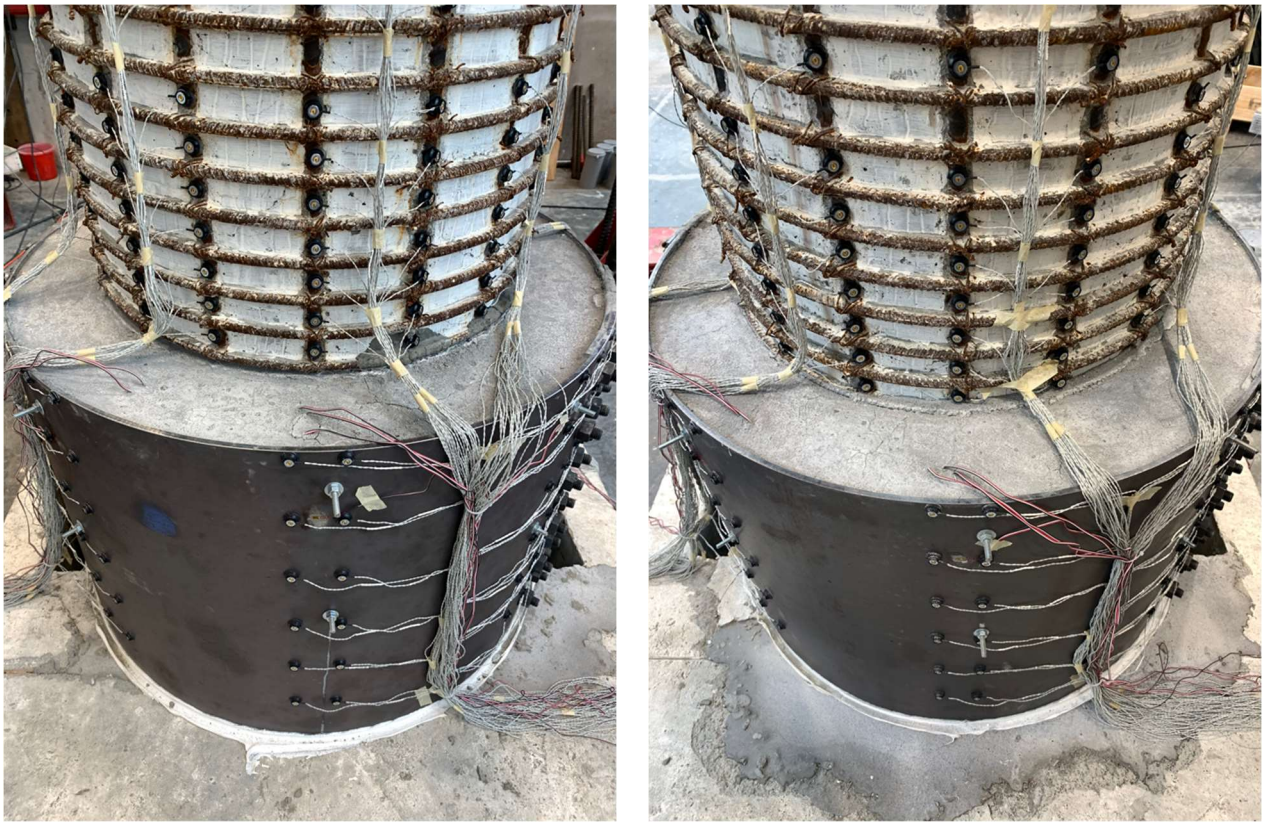

Figure 4.43: Comparison of grout cracking during ductility 1 for the North (left) and South (right) sides.

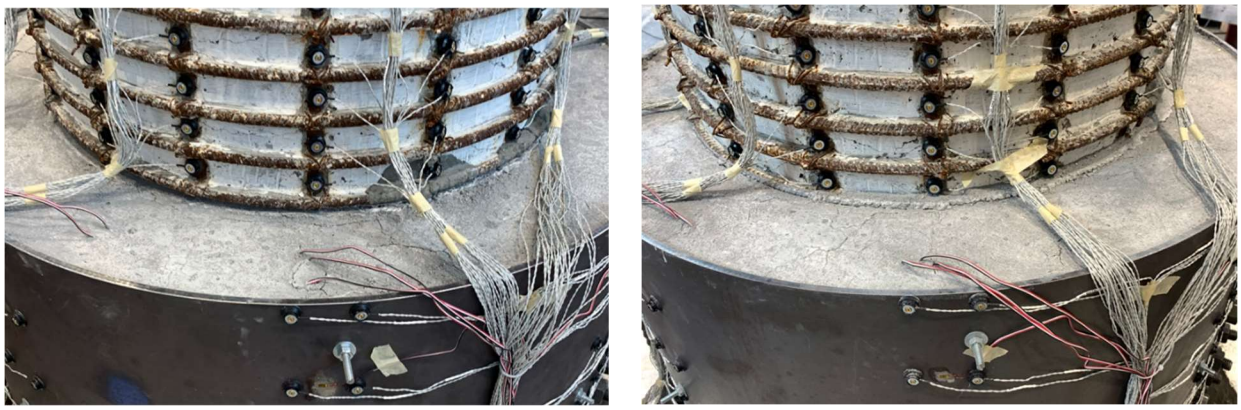

Figure 4.44: Damage Comparison after Ductility 1.5 of the North (left) and South (right) sides.

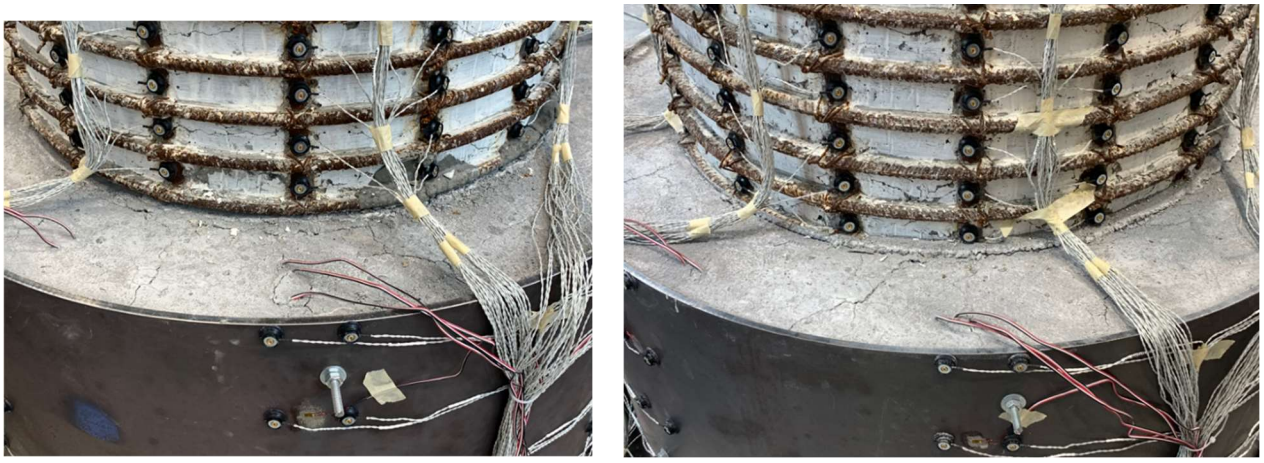

Figure 4.45: Damage Comparison after Ductility 2 of the North (left) and South (right) sides.

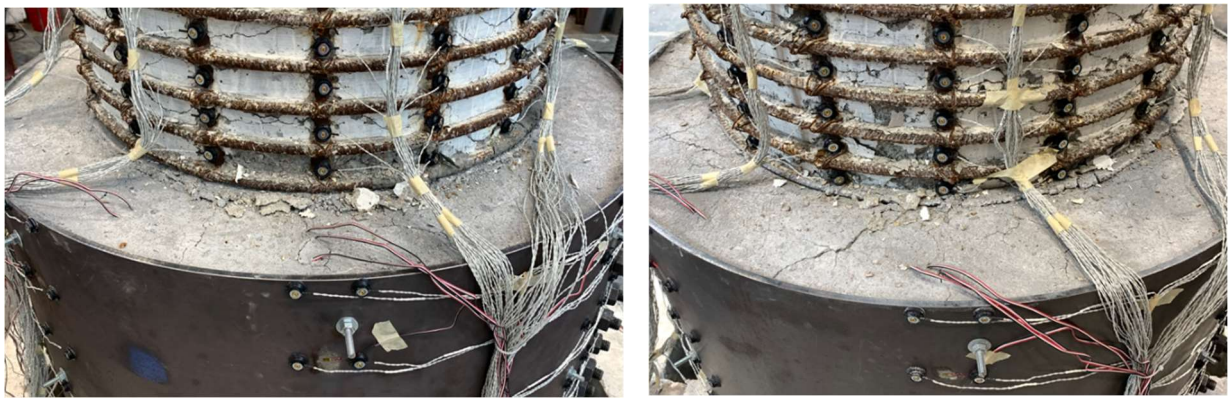

Figure 4.46: Damage Comparison after Ductility 3 of the North (left) and South (right) sides.

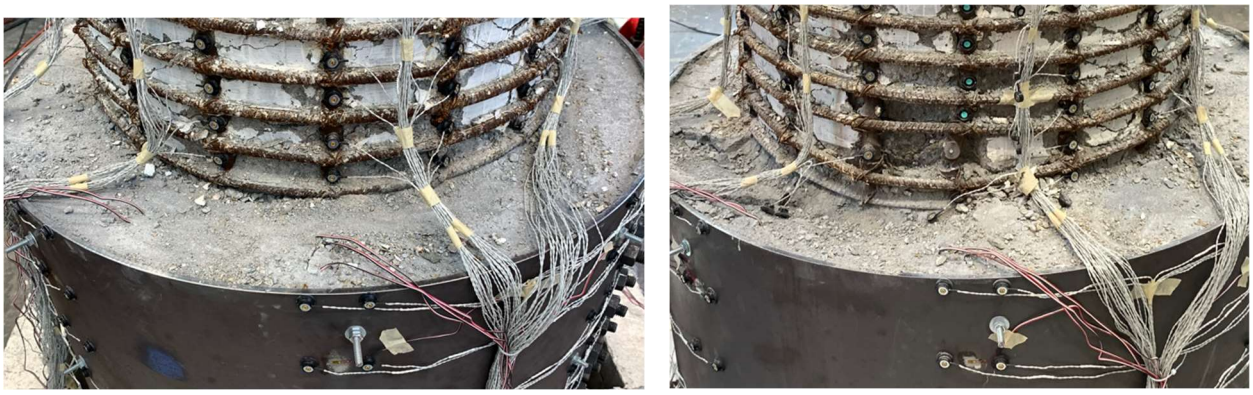

Figure 4.47: Damage Comparison after Ductility 4 of the North (left) and South (right) sides.

Figure 4.48: Damage Comparison after the test when all loose grout was removed of the North (left) and South (right) sides.

4.4.4 Global response

Figure 4.49 compares the Force vs. Displacement response of the repaired column with the original column. Similar to the third repair test, the repaired column did not reach the same ductility cycle as the original. The repaired column test ended after the first cycle of ductility 5. The original test completed 3 cycles at ductility 5 and went on to 2 cycles of ductility 6. The decreased ductility capacity is a consequence of the decreased effective height of the column imposed by the steel sleeve.

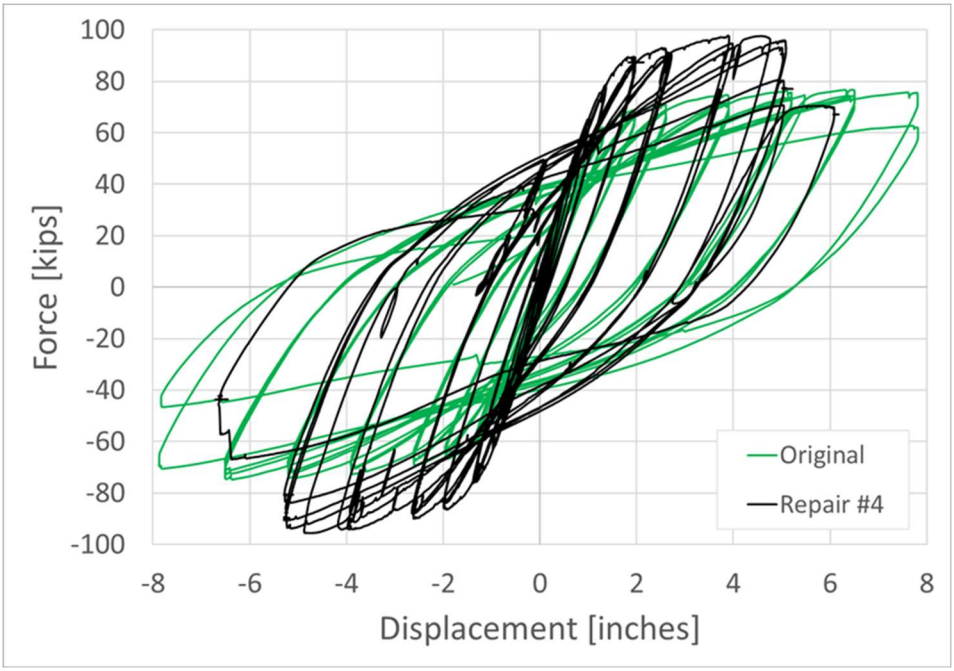

Figure 4.49: Force vs. Displacement Response of Repair #4.

The moment vs. displacement response is shown in Figure 4.50, and was produced following the procedure discussed in Section 4.3.4. The effective heights for the original column and repaired column are 96 inches and 74 inches, respectively. The graph shows that the performance of the repaired column is very similar to that of the original column. The repaired column does not exhibit the pinching behavior seen in previous repairs; this is expected due to the pre-tensioning of the steel sleeve and improved bond conditions on both sides. The behavior of the repaired column is also fairly symmetric, indicating that the additional chipping of concrete away from bars that did not previously fracture did not provide additional benefits.

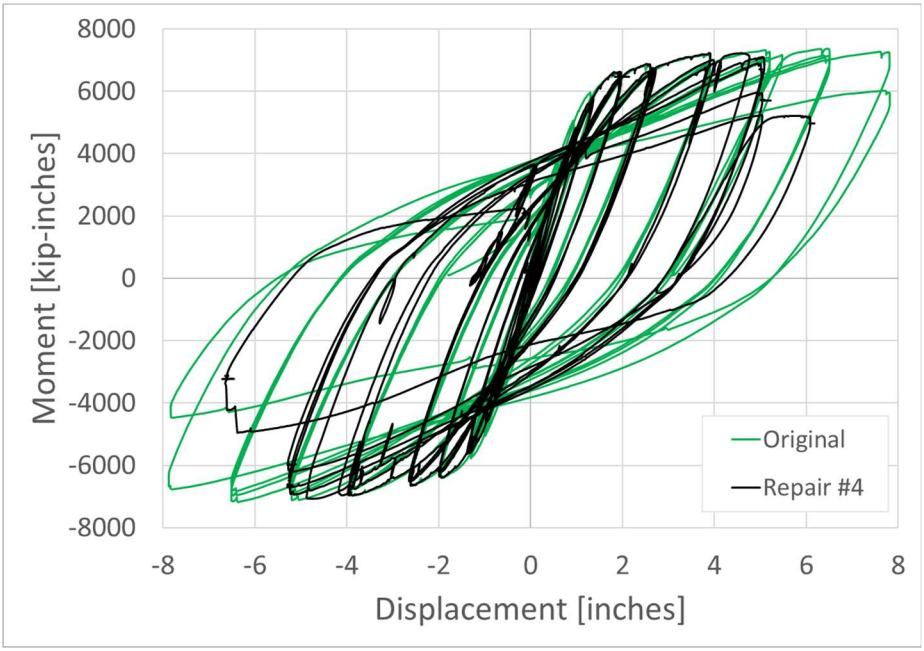

Figure 4.50: Moment vs. Displacement Response of Repair #4.

4.4.5 Local Response

The most extreme bar on each side of the column (N4 and S4) fractured during the repair test. These bars had both fractured in the initial column test, and were anchored in the repair such that they were able to buckle and fracture above the repair. The strain history is shown for the S4 and N4 bars in Figure 4.51 and Figure 4.52, respectively. Both bars reached a maximum tensile strain of around 0.05 before buckling, which is larger than the peak strain prior to debonding for any of the previous repairs. This shows that the removal of perimeter concrete around fractured bars along with the sleeve thickness designed to remain elastic are necessary to anchor fractured bars.

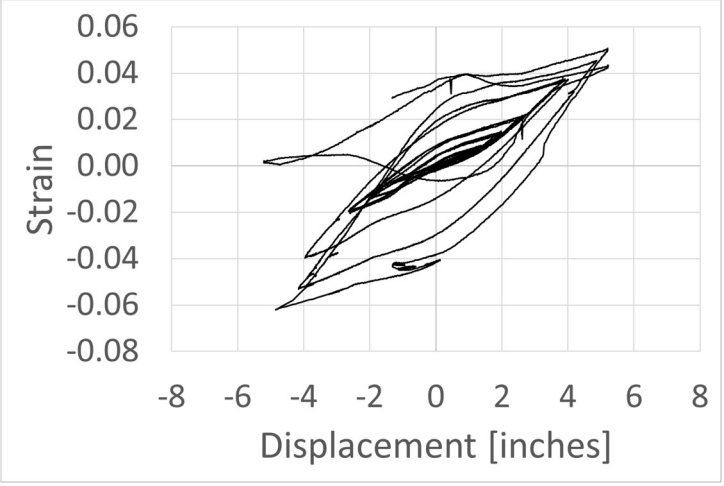

Figure 4.51: Strain History of S4 in Repair #4.

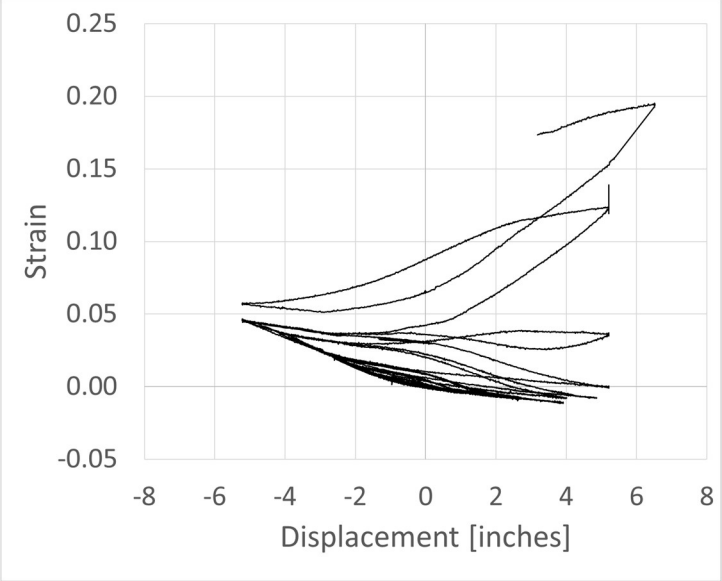

Figure 4.52: Strain History of N4 in Repair #4.

4.4.6 Conclusions

For this repair, concrete was chipped around the perimeter of the fractured bars on the South side and all of the bars on the North side. Chipping the perimeter concrete from the fractured bars proves to be successful for improving bond conditions and anchoring fractured bars on both sides of the column. The additional chipping of concrete around bars that were not originally fractured does not provide additional benefit, and should be neglected in interest of time and effort.

4.5 Repair #5

4.5.1 Primary Objective

Repair #5 used coupled bars which were embedded in the footing during construction for the repair reinforcement. The purpose of building in this capability during the design and construction of new bridges is to dramatically reduce the effort to construct the repair at the time it is needed by eliminating the need to drill holes through the footing. In this case, the yield capacity of the anchor bars is developed by connecting to the embedded couplers. The objective was to ensure that the coupled bars would behave elastically and similar to bars anchored with epoxy. By changing the column diameter from 24 inches to 18 inches, this column also was the first to provide data for a different aspect ratio.

4.5.2 Damaged Column and Repair

The initial damage condition of this column consisted of 1 fractured bar on the North side and 2 fractured bars on the South side. Based on the results of the previous tests, the concrete was chipped just around the fractured bars to improve bond conditions. Figure 4.53 shows the damage conditions for the North and South sides. For repairs using epoxy anchored bars in holes drilled in the footings, the number and size of bar is determined using the design outlined in Section 5.1 based on the number of bars that fracture in the original test. For this test with embedded couplers, the number and size of bar couplers that must be embedded is determined based on an assumed level of damage. The repair cross section was designed assuming no more than 3 longitudinal bars would fracture on each side of the column during the original test, resulting in 5 couplers placed in each side of the footing. Grade 80 threaded bars with a diameter of 0.75 inches were used with compatible couplers to construct the repair. Figure 4.54 shows the cross section and completed repair.

The properties for the original column and repair are summarized in Table 4.5. The aspect ratio (L/D) for the column in Repair #5 is 5.33, compared to an aspect ratio of 4 for the previous repairs in this report. The steel sleeve height maintained the same ratio of 0.9D, which reduced the height to 16.5 inches. The diameter of the steel sleeve was reduced to 26 inches, which provided a 4 inch annular ring for the backfill material. The bolted connection was adapted to the new repair height, following the design presented in Section 5.3.

Figure 4.53: Repair conditions for the North (left) and South (right) sides.

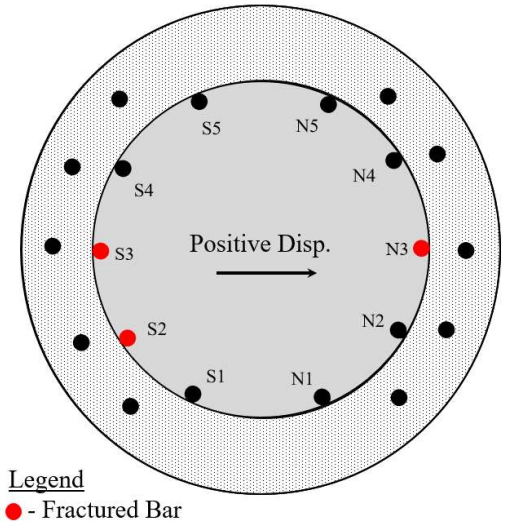

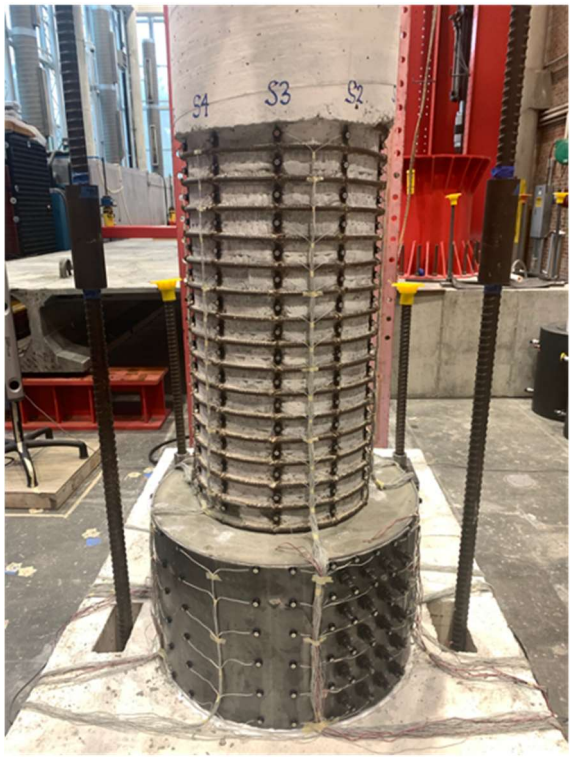

Figure 4.54: Repair cross section and bolt configuration for Repair #5.

Table 4.5: Column and Repair Properties for Repair #5.

	Original & Comparison Column	**Repair**
Column	Thangjitham Test 2	Repair #5
Geometry	Height = 8 ft Diameter = 18 inches	Height = 16.5 inches Diameter = 26 inches
Longitudinal Steel	10 #6 (ρ_l = 1.6%) f_y = 86.1 ksi ε_y = 0.30% f_u = 113.7 ksi ε_u = 9.0%	10 #6 bars f_y = 84.0 ksi ε_y = 0.35%
Transverse Steel	#3 Spirals @ 2" (ρ_s = 1.0%) f_y = 79 ksi ε_y = 0.48% f_u = 117 ksi ε_u = 7.6%	¼" A36 Steel Connected by 20 pre-tensioned ASTM A490 bolts with 5/8" diameter
Concrete/Grout Strength	f'_c = 6.51 ksi	f'_c = 7.41 ksi
Axial Load	ALR = 10% P = 144 kips	ALR = 10% P = 144 kips
Load Path	Δ_y' = 0.87 inches Δ_y = 1.15 inches	Δ_y' = 0.87 inches Δ_y = 1.15 inches
Bar Fractures	N3, S2, and S3	N4, S2, and S3

4.5.3 Test progression

The first grout cracks appeared during the first yield cycle, and were diagonal through the top of the repair, radiating from the area where the core column chipping stopped. Circumferential grout cracks formed in the ductility 1 cycles. The original column cracks also widened in this cycle. Beginning in ductility 1.5, new column cracks formed above the repair. Column concrete crushing happened during ductility 3.

To assess the potential differences in damage for the two sides, pictures were taken of each side after each ductility. The damage progression is shown in Figures 4.55 - 4.58 The North face of the column is shown in the pictures on the left, and the South face is shown on the right. The pictures were taken when the column was

brought to zero displacement. Cracks in the repair grout closed in compression on the North and South side throughout the test. Starting in ductility 4, loose concrete and grout was removed. Buckling was observed during the second cycle of ductility 5 for the extreme bars on both sides of the column (bars S3 and N3). On the third cycle of ductility 5, N3 fractured. During the next push, S3 fractured before surpassing the ductility 5 displacement. The final damage condition consisted of bars N3 and S3 fractured in the relocated hinge, along with the buckling of N2.

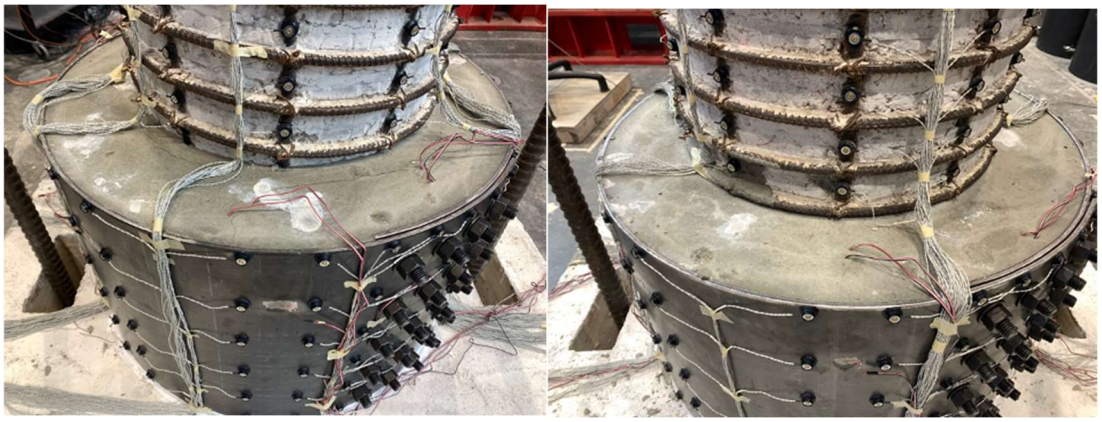

Figure 4.55: Damage after ductility 1 for the North (left) and South (right) sides.

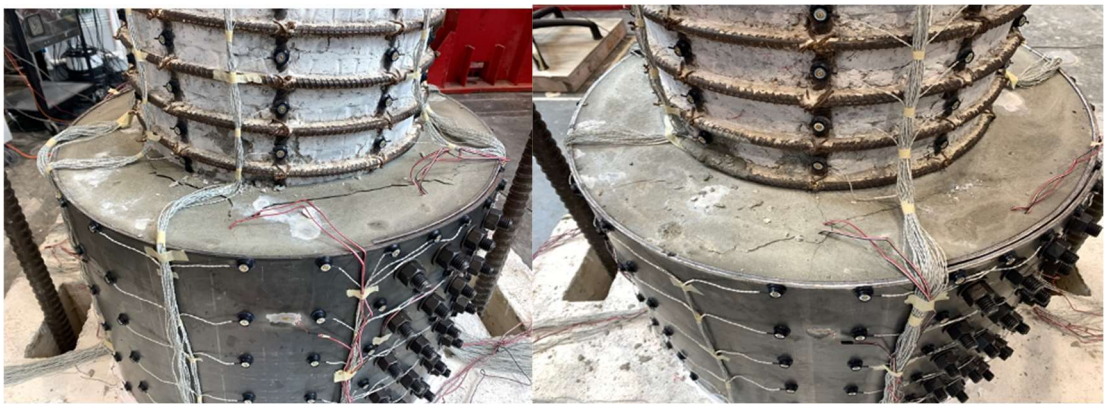

Figure 4.56: Damage after ductility 2 for the North (left) and South (right) sides.

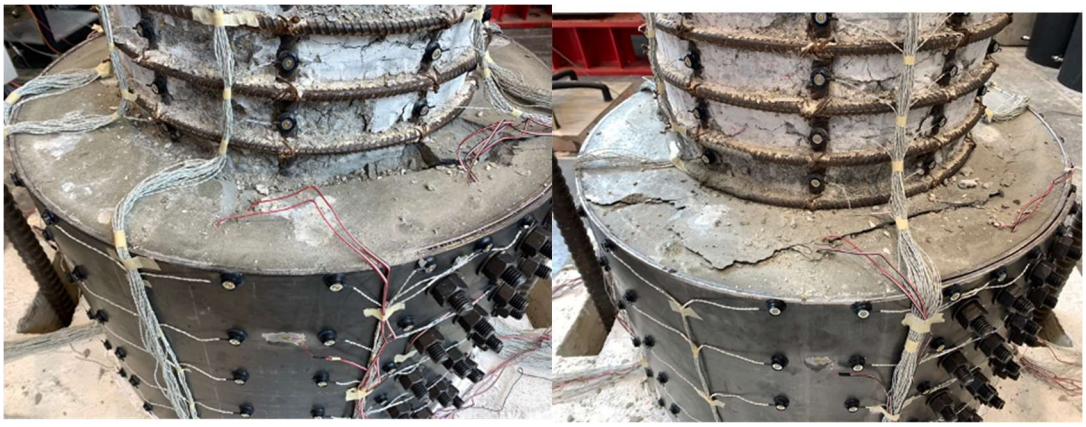

Figure 4.57: Damage after ductility 4 for the North (left) and South (right) sides.

Figure 4.58: Damage Comparison after the test when all loose grout was removed of the North (left) and South (right) sides.

4.5.4 Global response

Figure 4.59 compares the force vs. displacement response of the repaired column with the original column. In this repair test, the repaired column did reach the same displacement as the original column. The original column completed 3 cycles at ductility 6. At the end of ductility 6 for the repair test, the forces had dropped approximately 20%, which is typically considered failure, but the test was continued through ductility 7 to determine if the previously fractured bars would remain anchored with the new repair height.

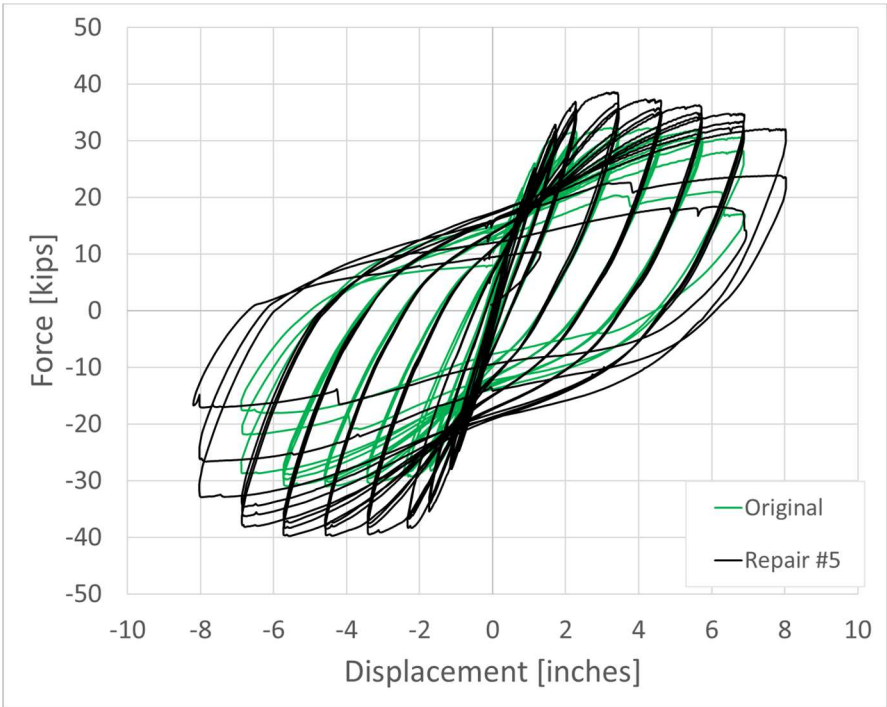

Figure 4.59: Force vs. Displacement of the Original and Repair Column Tests.

The moment vs. displacement response is shown in Figure 4.60, and was produced following the procedure discussed in Section 4.3.4. The effective heights for the original column and repaired column are 96 inches and 74 inches, respectively. The graph shows that the performance of the repaired column is similar to that of the original column; however, there is significantly more strength degradation in the repaired column compared to the original. Additionally, the repaired column has a lower initial stiffness. One factor that may contribute to the amount of strength loss and the lower initial stiffness is the level of initial damage, because the repaired column was more cracked in the relocated hinge region compared to previous repaired columns.

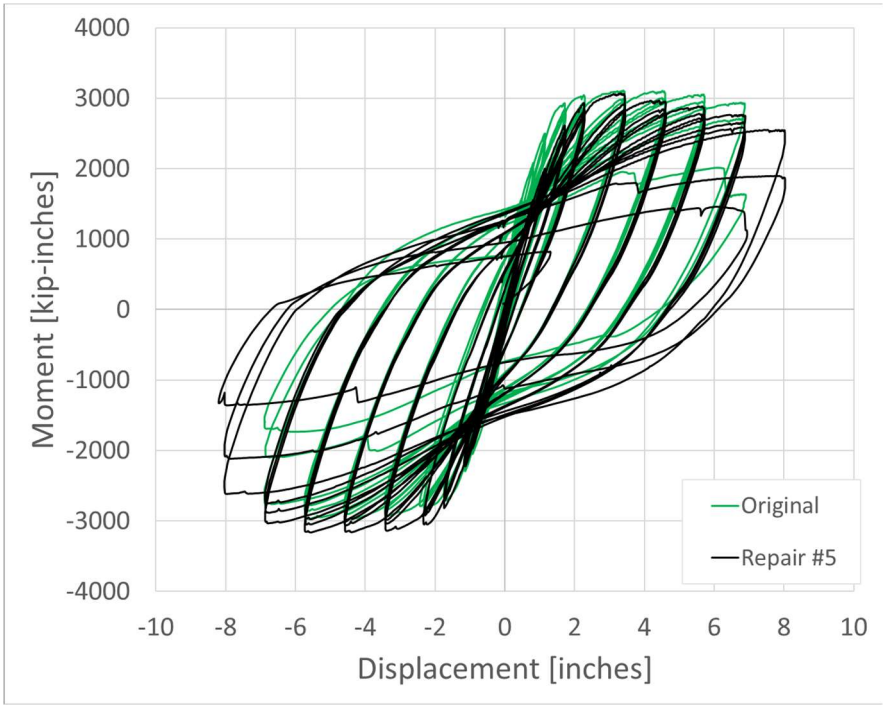

Figure 4.60: Moment vs. Displacement of the Original and Repair Column Tests.

4.5.5 Local Response

The goal for this test was to verify if coupled bars could be used to simplify construction while still behaving elastically and similar to the repair bars which are anchored in drilled holes in the footing with epoxy. Figures 4.61 and 4.62 show the strain in the coupled bars from strain gauges above the couplers, near the base of the repair on each side of the repair. The strains are well below the yield strain, and this is a result of determining the repair layout at the time of footing construction. The number and size of repair reinforcement was determined based on an assumption of the level of damage that the original column would experience. At the time of the repair, not all of the couplers need to be used if the column suffered less damage than expected, but the bar size would need to remain compatible with the couplers. For this repair, the repair reinforcement layout was not the most efficient given the level of damage, but reducing the quantity of repair bars without changing the bar size could have resulted in bars yielding within the repair.

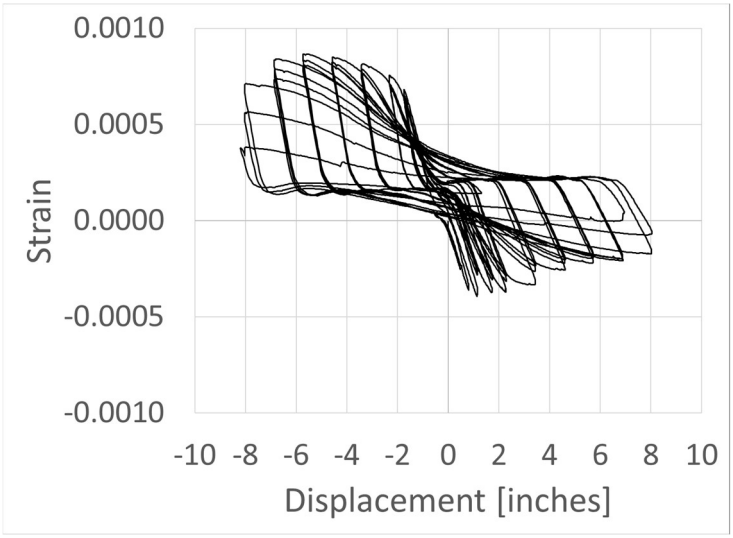

Figure 4.61: Strain History of North Side Extreme Repair Bar

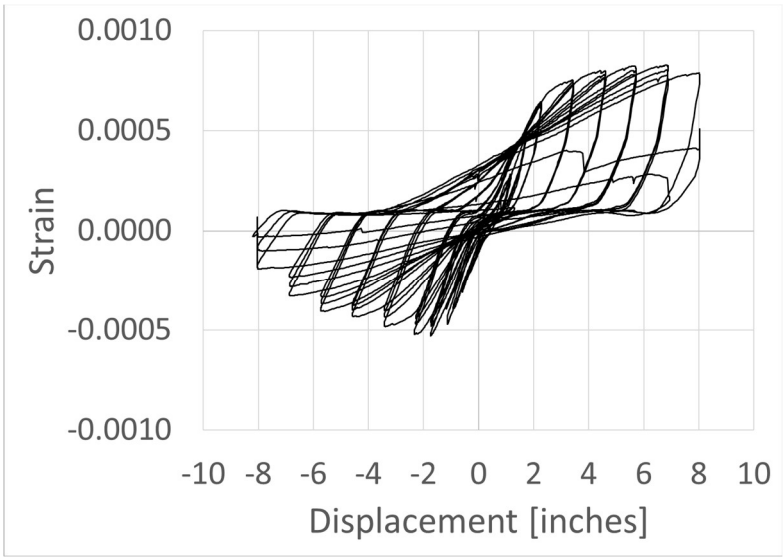

Figure 4.62: Strain History of South Side Extreme Repair Bar

As a qualitative comparison between methods of repair reinforcement anchorage, the strain in the repair bar from Repair #1 is presented in Figure 4.63. This shows the typical response of anchored repair bars. Both the epoxy anchored and coupled bars follow similar loading paths. The main difference is the decrease in stiffness as the bar transitions from tension to compression. For the epoxy anchored bar, the stiffness gradually changes from the tensile response to the compressive response. In the case of the coupled bar, the sections of

zero stiffness indicate that the bar experiences some level of socket action within the coupler. As the bar rocks within the coupler, it is engaged in tension and compression once it bears against the coupler.

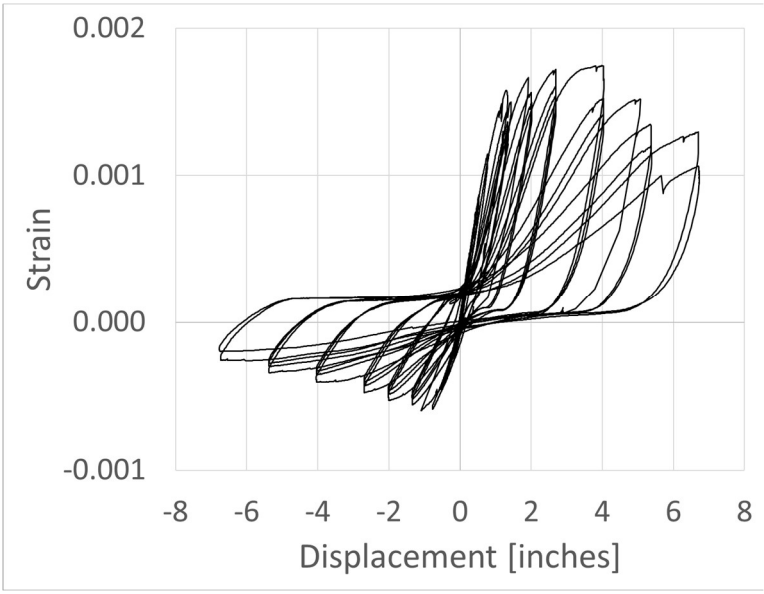

Figure 4.63: Strain History of Repair Bar in Repair #1

4.5.6 Conclusions

This repair used couplers in the footing to reduce the time and effort of repair construction. The coupled bars were effectively bonded in the repair and serve as a viable alternative to drilling and using epoxy anchored bars. For this repair, the couplers were embedded so the top surface was level with the top of the footing; however, embedding the couplers with cover above them would protect the couplers from environmental effects in the time between initial and repair construction while still significantly reducing the amount of time and effort to complete the repair.

4.6 Repair #6

4.6.1 Primary Objective

Similar to Repair #5, Repair #6 also used coupled bars which were embedded in the footing during construction for the repair reinforcement. The objective was to ensure that the coupled bars would behave elastically and similar to bars anchored with epoxy. Additionally, this column investigated a different aspect ratio, changing the height from 8 to 13 feet. The aspect ratio (L/d) for this column is 8.67.

4.6.2 Damaged Column and Repair

The initial damage condition of this column, shown in Figure 4.64, was one fractured bar on the North side and 3 fractured bars on the South side. The perimeter concrete was chipped around the fractured bars. The repair cross section is shown in Figure 4.65. In this design and the design of Repair #5, it was assumed that no more than 3 longitudinal bars would fracture on each side of the column, resulting in 5 couplers placed in each side of the footing during construction. For this repair, the actual damage of the original column was taken into account to decide how many bars would be placed in the couplers. On the South side, the assumed 3 bars fractured and therefore all 5 couplers were used. On the North side, only one bar fractured, so fewer repair bars could be used and still behave elastically according to the design, and two of the couplers were left empty.

The properties for the original column and repair are summarized in Table 4.6. The height of the steel sleeve was increased to 22 inches for this repair. The increase from 0.9D was to account for the increase in the extent of plasticity associated with the taller column height. The height of the repair was chosen to ensure that the strains of the original column and the location of relocated plastic hinge remained below 0.02, following the recommendations of Krish (2018). Because the design of the couplers must be determined before the original column is constructed, the equation for plastic hinge length was used to determine the proper height. The strain data from the original test showed the actual maximum strain at the relocated hinge was 0.027.

Figure 4.64 Repair #6 damage state of the North and South sides.

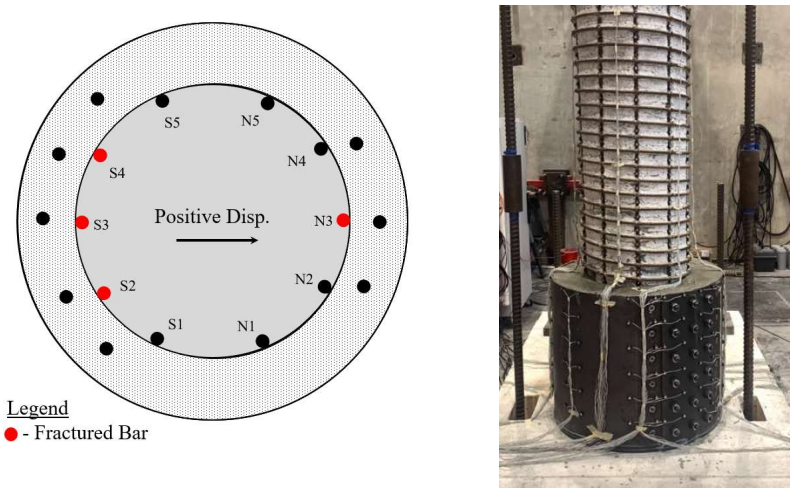

Figure 4.65: Repair #6 damage state of the (a) North and (b) South sides.

Table 4.6: Column and Repair Properties for Repair #6.

	Original & Comparison Column	**Repair**
Column	Thangjitham Test 5	Repair #6
Geometry	Height = 8 ft Diameter = 18 inches	Height = 22 inches Diameter = 26 inches
Longitudinal Steel	10 #6 (ρ_l = 1.6%) f_y = 86.1 ksi ε_y = 0.30% f_u = 113.7 ksi ε_u = 9.0%	8 #6 bars f_y = 84.0 ksi ε_y = 0.35%
Transverse Steel	#3 Spirals @ 2" (ρ_s = 1.0%) f_y = 79 ksi ε_y = 0.48% f_u = 117 ksi ε_u = 7.6%	¼" A36 Steel Connected by 18 pre-tensioned ASTM A490 bolts with 5/8" diameter
Concrete/Grout Strength	f'_c = 6.51 ksi	f'_c = 6.24 ksi
Axial Load	ALR = 10% P = 146.9 kips	ALR = 10% P = 146.9 kips
Load Path	Δ_y' = 2.16 inches Δ_y = 2.86 inches	Δ_y' = 2.16 inches Δ_y = 2.86 inches
Bar Fractures	N3, S2, S3, S4	N3 and S3

4.6.3 Test progression

The initial damage condition of this column consisted of 1 fractured bar on the North side and 3 fractured bars on the South side. The repaired column was subjected to the same axial load and displacement history as the original column.

The first grout cracks appeared during the first yield cycle, and were diagonal through the top of the repair, radiating from the area where the core column chipping stopped. Circumferential grout cracks formed in the ductility 1 cycles. As you can see in Figure 4.66 the column exhibited large cracks in the new hinge region from the initial loading of the original test. These original column cracks also widened in the ductility 1 cycles. Beginning in ductility 1.5, new column cracks formed above the repair. Column concrete crushing happened during ductility 3.

The damage progression is shown Figures 4.66-4.73. Each picture was taken at the peak displacements of each ductility cycle, with the shown side in tension. Cracks in the repair grout closed in compression on the North and South side throughout the test. Starting in ductility 4, loose concrete and grout was removed.

Buckling was observed during the second cycle of ductility 5 for the extreme bars on both sides of the column (bars S3 and N3). On the third cycle of ductility 5, N3 fractured. During the next push, S3 fractured before surpassing the ductility 5 displacement. In addition to N3 and S3 fracturing in the relocated hinge, N2 buckled.

Figure 4.66 Initial damage above repair.

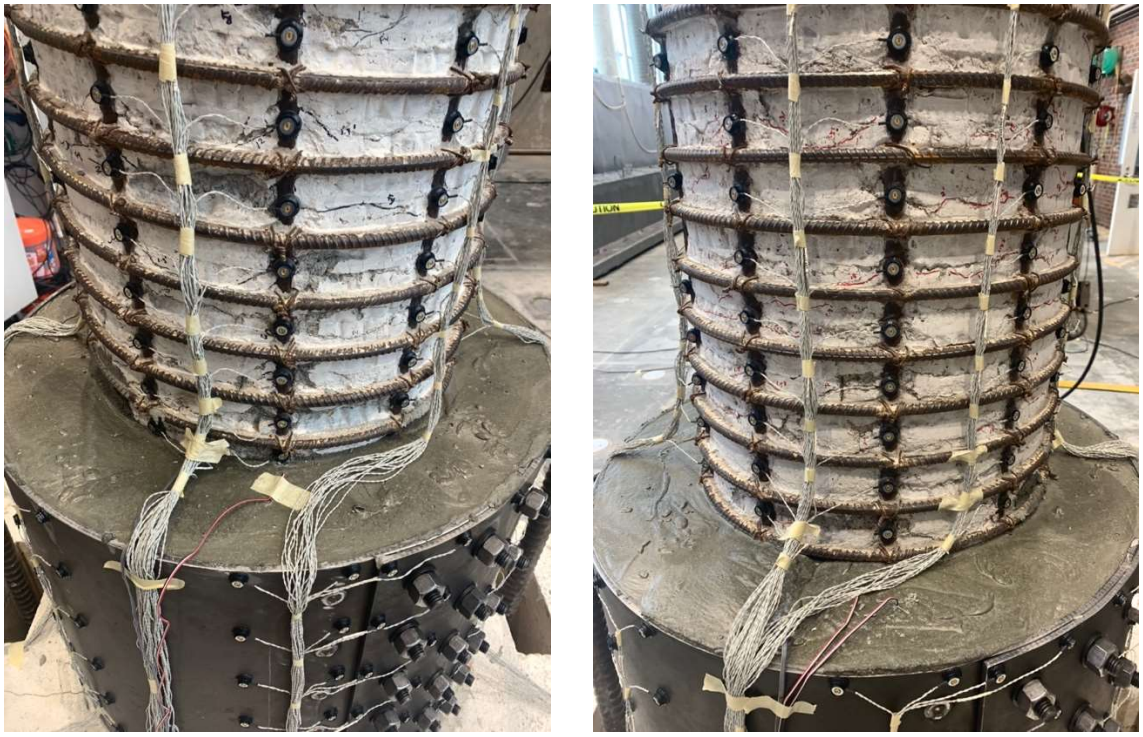

Figure 4.67: Damage During Ductility 1 of the North (left) and South (right) Sides.

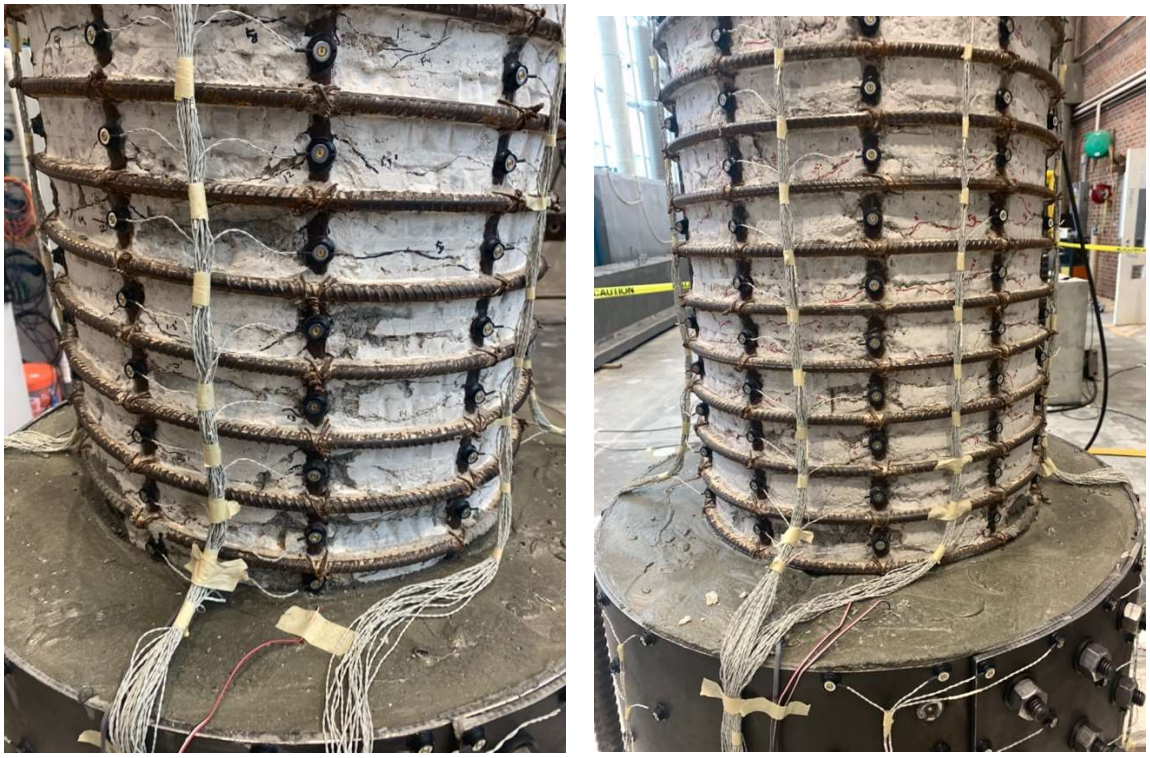

Figure 4.68: Damage During Ductility 1.5 of the North (left) and South (right) Sides.

Figure 4.69: Damage During Ductility 2 of the North (left) and South (right) Sides.

Figure 4.70: Damage During Ductility 3 of the North (left) and South (right) Sides.

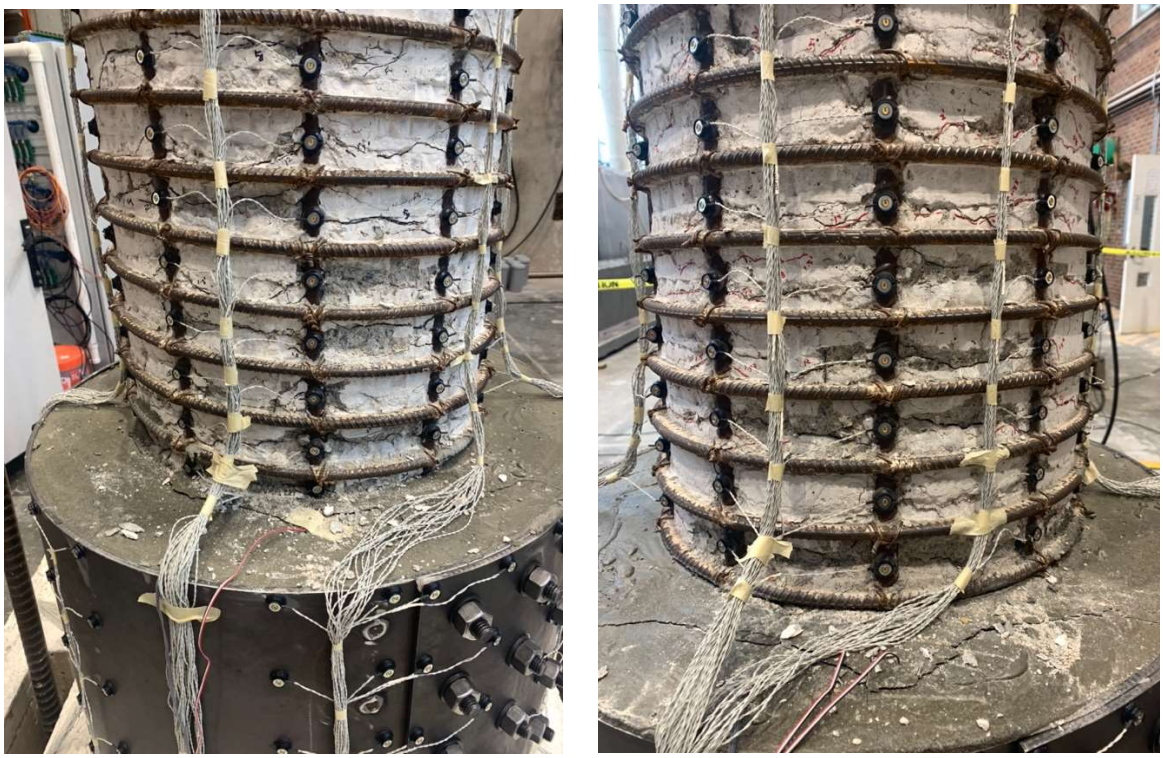

Figure 4.71: Damage During Ductility 4 of the North (left) and South (right) Sides.

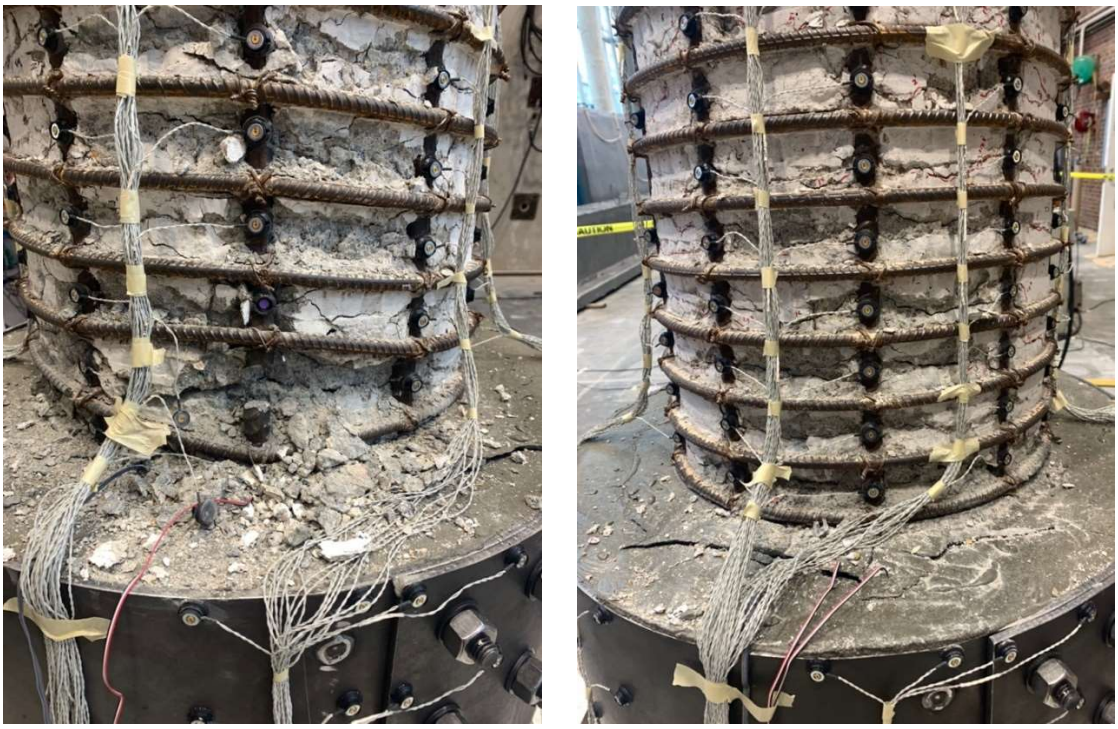

Figure 4.72: Damage During Ductility 5 of the North (left) and South (right) Sides.

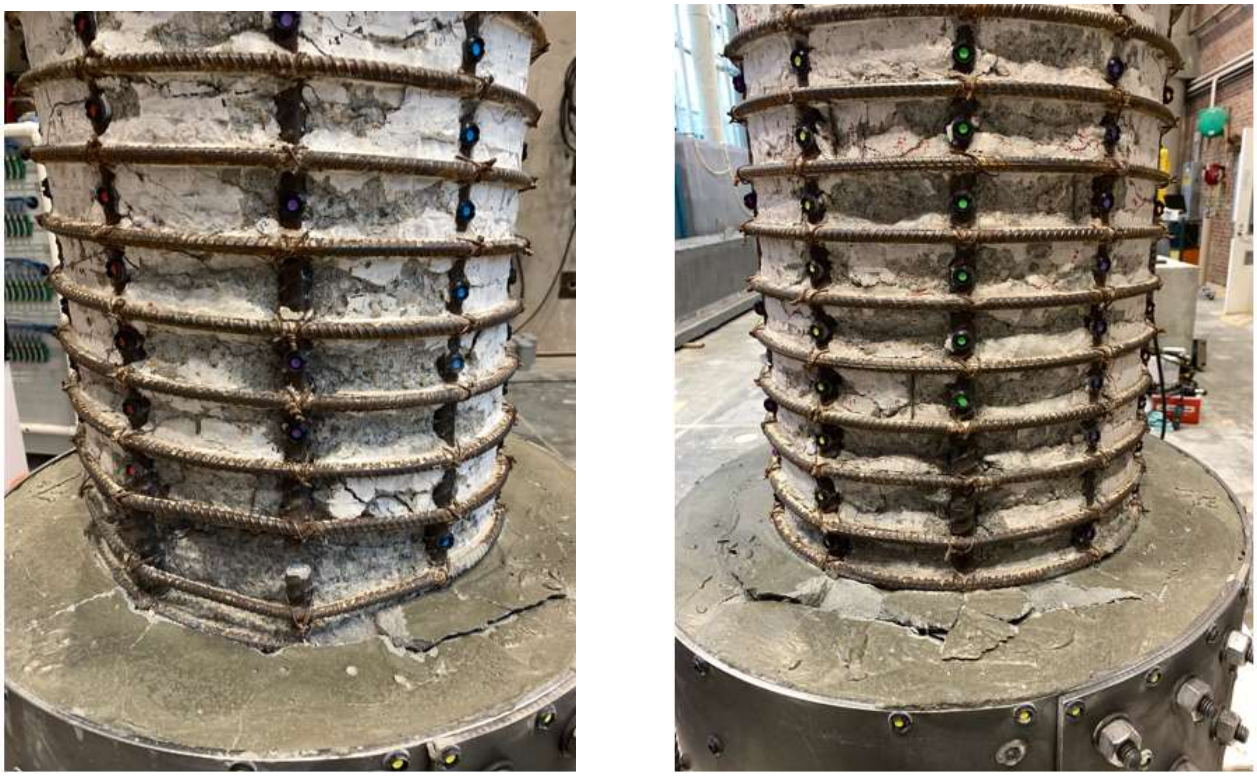

Figure 4.73: Damage after the test when all loose grout was removed of the North (left) and South (right) sides.

4.6.4 Global response

Figure 4.70 compares the force vs. displacement response of the repaired column with the original column. In this repair test, the repaired column was not able to reach the ductility level reached by the original column. After 3 cycles were completed at ductility 5, the South extreme bar (S3) fractured before surpassing the ductility 5 displacement, so a fourth cycle of ductility 5 was completed. The original column failed at the third cycle of ductility 6.

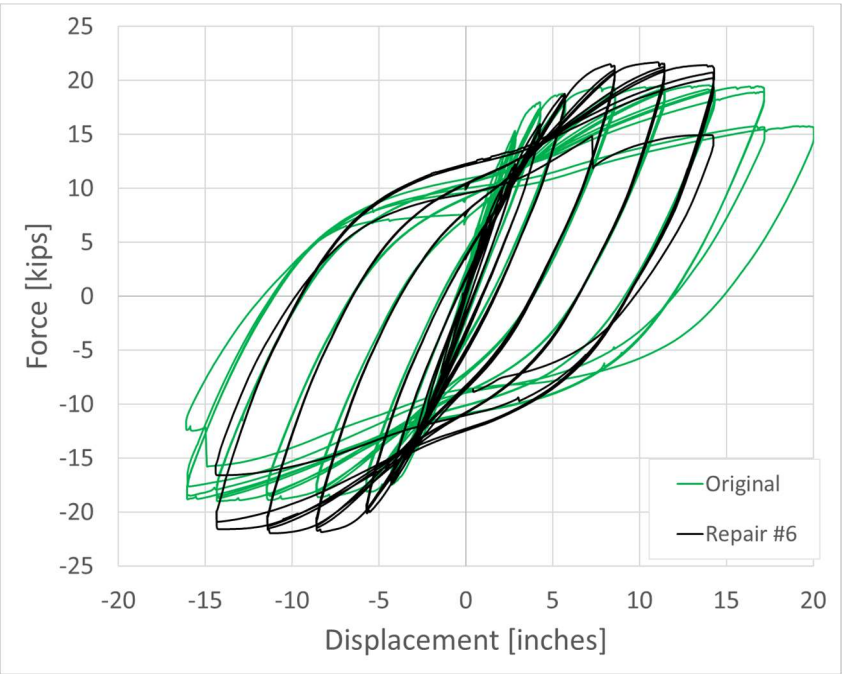

Figure 4.74: Force vs. Displacement of the Original and Repair Column Tests

The moment vs. displacement response is shown in Figure 4.75, and was produced following the procedure discussed in Section 4.3.4. The effective heights for the original column and repaired column are 156 inches and 134 inches, respectively. Figure 4.71 shows that the performance of the repaired column is similar to that of the original column. When the column is pulled to negative displacements, the behavior matches the original column except for a slight decrease initial stiffness. This decrease in stiffness is much more apparent when the column is pushed in the positive direction. While the column is pushed, the side with 3 originally fractured bars is placed in tension. Because these bars are anchored, they should be contributing fully to the moment capacity. Additionally, the strains in these bars would have initially been higher, resulting in a softer response.

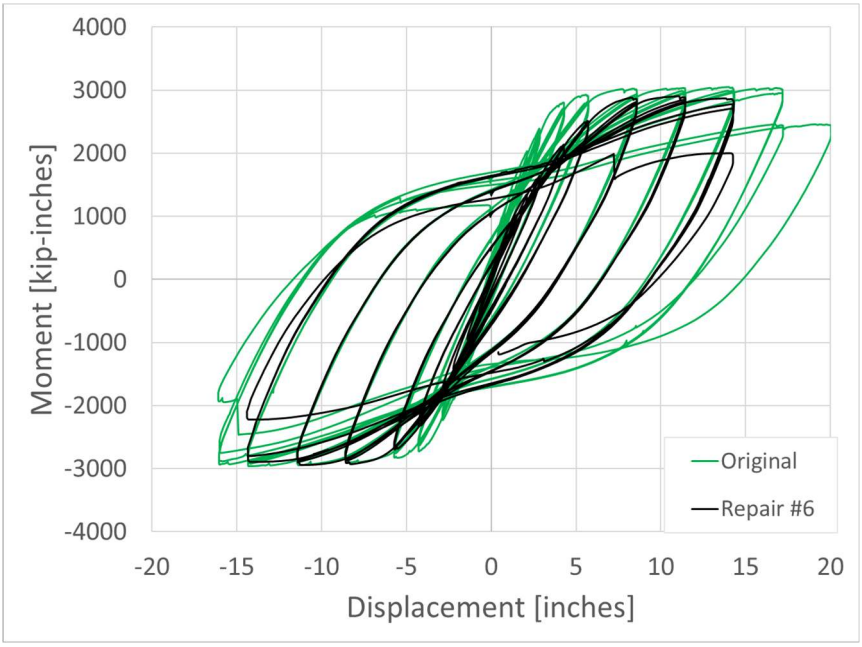

Figure 4.75: Moment vs. Displacement of the Original and Repair Column Tests.

4.6.5 Local Response

When coupled bars are used, the repair reinforcement layout must be chosen based on an assumed level of damage. For these columns, it was assumed that no more than 3 longitudinal bars would fracture on each side of the column during the original test, resulting in 5 couplers for #6 bars on each side being required for an elastic design. For this repair, the assumption of damage at the time of footing construction was better aligned with the actual level of damage. This is evident in the strain history in Figure 4.76, which shows the peak strain is closer to the yield limit, but still elastic, as designed. Similar to Repair #5, the repair bars experienced the rocking behavior.

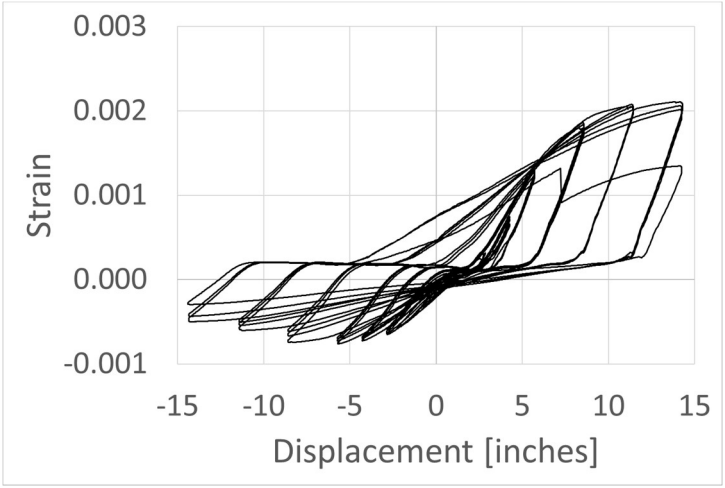

Figure 4.76: Strain History of South Side Extreme Repair Bar in Repair #6.

4.6.6 Conclusions

This repair used coupled bars for the repair reinforcement to simplify construction, and it was the first repair of a column with a height 13 feet. The coupled bars did behave elastically. In practice, the number of couplers embedded in the footing based on an assumed damage level may be more than the required number based on the true column damage. Either using all of the couplers or refining the design with the actual number of fractured bars provides an acceptable design solution. The damage level at the relocated hinge has an impact on the repaired column's response, and should be taken into account when determining the height of the repair.

4.7 Repair #7

4.7.1 Primary Objective

The objective of Repair #7 was to utilize an epoxy grout in the repair annular ring. One potential benefit of using an epoxy grout is that it can be poured underwater. Considering many column to footing connections are located underwater, equivalent performance of the repair with epoxy grout would expand the usability of this repair method. The repair and original column had nominally identical materials and aspect ratio to Repair #6 to compare the influence of the backfill material.

4.7.2 Damaged Column and Repair

The initial damage condition of this column consisted of 1 fractured bar on the South side and 3 fractured bars on the North side. The perimeter concrete was chipped around the fractured bars. 8 Grade 80 No.

6 bars were epoxy anchored into drilled holes in the footing. The strain from the previous test at the relocated hinge was less than the limit of 0.02 from Krish (2018). Epoxy grout was used as the backfill material and the completed repair is shown in Figure 4.77. The grout was poured to the same level as the top of the steel sleeve, but shrinkage resulted in a decreased height in addition to one large radial crack propagating through the entire height. Additional epoxy was poured into the crack, and after shrinkage the crack remained only at the surface. The properties for the original column and repair are summarized in Table 4.7.

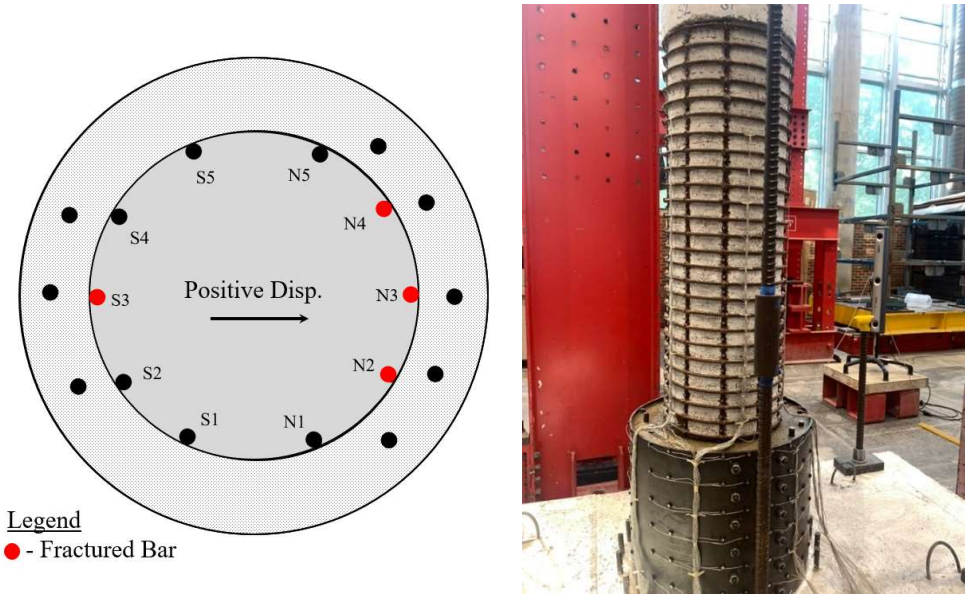

Figure 4.77: Repair Cross Section and Completed Repair.

Table 4.7: Column and Repair Properties for Repair #7.

	Original & Comparison Column	**Repair**
Column	Thangjitham Test 5	Repair #7
Geometry	Height = 8 ft Diameter = 18 inches	Height = 22 inches Diameter = 26 inches
Longitudinal Steel	10 #6 (ρ_l = 1.6%) f_y = 86.1 ksi ε_y = 0.30% f_u = 113.7 ksi ε_u = 9.0%	8 #6 bars f_y = 84.0 ksi ε_y = 0.35%
Transverse Steel	#3 Spirals @ 2" (ρ_s = 1.0%) f_y = 79 ksi ε_y = 0.48% f_u = 117 ksi ε_u = 7.6%	¼" A36 Steel Connected by 18 pre-tensioned ASTM A490 bolts with 5/8" diameter
Concrete/Grout Strength	f'_c = 6.51 ksi	f'_c = 9.28 ksi
Axial Load	ALR = 10% P = 146.9 kips	ALR = 10% P = 146.9 kips
Load Path	Δ_y' = 2.16 inches Δ_y = 2.86 inches	Δ_y' = 2.16 inches Δ_y = 2.86 inches
Bar Fractures	N3, S2, S3, S4	N2, N3, N4, S2, and S3

4.7.3 Test progression

The original condition of the grout can be seen in Figure 4.78. The radial grout crack maintained the same size throughout the test, and no cracks formed in the grout for the majority of the test. One circumferential hairline crack formed on the South side during the first push of ductility 5. Cracks formed in the concrete at the interface between the column and repair during the first cycles of ductility 1; the original column cracks widened in these cycles. Beginning in ductility 1.5, new column cracks formed above the repair. Column concrete crushing happened during ductility 3. The damage progression is shown in Figures 4.80-4.85. Each picture was taken at the peak displacement for ductility cycle, with the shown side in tension.

Buckling was observed above the steel sleeve during the second cycle of ductility 4 for the extreme bar on the North side of the column (N3). On the first cycle of ductility 5, N3 fractured. The two next bars (N2 and N4) buckled during the second push of ductility 5 and fractured during the second pull of ductility 5. On the South

side, the extreme bar (S3) and one next to it (S2) buckled on the first cycle of ductility 5 and fractured during the third cycle of ductility 5. The final damage condition was 5 fractured bars and one buckled bar.

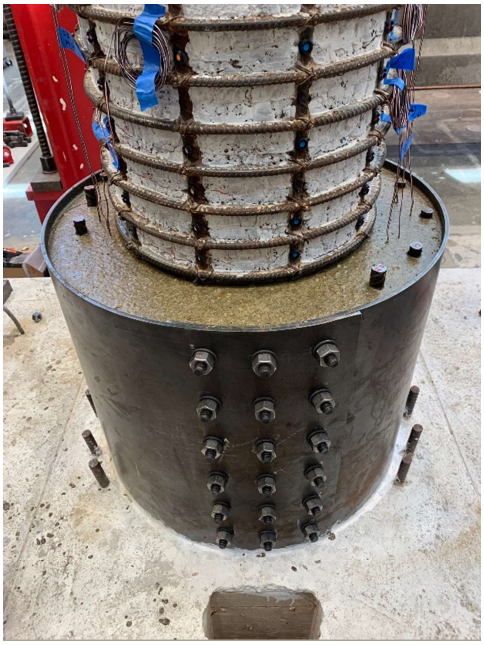

Figure 4.78: Initial Conditions

Figure 4.79: Initial Grout Crack

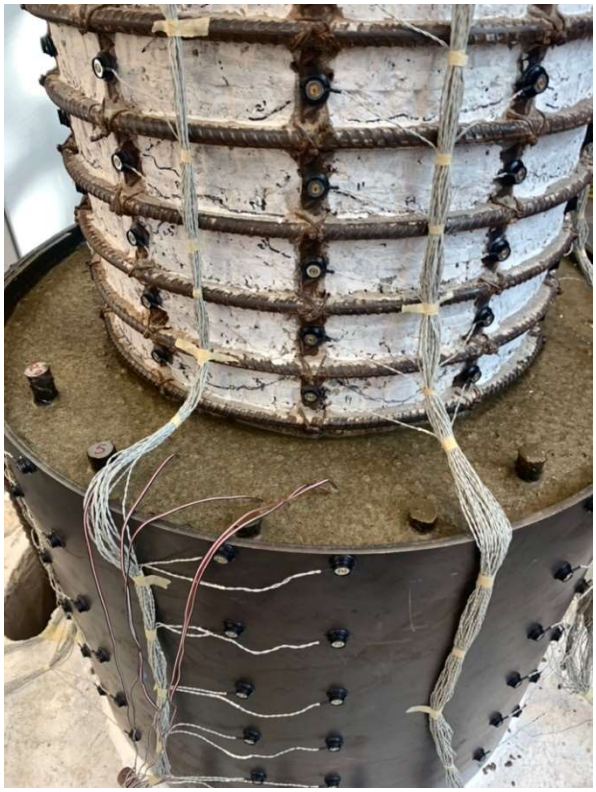


Figure 4.80: Damage During Ductility 1 of the North (left) and South (right) Sides.


Figure 4.81: Damage During Ductility 1.5 of the North (left) and South (right) Sides.

Figure 4.82: Damage During Ductility 2 of the North (left) and South (right) Sides.

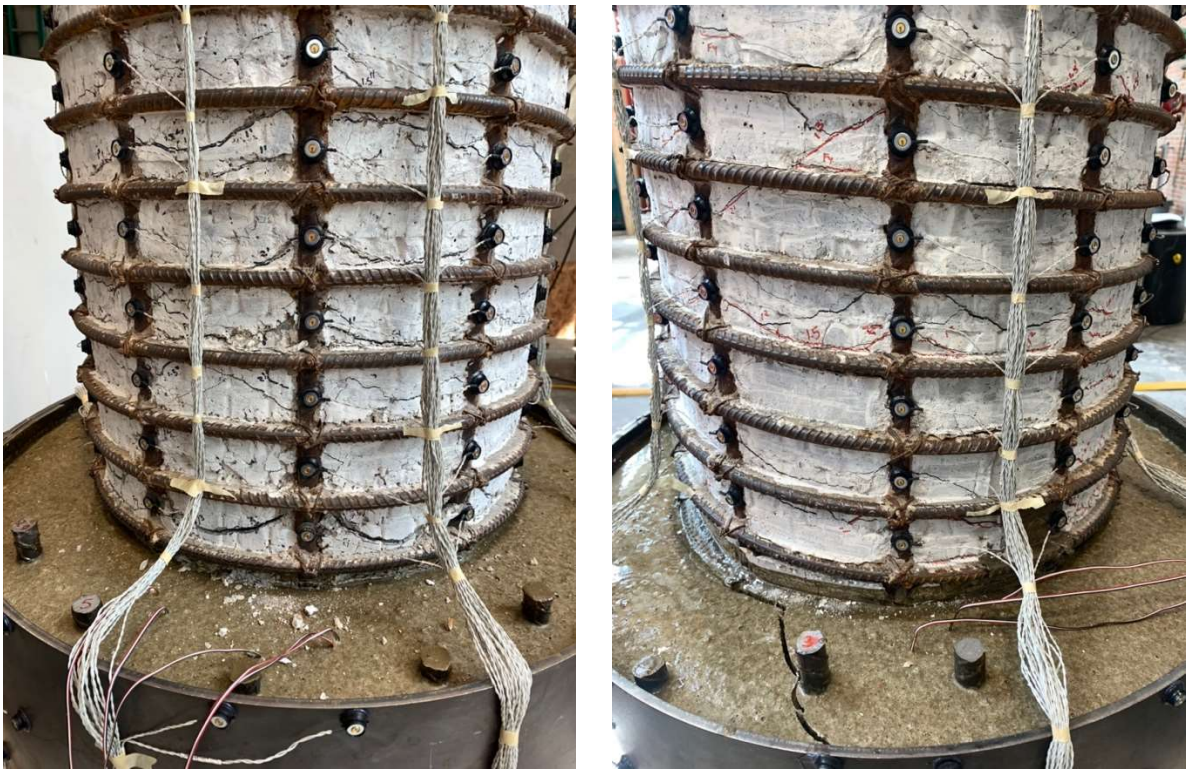

Figure 4.83: Damage During Ductility 3 of the North (left) and South (right) Sides.

Figure 4.84: Damage During Ductility 4 of the North (left) and South (right) Sides.

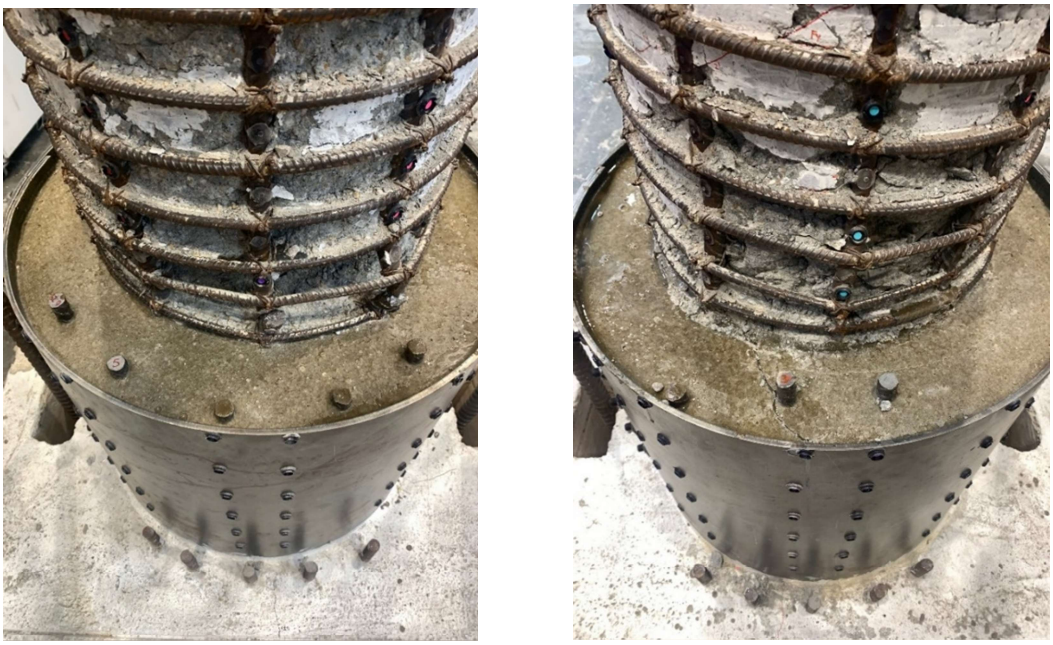

Figure 4.85: Damage after the test when all loose concrete was removed of the North (left) and South (right) sides.

4.7.4 Global response

Figure 4.86 compares the force vs. displacement response of the repaired column with the original column. In this repair test, the repaired column was not able to reach the ductility level reached by the original column. The repaired column test ended after ductility 5. The original column failed at the third cycle of ductility 6.

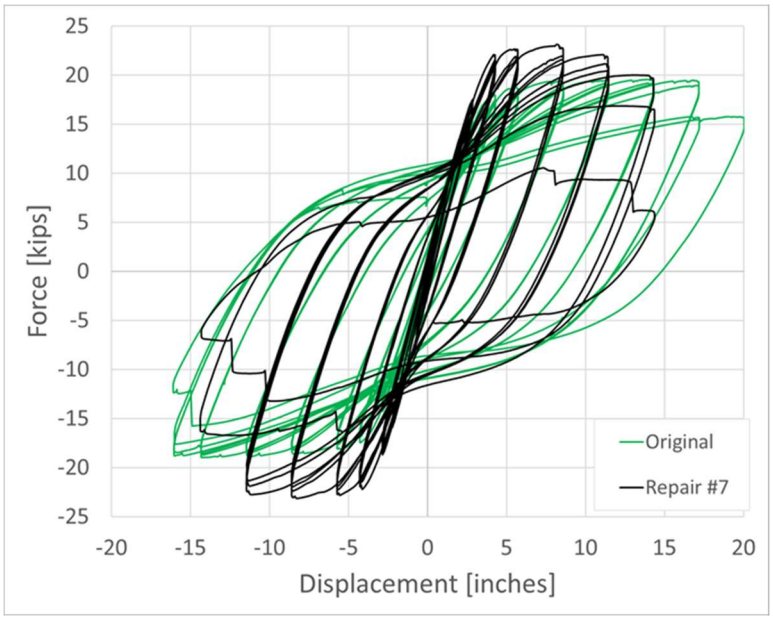

Figure 4.86: Force vs. Displacement of the Original and Repair Column Tests.

The moment vs. displacement response is shown in Figure 4.87, and was produced following the procedure discussed in Section 4.3.4. The effective heights for the original column and repaired column are 156 inches and 134 inches, respectively. For the original column, the distance between the applied load and the top of the footing was 13 feet (156 inches). 4.81 shows that the performance of the repaired column is similar to that of the original column and even has similar stiffness. This is different from the previous repairs where the previous maximum strains above the repair are higher resulting in a softened response.

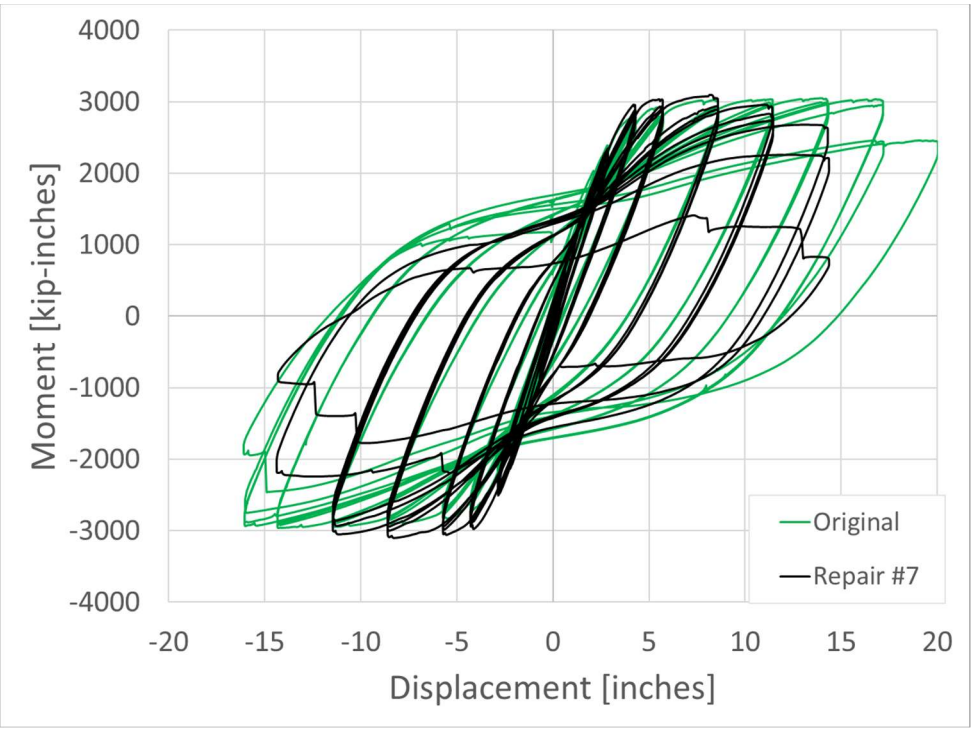

Figure 4.87: Moment vs. Displacement of the Original and Repair Column Tests.

A direct comparison between the force vs. displacement responses for Repairs #6 and #7 is shown in Figure 4.88. It is obvious that Repair #7 has a higher stiffness than Repair #6. The difference in damage conditions at the relocated hinge contribute to this difference in behavior. For Repair #6, the maximum strain from the original test above in the relocated hinge was 0.027, compared to 0.015 for Repair #7. As a reminder, the suggested maximum allowable strain in the relocated hinge is 0.02 based on the recommendations of Krish (2018).

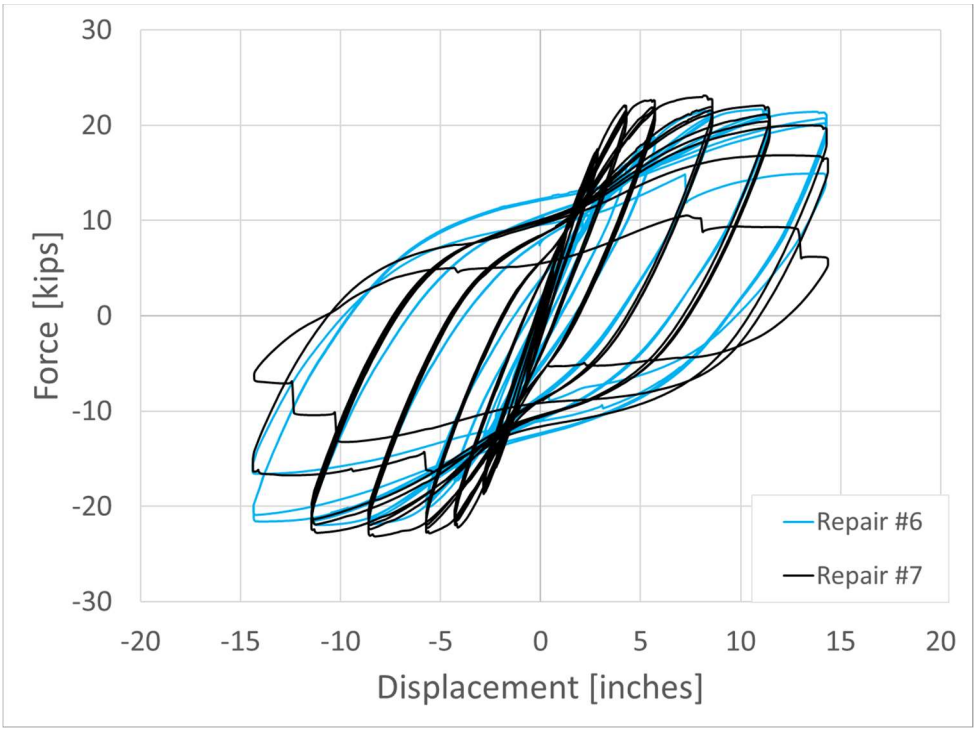

Figure 4.88: Force vs. Displacement of Repair #6 and Repair #7

4.7.5 Local response

A comparison of the strains on the repair bars is not available due to the heat generated by the epoxy grout during casting, which resulted in the strain gauges not working. Optotrak data from the exterior of the repair will be used to discuss the difference in repair performance. The LED markers allow for comparison of the repair rotation. The bottommost row of LED markers was used to trace the displacement relative to an LED on the fixed footing, and the line of best fit was used to determine the angle of repair rotation. Repair #6 (the cementitious grout comparison column) showed more repair rotation, which demonstrates that the epoxy grout did result in a more fixed condition.

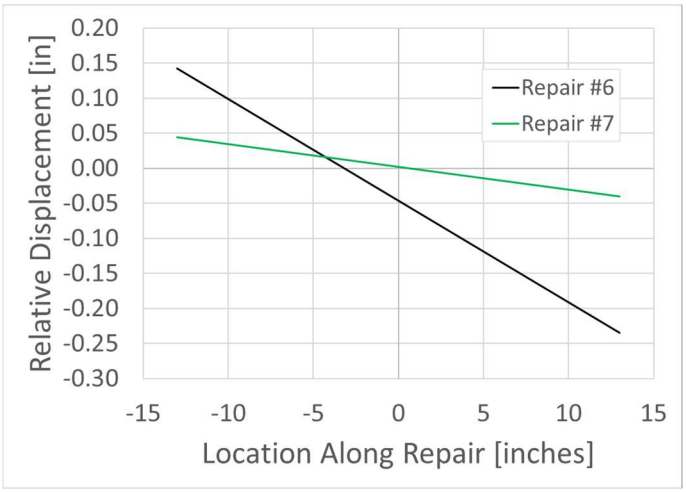

Figure 4.89: Repair Rotation at Ductility 4 for Repair #6 and Repair #7

One implication of this result is that less rotation of the repair leads to an increased flexural demand of the column section to reach the same displacement. The slope of the lines shown in Figure 4.89 at ductility 4 for Repairs #6 and #7 represents the angle of repair rotation.A comparison of the angle at the end of the first push cycle of each ductility level is shown for the two repairs in Figure 4.90. This decrease in repair rotation also suggests that the strain in the repair bars is less than Repair #6, and did not yield.

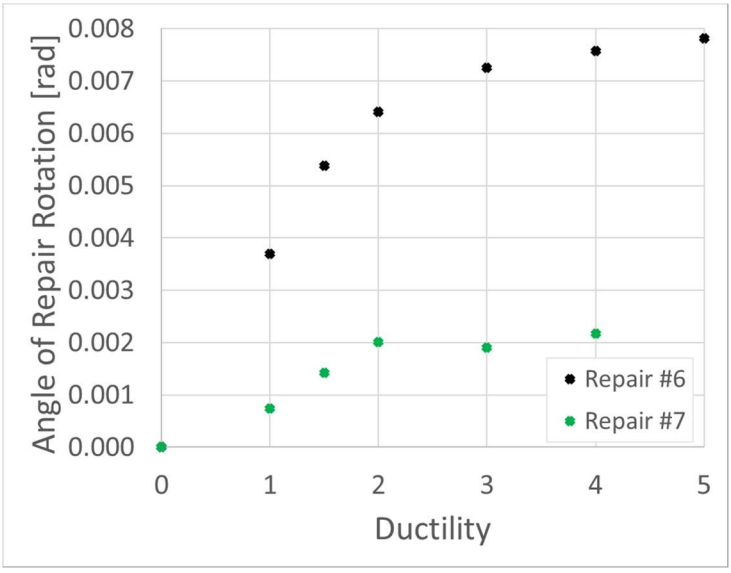

Figure 4.90: Angle of Repair Rotation throughout loading for Repair #6 and Repair #7

4.7.6 Conclusions

This repair used an epoxy grout as the backfill material to determine if it was an acceptable alternative to a cementitious grout in conditions where an epoxy grout would be desirable, such as column to footing connections occurring underwater. The repair performed similarly to Repair #6 with cementitious grout, but experienced less repair rotation; this implies that the design of repair reinforcement is acceptable and perhaps conservative when using an epoxy grout.

4.4 Repair #8

4.8.1 Primary Objective

All of the previous repairs used a lower limit of the steel jacket height equal to 0.9D . This produces an increase in moment demand at the footing, which may overload it in practice. The objective of Repair #8 was to determine the effect of decreasing the repair height, which would also decrease the moment demand at the footing. An additional benefit of reducing the steel jacket height is that it would lead to savings in material costs for the backfill material; however, the height may be limited by the strains in the relocated hinge from previous loading, or by the bond conditions of the fractured bars. The reduced steel jacket height was determined by the development length of the repair reinforcing bars, resulting in a height of 13.5 inches , or 0.75D.

4.8.2 Damaged Column and Repair

The initial damage condition of this column consisted of 2 fractured bars on the South side and 1 fractured bar on the North side. The perimeter concrete was chipped around fractured bars. The repair reinforcement consisted of 8 Grade 80 No. 5 bars which were anchored using epoxy in drilled holes. The cross section for the repair is shown in Figure 4.91. The properties for the original column and repair are summarized in Table 4.8.

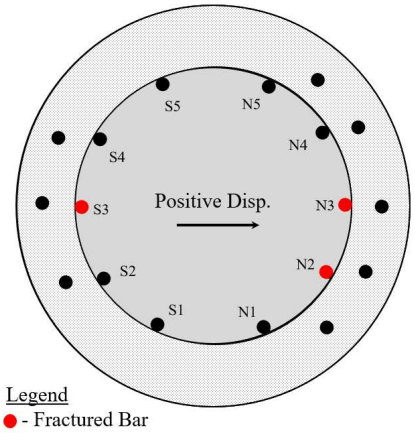

Figure 4.91: Cross section for Repair #8 and Completed Repair

Table 4.8: Column and Repair Properties for Repair #8.

	Original & Comparison Column	**Repair**
Column	Thangjitham Test 2	Repair #8
Geometry	Height = 8 ft Diameter = 18 inches	Height = 13.5 inches Diameter = 26 inches
Longitudinal Steel	10 #6 (ρ_l = 1.6%) f_y = 86.1 ksi ε_y = 0.30% f_u = 113.7 ksi ε_u = 9.0%	8 #5 bars f_y = 84.0 ksi ε_y = 0.35%
Transverse Steel	#3 Spirals @ 2" (ρ_s = 1.0%) f_y = 79 ksi ε_y = 0.48% f_u = 117 ksi ε_u = 7.6%	¼" A36 Steel Connected by 12 pre-tensioned ASTM A490 bolts with 5/8" diameter
Concrete/Grout Strength	f'_c = 6.51 ksi	f'_c = 5.48 ksi
Axial Load	ALR = 10% P = 144 kips	ALR = 10% P = 144 kips
Load Path	Δ_y' = 0.87 inches Δ_y = 1.15 inches	Δ_y' = 0.87 inches Δ_y = 1.15 inches
Bar Fractures	N3, S2, and S3	N2, N3, N4, and S2

4.8.3 Test progression

The damage progression is shown in the following series of Figures 4.92 through 4.98. Each picture was taken at the peak displacement of each ductility cycle, with the shown side in tension.

Hairline cracks in the repair grout formed on the South side at 0.75Fy'. Circumferential grout cracks formed in the repair at the base of the column during the first yield cycle. During ductility 1, the largest grout crack measured was 0.02 inches while the largest crack in the column measured was around 0.01 inches. The column continued to crack along the height and hairline cracks continued to form during ductility 1.5. During ductility 2, the grout cracks remained constant while the column cracks increased to 0.025 in. At the end of ductility 2, the column concrete began to crush.

During ductility 3, a difference in behavior was noticed for the North and South sides. On the North side, the most extreme bar (N3) began to exhibit low levels of buckling. The most extreme bar on the South side (S3) remained straight and the repair grout cracks remained open, even when that side was in compression. The grout uplifted and large chunks were removed during ductility 5. Buckling of the most extreme bar (N3) became more severe during the second cycle of ductility 5, and the bar fractured at the end of the first cycle of ductility 6. During the second cycle, two more bars on the North side (N2 and N4) buckled. The extreme bar on the South side (S3) never buckled or fractured, and the next most extreme bar (S2) buckled and fractured during ductility 6.

Figure 4.92: Initial Damage of the North (left) and South (right) Sides.

Figure 4.93: Damage During Ductility 1 of the North (left) and South (right) Sides.

Figure 4.94: Damage During Ductility 2 of the North (left) and South (right) Sides.

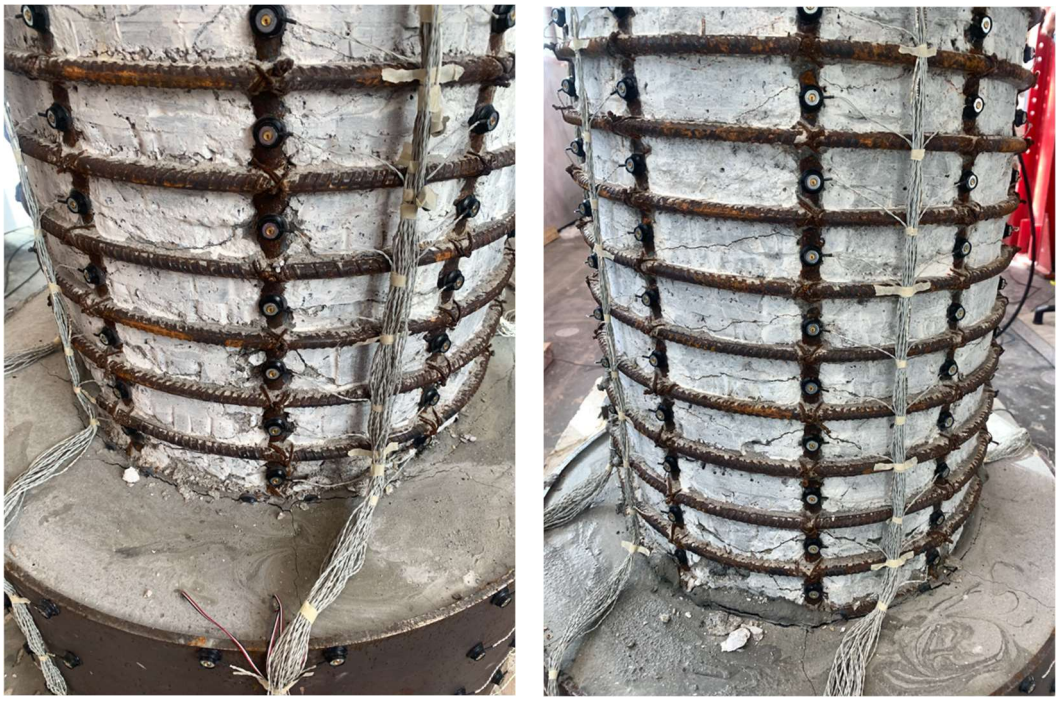

Figure 4.95: Damage During Ductility 3 of the North (left) and South (right) Sides.

Figure 4.96: Damage During Ductility 4 of the North (left) and South (right) Sides.

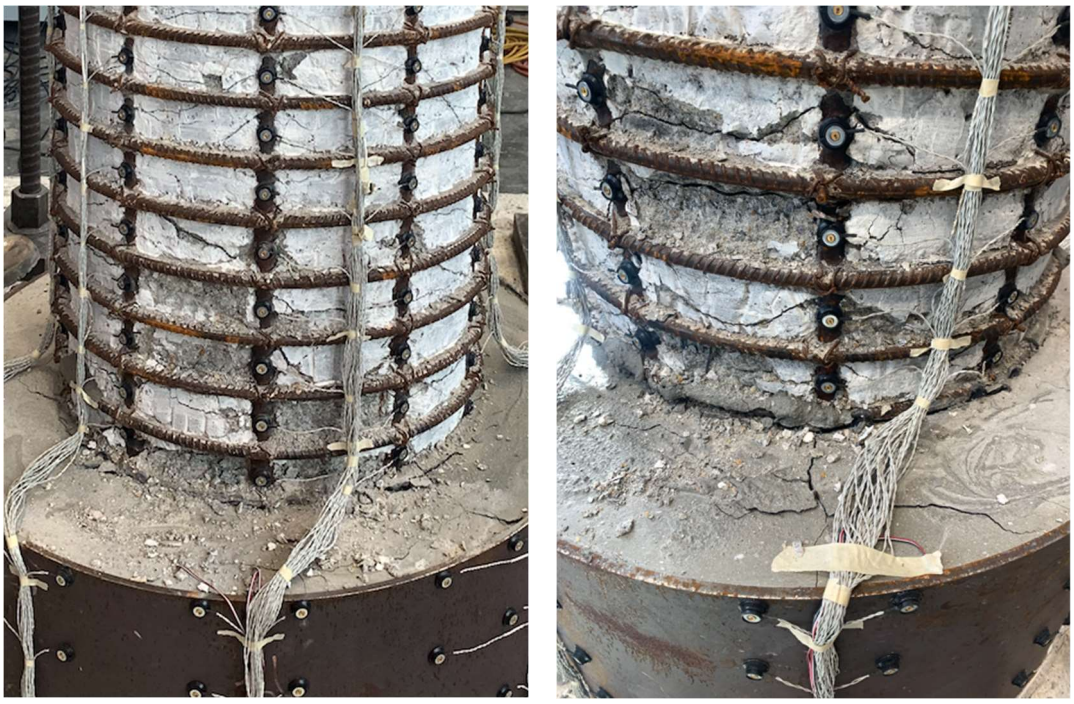

Figure 4.97: Damage During Ductility 5 of the North (left) and South (right) Sides.

Figure 4.98: Final Damage of the North (left) and South (right) Sides.

4.8.4 Global response

Figure 4.99 shows the force vs. displacement response in which this column reached the same displacement capacity as the original; the repair first experienced fracture during the first cycle of ductility 6, while the original completed an additional cycle before fracture. The repair response does display some strength degradation, especially after the extreme bar on the South side debonds during the second cycle of ductility 5.

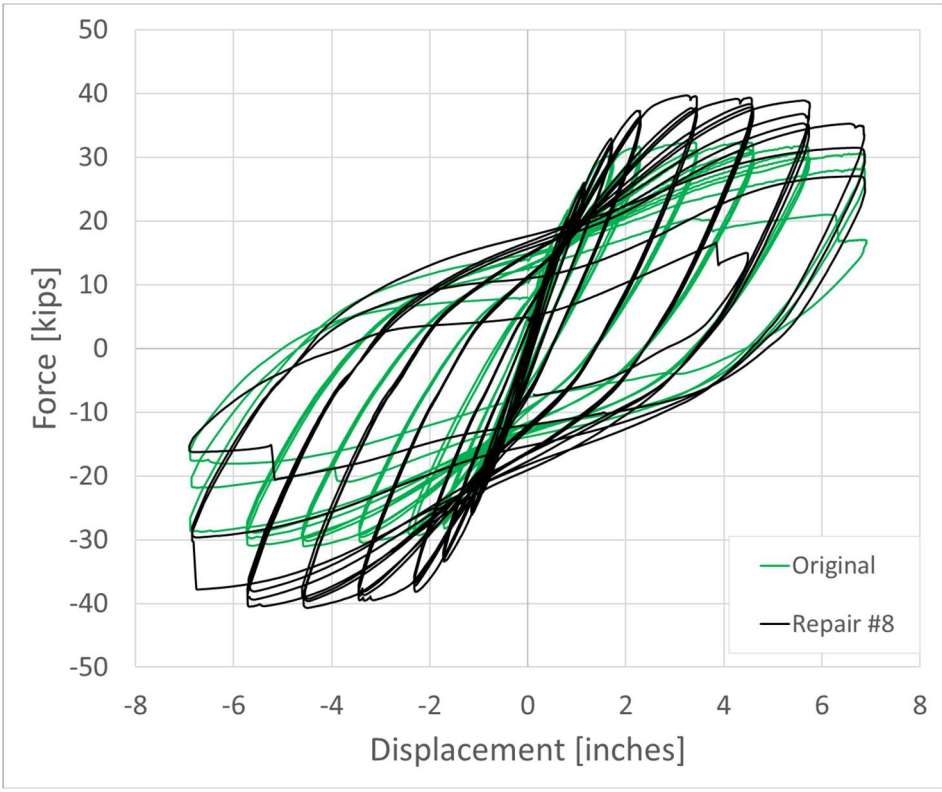

Figure 4.99: Force vs. Displacement of the Original and Repair Column Tests.

Figure 4.100 shows the moment vs. displacement response where it can be seen that the repaired column had an increased moment capacity compared to the original column. However, the stiffness of the repaired column was lower, because decreasing the height of the repair results in higher levels of damage at the relocated hinge, resulting in lower stiffness.

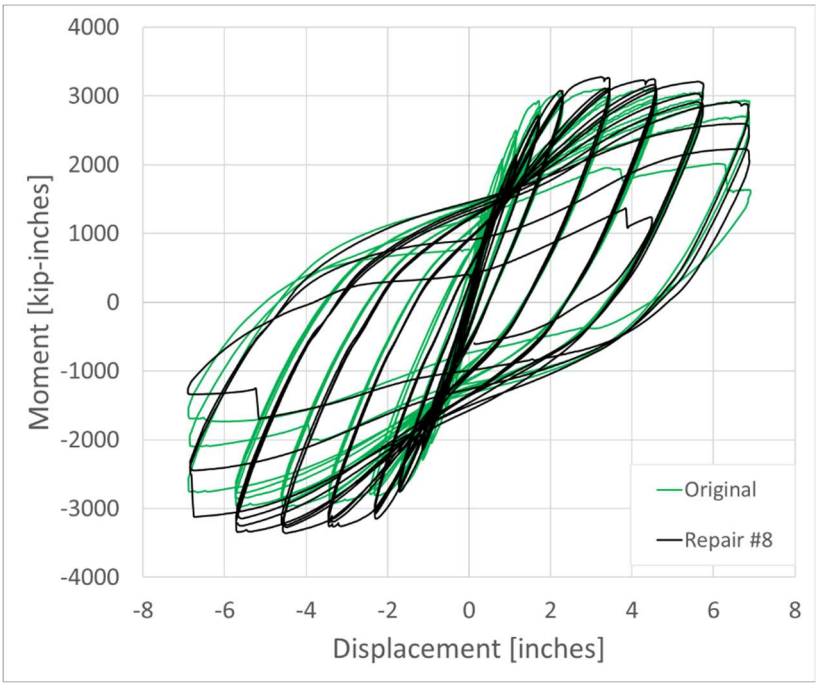

Figure 4.100: Moment vs. Displacement of the Original and Repair Column Tests.

4.8.5 Local response

During the test, the most extreme bar on the North side (N3) buckled and fractured above the steel jacket. On the South side, however, S3 did not fracture and the test ended with the fracture of the next most extreme bar (S2). Figure 4.101 shows the strain history of S3, which shows the tensile strains decreasing in ductility 5, demonstrating that this bar debonded and stopped contributing to the strength of the repaired column. This is also apparent in the force vs. displacement response in Figure 4.99 as the difference in forces between the first and second push cycles of ductility 5.

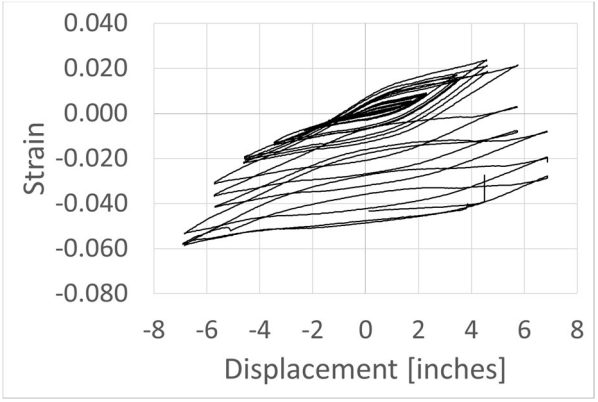

Figure 4.101: Strain History of S3 in Repair #8.

4.8.6 Conclusions

This repair investigated the use of a shorter repair height with the aim of decreasing the moment demand on the footing. The performance of the repaired column was similar to those with repair heights of 0.9D. Decreasing the limit of repair height below 0.9D is possible, provided the damage level at the relocated hinge is considered and the repair is designed so fractured bars are anchored within the repair.

4.9 Repair #9

4.9.1 Primary Objective

In all of the previous repairs with fully anchored bars, the displacement capacity of the repaired column is reduced relative to the original column response, due to the change in stiffness associated with relocating the plastic hinge. The objective of Repair #9 was to improve the displacement capacity of the repaired column by using a Carbon FRP wrap on the relocated plastic hinge region to match or exceed the original global performance. The CFRP was designed to provide sufficient confinement such that the repaired section has an increased curvature capacity.

4.9.2 Damaged Column and Repair

The initial damage condition of this repair was 1 fractured bar on the North side and 2 fractured bars on the South side. The perimeter concrete was chipped around the fractured bars. The cross section and completed repair is shown in Figure 4.102. To compare the influence of the CFRP wrap with Repair #8, the repair height was 13.5 inches. Although 13.5 inches was not sufficient to anchor all of the previously fractured bars in Repair #8, the CFRP wrap could improve the bond conditions, while minimizing the increase in moment demand at the footing. The properties for the original column and repair are summarized in Table 4.9.

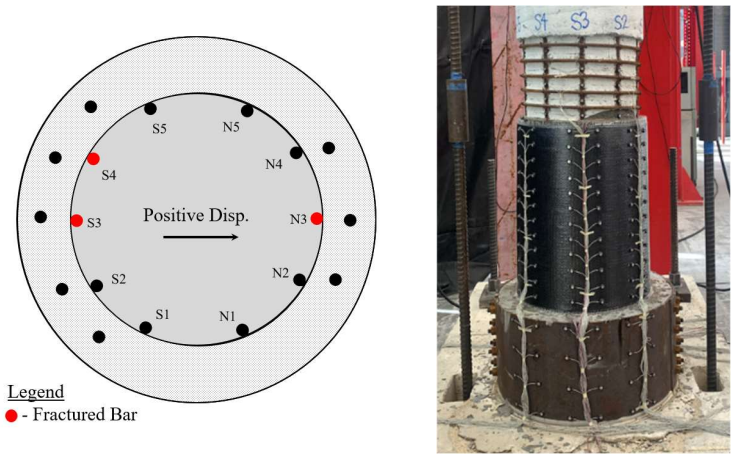

Figure 4.102: Cross Section for Repair #9.

Table 4.9: Column and Repair Properties for Repair #9.

	Original & Comparison Column	**Repair**
Column	Thangjitham Test 2	Repair #9
Geometry	Height = 8 ft Diameter = 18 inches	Height = 13.5 inches Diameter = 26 inches
Longitudinal Steel	10 #6 (ρ_l = 1.6%) f_y = 86.1 ksi ε_y = 0.30% f_u = 113.7 ksi ε_u = 9.0%	8 #5 bars f_y = 84.0 ksi ε_y = 0.35%
Transverse Steel	#3 Spirals @ 2" (ρ_s = 1.0%) f_y = 79 ksi ε_y = 0.48% f_u = 117 ksi ε_u = 7.6%	¼" A36 Steel Connected by 12 pre-tensioned ASTM A490 bolts with 5/8" diameter 3 layers CFRP wrap
Concrete/Grout Strength	f'_c = 6.51 ksi	f'_c = 7.50 ksi
Axial Load	ALR = 10% P = 144 kips	ALR = 10% P = 144 kips
Load Path	Δ_y' = 0.87 inches Δ_y = 1.15 inches	Δ_y' = 0.87 inches Δ_y = 1.15 inches
Bar Fractures	N3, S2, and S3	N2, N3, N4, and S3

4.9.3 Test progression

At the first yield displacement, the epoxy of the CFRP wrap began to audibly crack between the fibers, along the height of the column, as shown in Figure 4.103. These noises continued each time the column was pushed or pulled to a larger displacement. Transverse cracks between the fibers of the CFRP were distributed along the height. At the base of the CFRP, a circumferential crack formed in the grout, while the majority of the grout remained undamaged. The circumferential crack was measured to be .08 inches at ductility 1.5 and grew with each ductility cycle. During ductility 3, the concrete at the top of the footing began to uplift, which indicated that the repair was rotating and not fully fixed at the base.

Because of the presence of the CFRP wrap, the longitudinal bars were not visible during the test, and they could not be instrumented with Optotrak LEDs to obtain direct strain measurements. The inferences about longitudinal bar behavior throughout the progression of the test were based on the changes in force applied by the actuator. During the first cycle of ductility 8, there was a loud noise and drop in force which indicated a bar fracture on the South side. In the following pull, 3 distinct noises and drops in force occurred. After the test concluded, the grout at the interface between the steel repair and CFRP was removed to determine the fracture locations. All 4 bar fractures that were heard in the test were found approximately one inch below the FRP, as shown in Figure 4.108. The bars did not show any sign of buckling.

Figure 4.103: Damage During Ductility 1.5 of the North (left) and South (right) Sides.

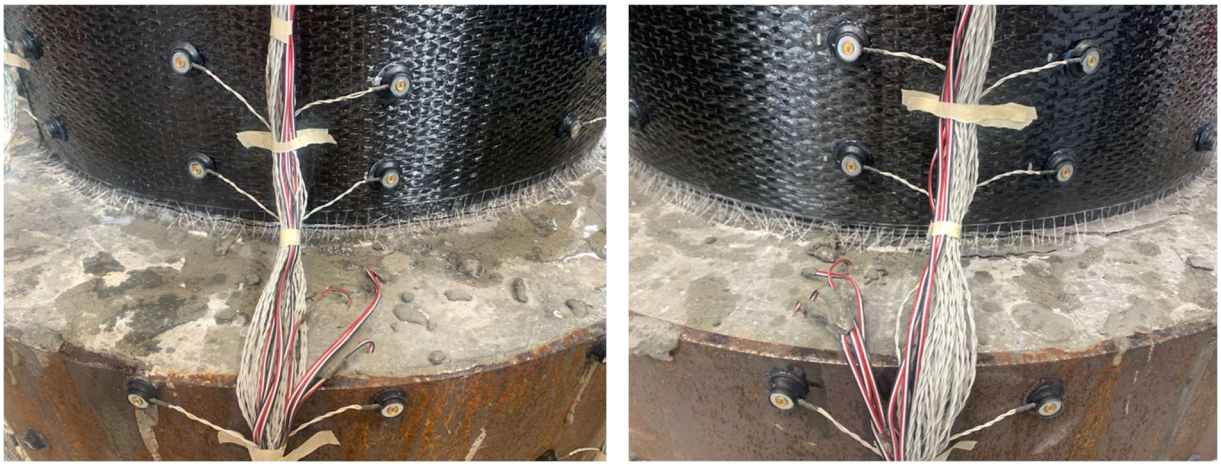

Figure 4.104: Damage During Ductility 2 of the North (left) and South (right) Sides.

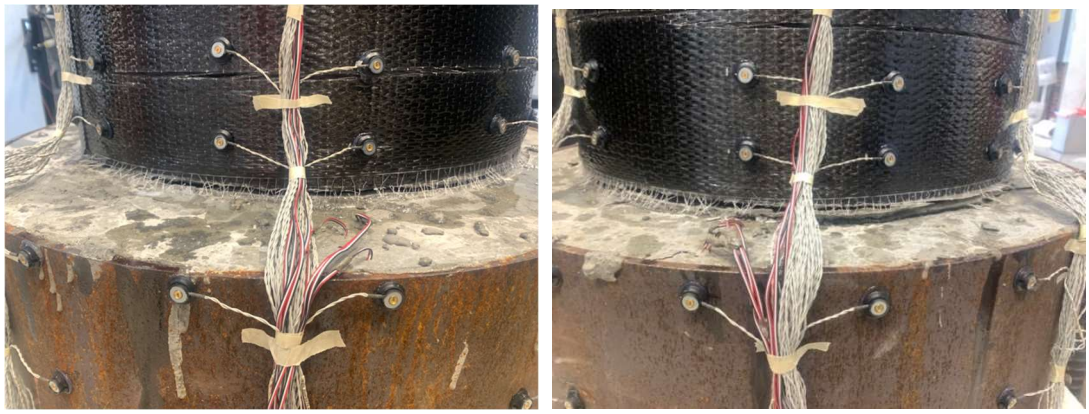

Figure 4.105: Damage During Ductility 4 of the North (left) and South (right) Sides.

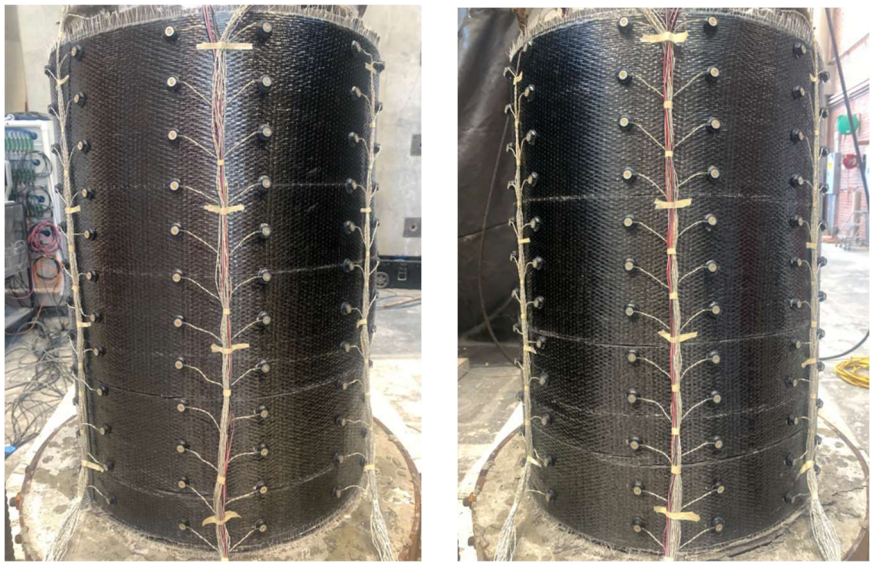

Figure 4.106: Damage During Ductility 6 of the North (left) and South (right) Sides.

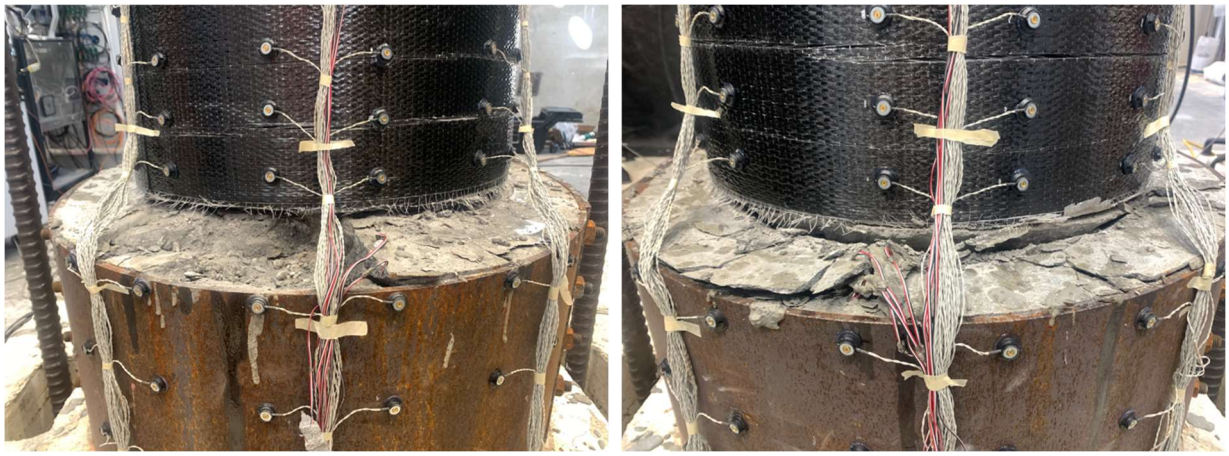

Figure 4.107: Final Damage of the North (left) and South (right) Sides.

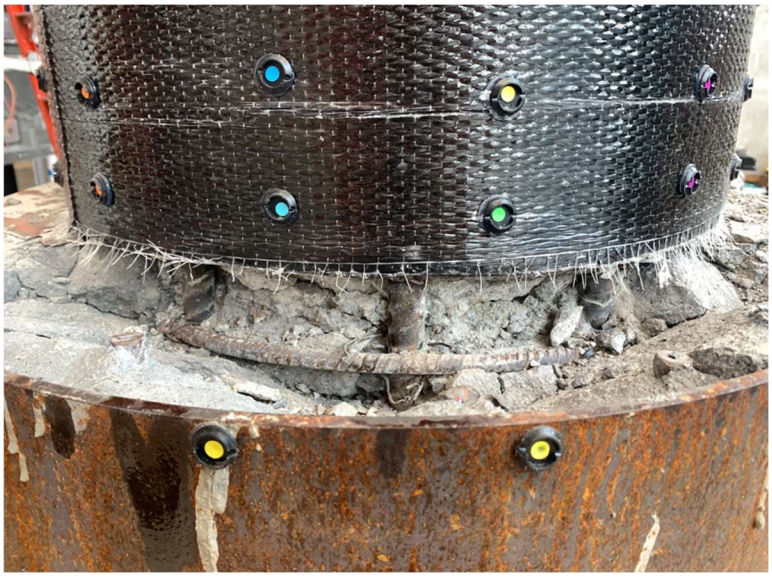

Figure 4.108: Removal of Grout to Locate Fracture Points.

4.9.4 Global response

In Figure 4.109, the force vs. displacement response shows that the repair was able to maintain strength without degradation until bars began to fracture. In previous repairs where the original ductility capacity was met, the response softened before reaching the target ductility. The displacement capacity for this repair exceeded that of the original column. The original column completed 3 cycles at ductility

6, while the repaired column completed 3 cycles at ductility 7 and bars fractured during the first push and pull of ductility 8.

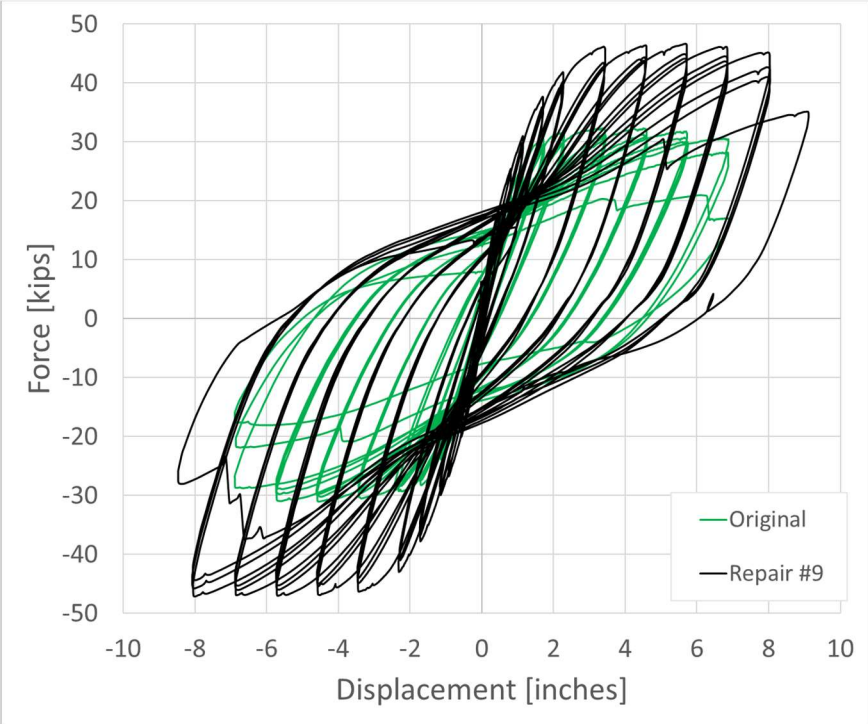

Figure 4.109: Force vs. Displacement of the Original and Repair Column Tests.

It is evident in the moment vs. displacement response shown in Figure 4.110 that the moment is higher for the repaired column compared to the original. Part of the reason for this increased moment at the relocated hinge is the presence of the confined cover concrete. In the original column, the cover is blocked out to allow for instrumentation of the reinforcing steel, and the moment would theoretically be larger if the cover was included. Including the cover in the original column moment would reduce the difference in moments for the two tests, but the moment capacity would still increase because of the confinement from the CFRP wrap, which engages the concrete cover as well as increases the compressive strength and strain capacity of the concrete core.

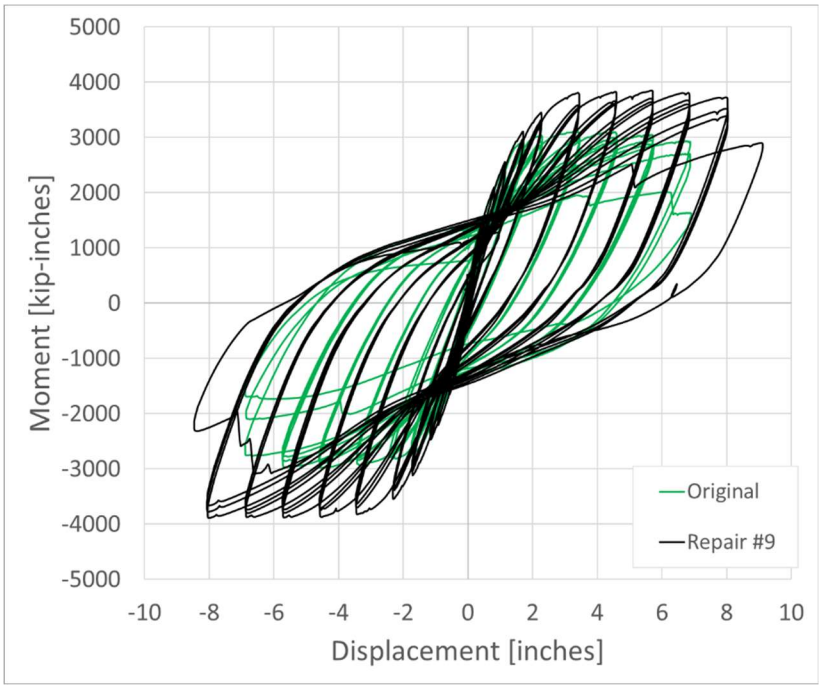

Figure 4.110: Moment vs. Displacement of the Original and Repair Column Tests.

Figure 4.111 provides a direct comparison of the moment vs. displacement response between Repairs #8 and #9. The repairs are nominally identical, except Repair #9 has the addition of the CFRP wrap. The main difference in response is the additional moment capacity from the engaged cover and increased strength of the confined core. The CFRP wrap did result in a larger displacement capacity than Repair #8, as well as a decrease in strength degradation at larger ductilities.

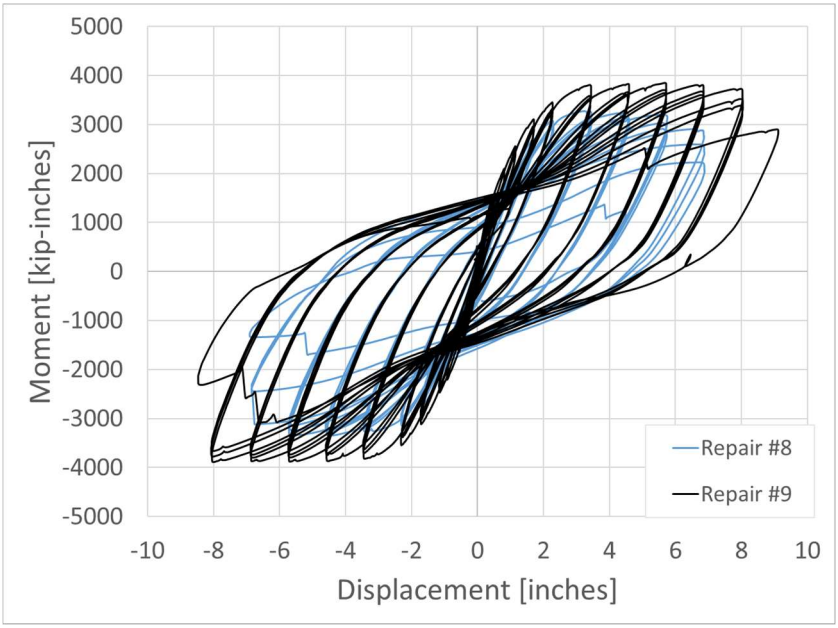

Figure 4.111: Moment vs. Displacement of Repair #8 and Repair #9.

4.9.5 Local response

Figure 4.112 shows the strain history for the hoop strains in the FRP, calculated using Optotrak LEDs placed on the CFRP wrap. This is shown for the maximum measured hoop strain, which was found at the base of the CFRP wrap on the South side of the column. When the column is pulled to negative displacements, the South side of the column is in compression, resulting in larger dilation and therefore leading to larger strains. The maximum measured CFRP hoop strain was approximately 0.5%. The ultimate tensile elongation is determined by testing the CFRP in uniaxial tension, and experimentation shows that the true failure strain is reduced for hoop fibers. Considering the ultimate tensile elongation for the CFRP used in this repair is 1.7%, according to the manufacturer data sheet, and the efficiency factor of 0.55 (ACI 440.2R-08, 2008), the expected maximum CFRP hoop strain would be 0.935%. This suggests that the number of CFRP wrap layers could be reduced while still providing effective confinement, which was tested in Repair #10.

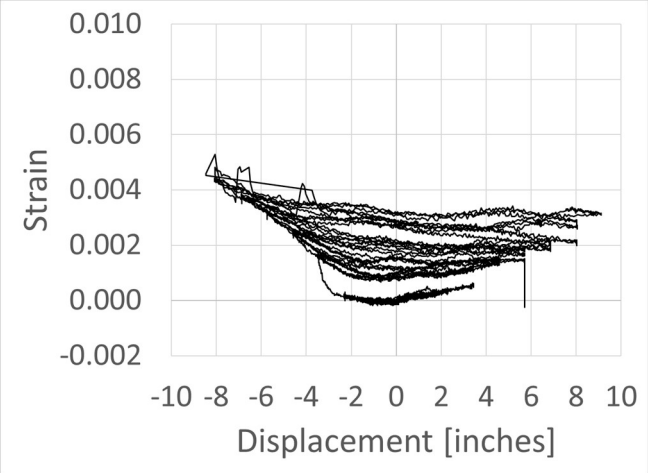

Figure 4.112: Hoop Strain History of CFRP wrap in Repair #9.

4.9.6 Conclusions

This repair used a CFRP wrap to increase the displacement capacity of the repaired column to match the original column. The results of this test showed that the CFRP wrap was effective in delaying buckling and bar fracture in the new plastic hinge location. The increased confinement from the CFRP wrap resulted in a larger moment capacity of the repaired section compared to the original column section. The measured hoop strains in the CFRP indicate that the confinement could be reduced by reducing the number of CFRP wrap layers, while still achieving similar displacement capacities and reducing the increase in moment demand on the footing.

4.10 Repair #10

4.10.1 Primary Objective

The data from Repair #9 showed that the CFRP wrap could potentially be used more efficiently because the maximum experimental strain was sufficiently less than the expected rupture strain of the CFRP wrap. The objective of Repair #10 was to determine the effect of reducing the number of CFRP layers, which would be beneficial in reducing construction effort, installation time, and material use, as well as reduce the increase in moment demand on the footing.

4.10.2 Damaged Column and Repair

The damage condition for this column was 1 fractured bar on the North side and 2 fractured bars on the South side. The perimeter concrete was chipped around the fractured bars. The cross section of the repair consisted of 8 Grade 80 No. 6 bars and is shown in Figure 4.113. To ensure that all of the previously fractured bars would remain anchored, the repair height was 0.9D, or 16.5 inches. The number of layers used for the CFRP wrap was reduced from 3 layers to 2 layers. The properties for the original column and repair are summarized in Table 4.10.

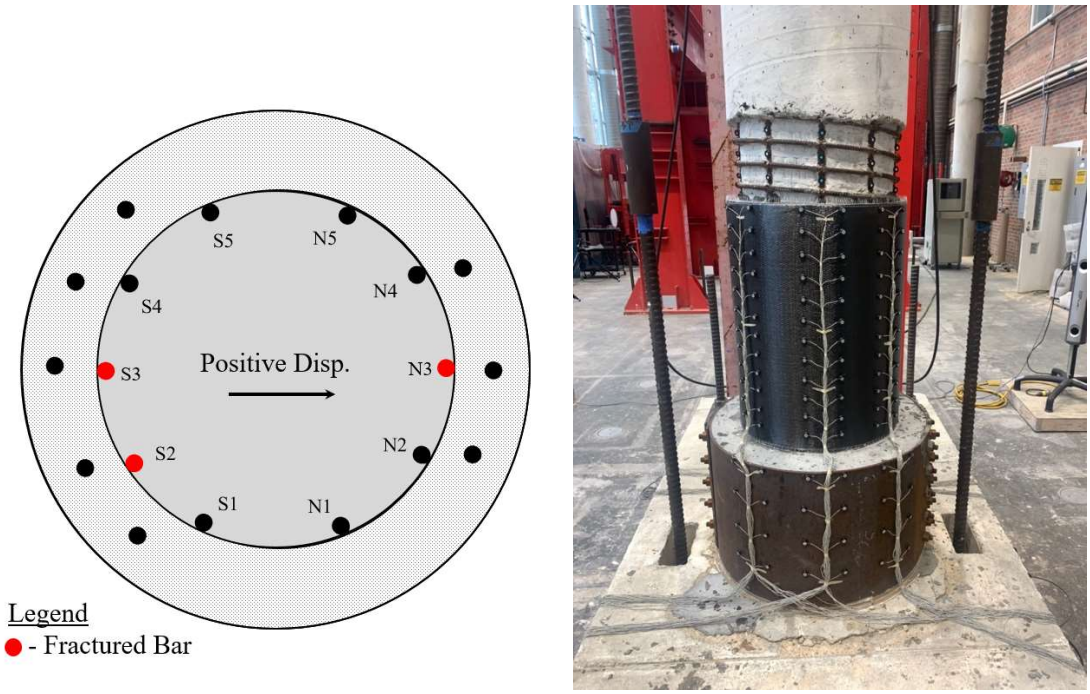

Figure 4.113: Cross section for Repair #10

Table 4.10: Column and Repair Properties for Repair #10.

	Original & Comparison Column	**Repair**
Column	Thangjitham Test 2	Repair #10
Geometry	Height = 8 ft Diameter = 18 inches	Height = 16.5 inches Diameter = 26 inches
Longitudinal Steel	10 #6 (ρ_l = 1.6%) f_y = 86.1 ksi ε_y = 0.30% f_u = 113.7 ksi ε_u = 9.0%	8 #5 bars f_y = 84.0 ksi ε_y = 0.35%
Transverse Steel	#3 Spirals @ 2" (ρ_s = 1.0%) f_y = 79 ksi ε_y = 0.48% f_u = 117 ksi ε_u = 7.6%	¼" A36 Steel Connected by 15 pretensioned ASTM A490 bolts with 5/8" diameter 2 layers CFRP wrap
Concrete/Grout Strength	f'_c = 6.51 ksi	f'_c = 7.62 ksi
Axial Load	ALR = 10% P = 144 kips	ALR = 10% P = 144 kips
Load Path	Δ_y' = 0.87 inches Δ_y = 1.15 inches	Δ_y' = 0.87 inches Δ_y = 1.15 inches
Bar Fractures	N3, S2, and S3	N3, S2, S3, and S4

4.10.3 Test progression

Photos of the test progression are shown in Figure 4.114 through Figure 4.121. Similar to the previous repair, the epoxy began to audibly crack around the first yield displacement, and a hairline circumferential grout crack formed at the base of the CFRP. However, this repair displayed more cracking in the grout, starting around ductility 2. Similar to Repair #9, transverse cracks formed in the FRP around ductility 1.5, and a concentrated crack at the base of the FRP formed during ductility 2. Cracks at the top of the grout also formed. The extreme bar on the South side (S3) fractured during

ductility 5. During the final cycles of ductility 6, the extreme bar on the North side (N3) fractured, as well as the two adjacent South side bars (S2 and S4).

After the test concluded, the grout was chipped away to find the fracture points at similar locations to Repair #9. However, this time the bars did exhibit a buckled shape. This is believed to be due to either: the 2 layers of CFRP wrap not providing sufficient confinement to prevent or delay bar buckling; or a weaker top surface of grout which allowed the bars to buckle.

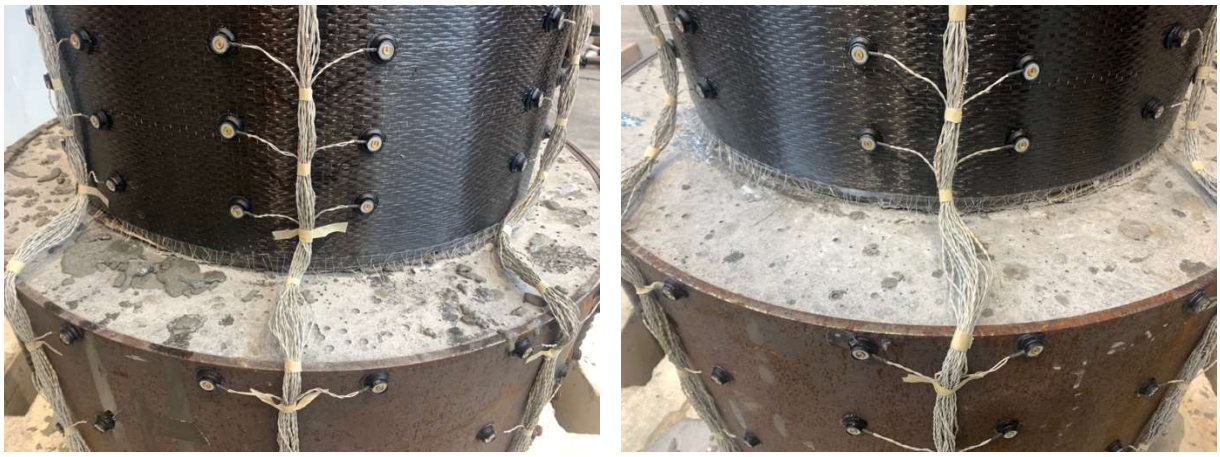

Figure 4.114: Damage During Ductility 1.5 of the North (left) and South (right) Sides.

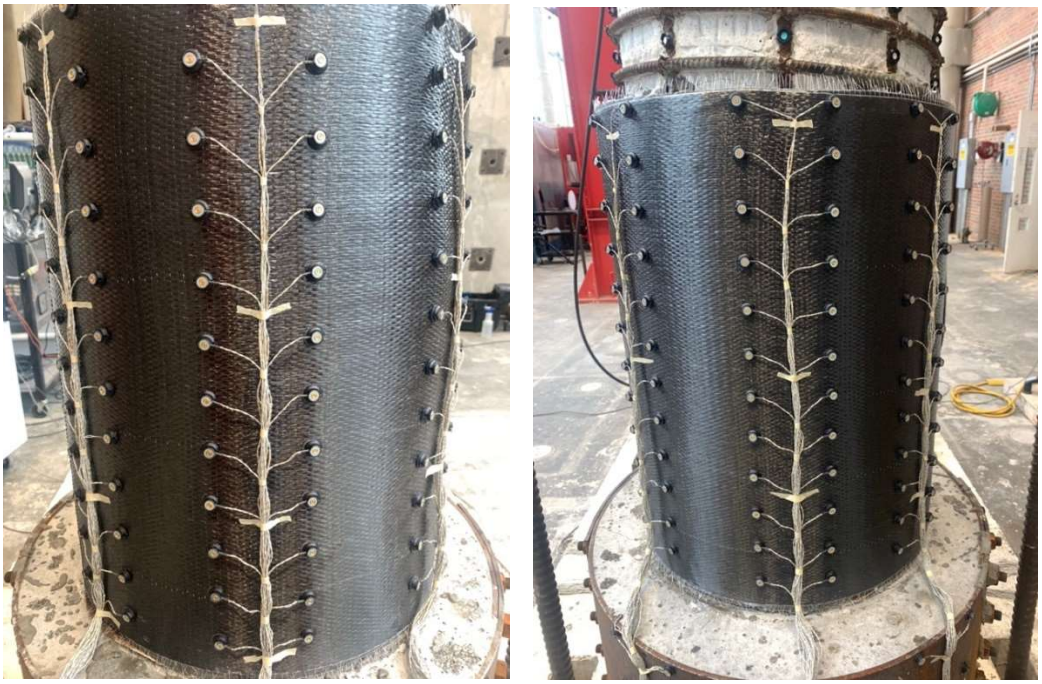

Figure 4.115: Damage During Ductility 2 of the North (left) and South (right) Sides.

Figure 4.116: Damage Below CFRP During Ductility 2 of the North (left) and South (right) Sides.

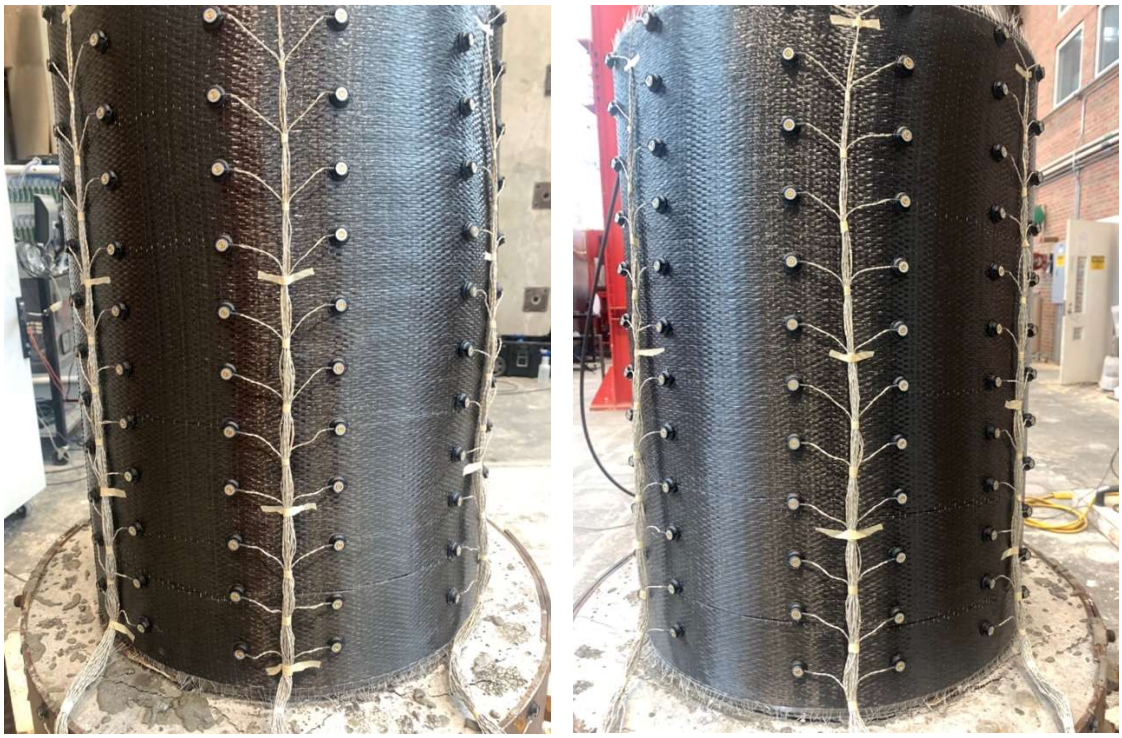

Figure 4.117: Damage During Ductility 3 of the North (left) and South (right) Sides.

Figure 4.118: Damage Below CFRP During Ductility 3 of the North (left) and South (right) Sides.

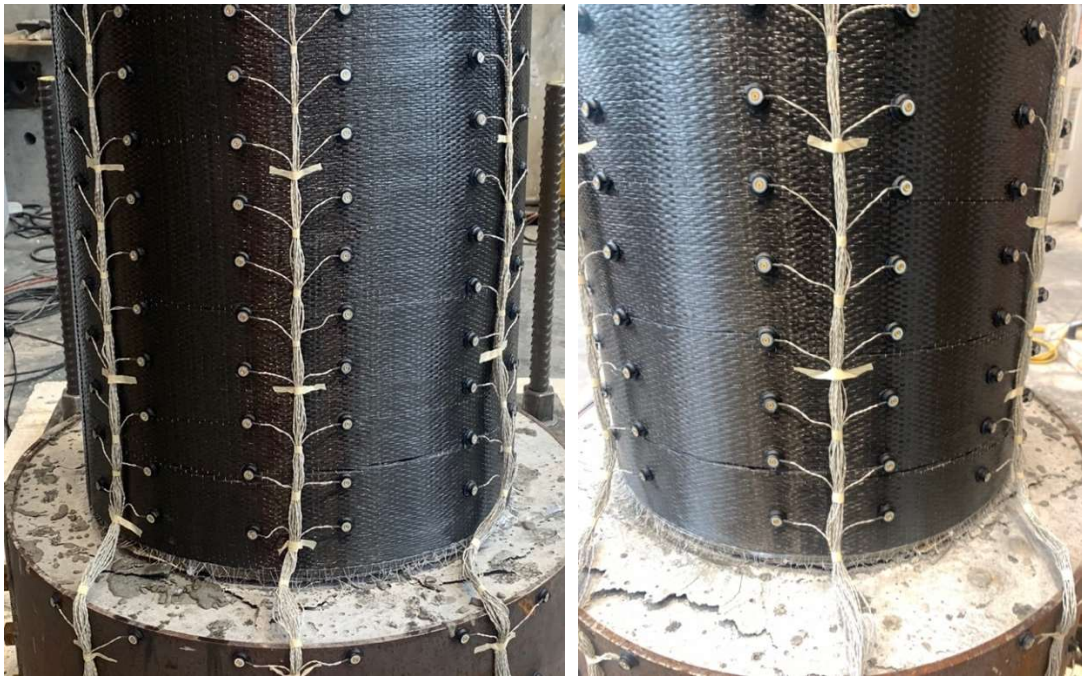

Figure 4.119: Damage During Ductility 4 of the North (left) and South (right) Sides.

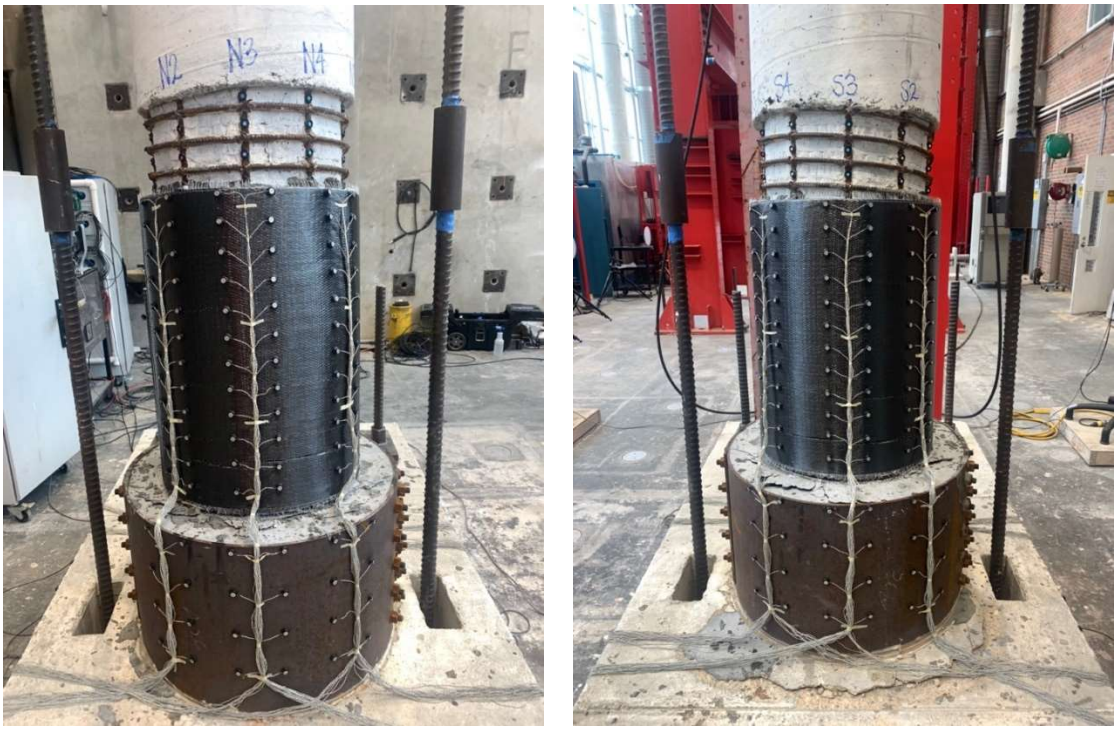

Figure 4.120: Damage During Ductility 5 of the North (left) and South (right) Sides.

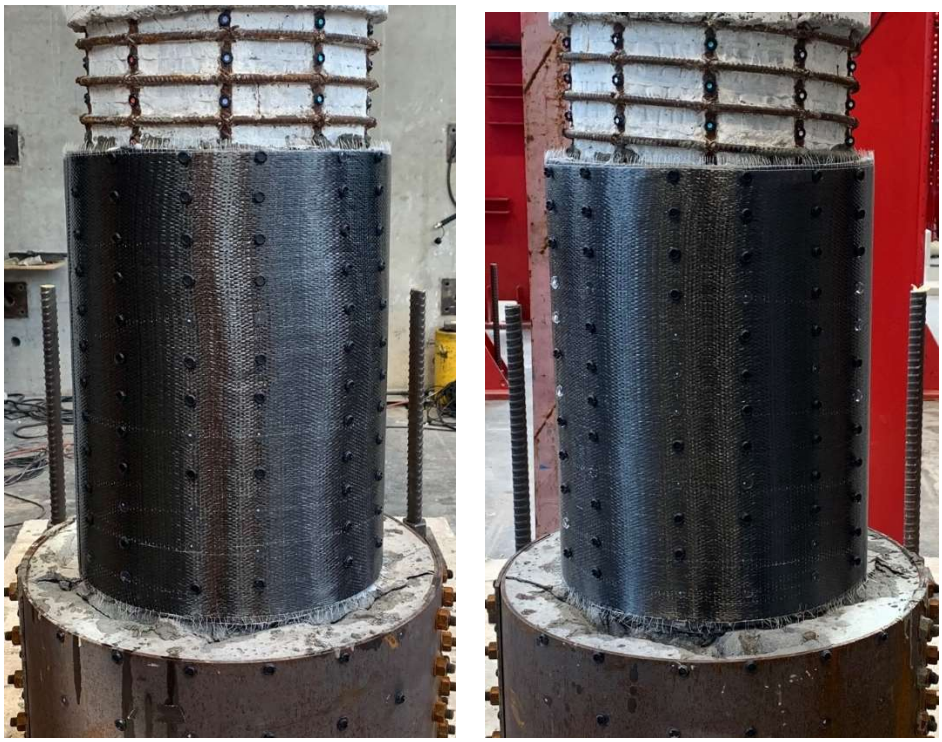

Figure 4.121: Final Damage of the North (left) and South (right) Sides.

4.10.4 Global response

Figure 4.122 shows the force vs. displacement response for Repair #10. In this test, the first fracture for the repaired column occurred during ductility 5 while the original column had an ultimate displacement ductility of 6. Compared to Repair #9 which had an additional layer of the CFRP wrap, this column exhibits slightly more strength degradation, but still maintains most of its strength until bar fracture.

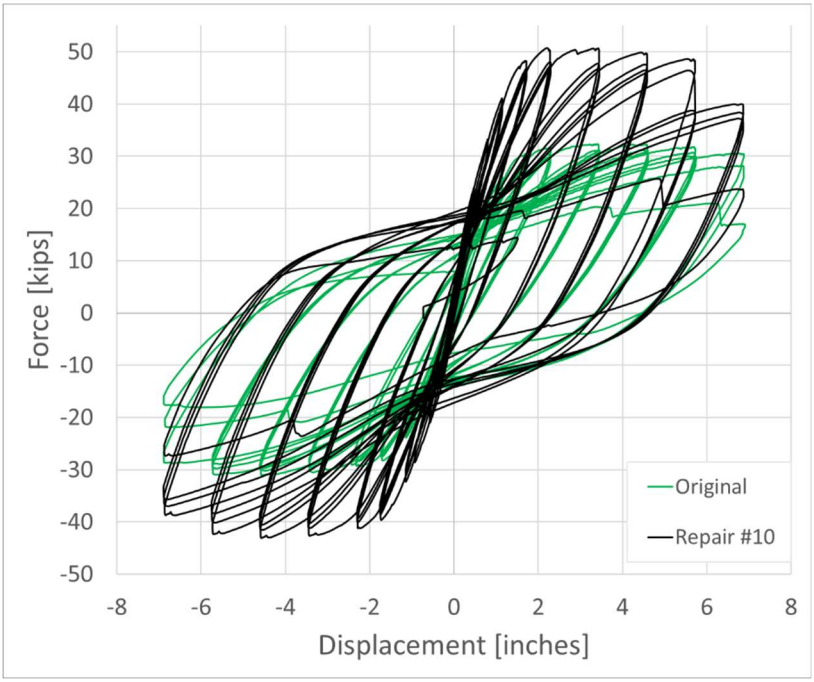

Figure 4.122: Force vs. Displacement of the Original and Repair Column Tests.

Comparing the moment vs. displacement responses in Figure 4.108, the moment in the repair is significantly higher than the original column. This is because of the concrete cover that is now confined and providing additional capacity, as discussed in Section 4.9.4.

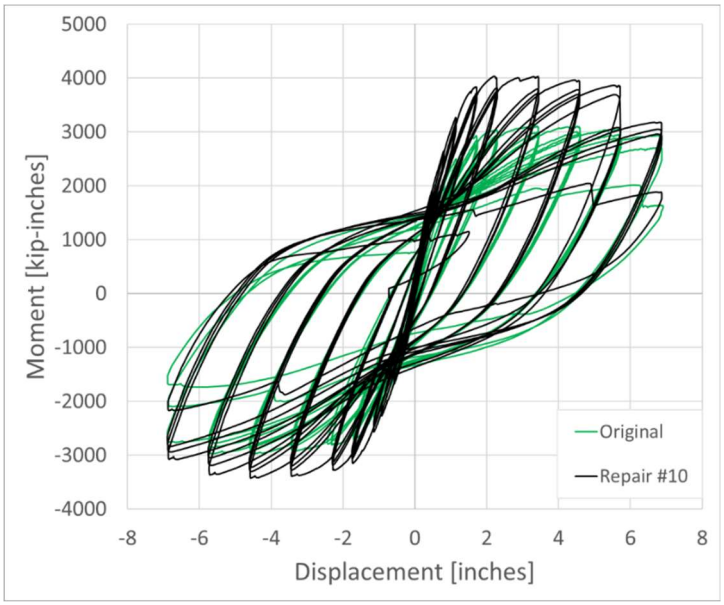

Figure 4.123: Moment vs. Displacement of the Original and Repair Column Tests.

The moment vs. displacement response is compared for Repairs #9 and #10 in Figure 4.124. Repair #9 used 3 layers of CFRP wrap and a repair height of 13.5 inches, while Repair #10 used 2 layers of CFRP wrap and a repair height of 16.5 inches. The influence of repair height should be negligible when comparing the moment response, although the increased stiffness of Repair #10 indicates that changing the repair height influences the stiffness. Repair #10 exhibits more strength degradation, and reaches a lower ductility level.

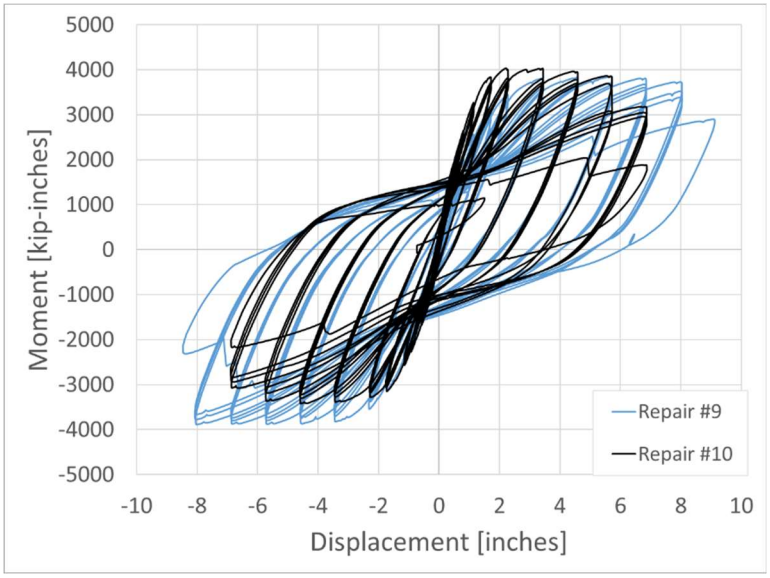

Figure 4.124: Moment vs. Displacement of Repair #9 and Repair #10.

4.10.5 Local response

Figure 4.125 shows the strain history for the hoop strains in the FRP, calculated using Optotrak LEDs placed on the CFRP wrap. The maximum measured hoop strains were found at the base of the FRP on the North side. For positive displacements, the North side is in compression which causes more dilation and the strains to be higher than negative displacements. Using fewer layers of CFRP wrap did result in an increase in measured hoop strain compared to Repair #9. The maximum measured hoop strain was 0.006; this is 50% higher than the measured hoop strain at the same ductility level in Repair #9. However, the fewer layers were not able to prevent the reinforcement from buckling, which led to column failure at a ductility level less than the original column.

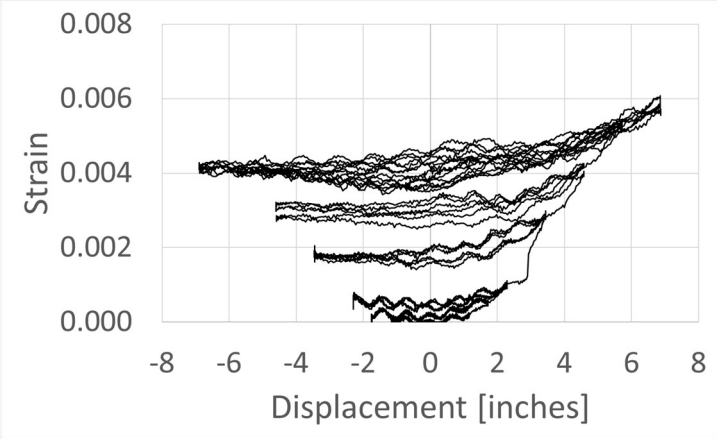

Figure 4.125: Hoop Strain History of CFRP wrap in Repair #10.

4.10.6 Conclusions

This repair used a reduced number of layers of the CFRP wrap to determine if it could be more efficiently designed. The results show that decreasing the number of CFRP wrap layers was not sufficient to prevent buckling and delay fracture in the relocated hinge. If more displacement capacity is required, the originally designed number of CFRP wrap layers should be applied, and other measures to extend the plasticity of the reinforcing steel could be implemented. One method to extend the plasticity could be debonding the reinforcing steel around the interface between the CFRP wrap and steel jacket.

4.11 Comparison of Repair Performance

In this section, the results of the repair tests are summarized. For convenience, the important properties of the columns and repairs are provided in Table 4.11.

Table 4.11: Repair Properties.

Repair	Sleeve Thickness	Bolt Pretension	Removal of Loose Concrete	Column Height	Column Diameter	Sleeve Height	Grout	CFRP Layers
1	10-ga	No	No	8’	24”	0.9D	Cementitious	--
2	10-ga	Yes	No	8’	24”	0.9D	Cementitious	--
3	0.25”	Yes	On one side	8’	24”	0.9D	Cementitious	--
4	0.25”	Yes	Yes	8’	24”	0.9D	Cementitious	--
5	0.25”	Yes	Yes	8’	18”	0.9D	Cementitious	--
6	0.25”	Yes	Yes	13’	18”	1.2D	Cementitious	--
7	0.25”	Yes	Yes	13’	18”	1.2D	Epoxy	--
8	0.25”	Yes	Yes	8’	18”	0.75D	Cementitious	--
9	0.25”	Yes	Yes	8’	18”	0.75D	Cementitious	3
10	0.25”	Yes	Yes	8’	18”	0.9D	Cementitious	2

For a typical reinforced concrete column, there are two main components of deformation: column flexure and column rotation due to strain penetration. Column flexure is a result of the curvature sustained by the column from the base to the top, and column rotation comes from the bond slip that occurs at the column-footing joint. For the repaired columns, Krish (2018) found that these two components are still the main methods of deformation, but the column rotation can be split into two parts since bond slip can be determined at both the top of repair to column interface and the bottom of repair to footing interface. Using the methods Krish (2018) described, the components of deformation can be found for each of the repairs at any point throughout the test. This was done for the peak displacement of the first cycle at each ductility level for the first four repairs, and is compared to the comparison columns in Figure 4.126. For most cases, the sum of each component is slightly less than the measured displacement. In other cases, the total displacement overestimates the measured displacement. These slight inaccuracies are attributed to measurement errors, as well as other forms of deformation like shear or sliding.

To best compare the effects of the changes to the steel sleeve, consistent damage and repair conditions are needed. Fortunately, at least one side of each of the columns originally had three

longitudinal bars fractured and were repaired with five repair bars of the same size. Using the push or pull cycle when these bars are in tension is therefore the best way to see the benefits of each variation of the steel sleeve and bolts and allows for the four variations outlined in Table 4.12 to be compared. Since the repairs and column tests were subjected to different displacements at each ductility cycle, a comparison of the absolute values of the components of displacement would make it difficult to compare the effects of the sleeve and bolt variations. Instead, the proportion of each component of deformation to the total deformation can be used.

Table 4.12: Sleeve and Bolt Variation Comparisons.

Repair	Cycle	Sleeve and Bolt Variation
Repair #1	Push	10-ga steel sleeve with snug-tight bolts
Repair #2	Push	10-ga steel sleeve with pre-tensioned bolts
Repair #3	Push	¼" steel sleeve with pre-tensioned bolts
Repair #3	Pull	¼" steel sleeve with pre-tensioned bolts and improved bond conditions
Repair #4	Push	¼" steel sleeve with pre-tensioned bolts and improved bond conditions

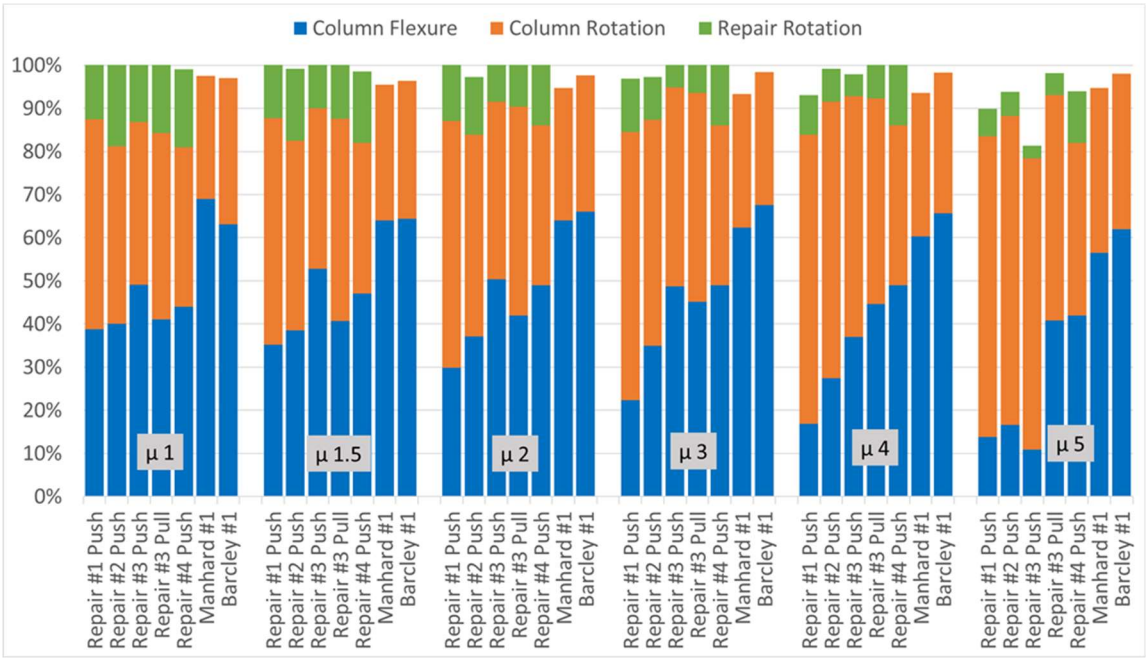

Figure 4.126: Proportional comparison of the components of deformation for 24" diameter columns.

Looking first at the two comparison columns on the far right of each ductility in Figure 4.114, it can be seen that flexural deformation accounts for about 60-65% of the column's displacement, with only a slight drop in proportion in the largest ductilities. In comparison, all of the repairs begin with flexural deformation accounting for about 45% of the displacement in ductility 1. For Repair #1 push cycles, this proportion steadily dropped through every cycle and was essentially replaced by column rotation. This is because the plate slip in this repair, which reduced confinement inside the repair, provided a weak anchorage of the column inside the repair making rotation easier. Repair #2 sought to improve this anchorage by using pre-tensioned bolts to prevent slip of the plates. It can be seen in Figure 4.114 that initially there is only a minor drop in the proportion of flexural deformation, but once the fractured bars debonded in ductility 3, the proportion rapidly drops and causes more column rotation as was seen with Repair #1.

In the third repair, a larger sleeve thickness was used to further improve the confinement inside the repair. Additionally, the fractured bars on the North side had the perimeter concrete removed and re-fractured in the repair test, while the South side was prepared the same as the previous repairs and still debonded. For the push cycles the South side was in tension, and while there was initially more flexural displacement, after the bars debond the proportion drops and column rotation increases. The pull cycles of Repair #3 and push cycles of Repair #4 do not have the large drop in flexural deformation and increase in column rotation at the final ductilities, as the fractured bars in tension did not debond for these repair conditions. This increase in column flexure and reduction in column rotation is considered an improvement of the repair response because it means the column is deforming more like the original column would have. While the proportion of flexural deformation is lower (37-44%), this is unavoidable given the increase in rotational demand due to the reduced effective height to the column-repair joint.

Figure 4.127 compares the components of deformation for the columns of 18" diameter. Repair #5 and Repair #6 compare columns of different heights. For Repair #6, which was 13 ft tall, the effective height considering the height of the repair was closer to the original column height; this results in proportions of flexure similar to what would be seen in an original column (around 60% at ductility 4). Repair #7 was also 13 ft tall and also exhibited a large proportion of column flexure. The contribution due to repair rotation was less for this repair, which used an epoxy grout, compared to all of

the other repairs using cementitious grout. The proportion of repair rotation was similar (~10%) for all of the repairs with cementitious grout.

The difference between Repair #5 and Repair #8 was the height of the steel sleeve. For Repair #8, the height of the sleeve was decreased. While the amount of repair rotation remained similar, one previously fractured bar debonded in Repair #8, which resulted in a reduction of column flexure and increase in column rotation. Repair #9 was similar to Repair #8, with the addition of 3 layers of CFRP wrap. The flexural rotation was decreased for Repair #9, which shows that the displacement capacity can be increased with the addition of the CFRP wrap, because the section will have less flexural demand; however, the increased column rotation concentrates large strains at the base of CFRP wrap, which could limit the displacement capacity.

Repair #10 reduces the amount of CFRP layers from 3 (in Repair #9) to 2, and has an increased repair height. The response of Repair #10 can also be compared to Repair #5 which had the same repair height, but did not include the CFRP wrap. The behavior of Repair #10 is very similar to Repair #5, indicating that the 2 layers of CFRP were not sufficient to improve the behavior of the repaired column.

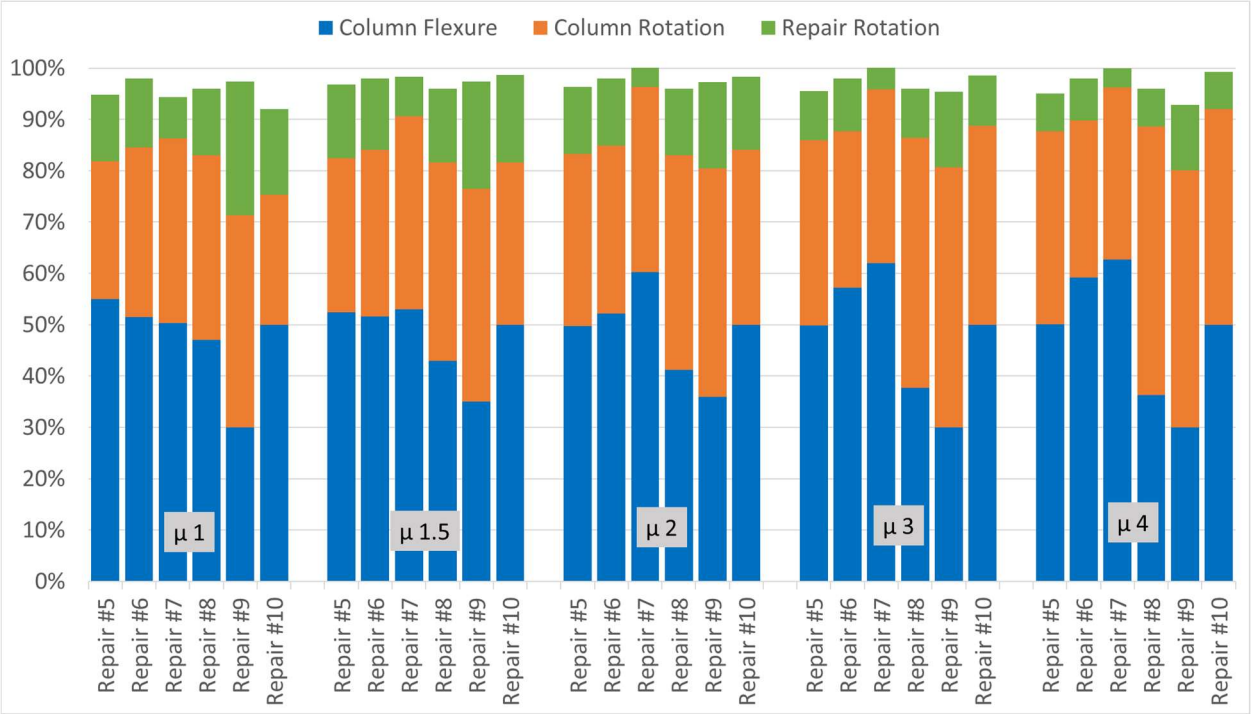

Figure 4.127: Proportional comparison of the components of deformation for 18" diameter columns

Chapter 5: Repair, Steel Sleeve, and CFRP Wrap Designs

In this chapter, the design processes for the implementation of the repair presented in this research will be discussed. The first section will outline the results of following Krish's (2018) plastic hinge relocation design for the first three repairs, which were the basis for the design of the bolted connection; it will be shown that this methodology provided a conservative design for all three repairs. The next section will propose additional requirements to the required sleeve thickness in this repair based off the experimental tests in this report. In Krish's (2018) design, the only consideration for the sleeve thickness was regarding the shear capacity of the repair. The proposed design requires a much thicker sleeve thickness based off confinement requirements, then shear capacity and flexural ductility are checked afterwards. The next two sections of this chapter will then present the design assumptions used for the bolts and their pre-tensioning for the repairs in this project. The last section will present the design of the CFRP wrap.

5.1 Plastic Hinge Relocation Repair Design

This section will present a brief discussion and the key values found using Krish's (2018) design process for the first three repairs in this project, which varied sleeve thickness and bond conditions. A complete description of the repair design is given by Krish (2018). As a note, the following designs include both directions of loading for Repair #1 and #2 as they each had unsymmetrical damage.

Moment-curvature analysis was performed on the column cross section both with and without the fractured longitudinal bars, and the results of the two limit states are shown in Table 5.1. With this information, a repair design can be analyzed using the Mirrored Plasticity Model developed by Krish (2018). This involves finding the design moment for the repair and subjecting the repair cross section to that moment. An acceptable design should ensure that the longitudinal repair bars remain below yield, which was at a strain of 0.0035 for the steel in this project. Table 5.2 presents the design moment and predicted strain for the repair bars, followed by the maximum experimental value from strain gauges applied to the repair bars.

Table 5.1: Results of Moment-Curvature Analysis of Column.

		First Yield			Ultimate		
	Direction	**Φ'_y (1/in)**	**M_y (kip-in)**	**$M_{y,rup}$ (kip-in)**	**Φ_u (1/in)**	**M_u (kip-in)**	**$M_{u,rup}$ (kip-in)**
Repair #1	**Push**	0.00047	5002	3233	0.00282	7083	4935
	Pull			2779			4305
Repair #2	**Push**	0.00049	5064	3264	0.00285	7232	5023
	Pull			3863			5769
Repair #3	**Both**	0.00047	4837	3070	0.00324	7075	4849

Table 5.2: Repair Bar Strain Prediction vs Experimental.

		$M_{br,u}$ (kip-in)	**$\varepsilon_{Predicted}$ (in/in)**	**$\varepsilon_{Experiment}$ (in/in)**
Repair #1	**Push**	5721	0.00245	0.00207
	Pull	6164	0.00232	0.00162
Repair #2	**Push**	5853	0.00252	0.00171
	Pull	5329	0.00229	0.00221
Repair #3	**Push**	5771	0.00261	0.00203
	Pull			0.00182

For all three repairs, Krish's (2018) design conservatively estimated the peak strain in the repair bars and all remained elastic throughout the test. While this conservatism is good, in Krish's repairs the model was much more accurate in predicting the strains of the repair bars. Given that the findings of the experimental tests in this project led to recommendations of using a thicker steel sleeve and removing

concrete around fractured longitudinal bars, Krish's model could likely be adjusted if the fractured bars remain anchored inside the repair.

5.2 Sleeve Thickness Design Checks

A major development from the experimental tests in this project was in learning the important role confinement plays in the repair's response. With confinement primarily coming from the steel sleeve, a reliable design for the sleeve thickness is needed. In Krish's (2018) repair design, the only consideration for the sleeve thickness was in relation to the shear capacity of the repair. Given the results of this study, it is clear that the confining effects from the sleeve must also be considered in order to prevent debonding of fractured bars. To do this, Priestley's steel jacket column retrofit design that was described in Section 2.3 will be adapted for this column-repair geometry. The following sections present three requirements for the sleeve thickness for different elements of the repair. These requirements are not considered additive as each element occurs at different sides of the sleeve for any given direction of loading. As a note, the repair design discussed in Section 5.1 requires a sleeve thickness already be specified. It is recommended that the sleeve thickness initially be determined based off the results of Section 5.2.1, which does not require moment-curvature analysis of the section and is most likely to control. Then, once the repair has been designed, Sections 5.2.2 and 5.2.3 should be used to check that the sleeve thickness is acceptable.

5.2.1 Confinement to Prevent Lap-Splice Failure

The effects of confinement on the non-contact lap splice in the repair is likely to be the controlling factor in finding the required sleeve thickness. While Priestley's design method was intended for columns that were constructed using starter bars that extend from the footing and are lapped with column longitudinal bars in the plastic hinge, the splitting failure mechanism described is still considered to be the cause of the fractured bars debonding in this repair. In short, this mechanism assumes that a crack will form around the bars along the length of the splice and confining forces along the splice will act to anchor the bar through friction. If the force from the bar is too large, then the bar will slip at the crack and the lap-splice will fail. Based off the experimental tests, the splitting crack

surface is assumed to be along the radius of the column longitudinal bars which is shown in Figure 5.1 and can be calculated for each bar using Equation 5.1 where *D'* is the diameter of the spiral and *n* is the number of longitudinal bars. With this assumed crack shape, the required volumetric ratio for the steel sleeve can be found using Equation 5.2 according to Priestley's design and substituting Equation 5.1 and Equation 5.3 into Equation 5.2 results in the required thickness in Equation 5.4. This resulted in a required thickness of 0.20 inches for the columns in this repair and is why the 0.25 inch thick plate was used in Repair #3.

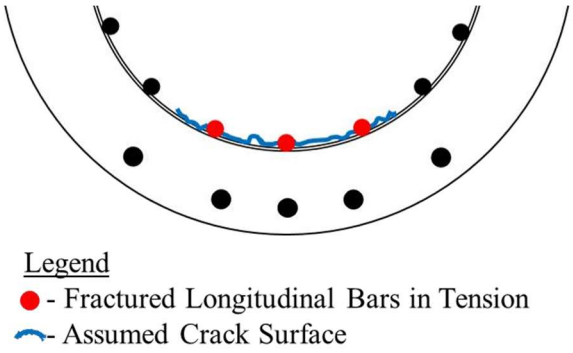

Figure 5.1: Assumed Crack Shape for Lap-Splice Failure.

$$p = \frac{\pi D'}{n} \qquad \textbf{Equation 5.1}$$

$$\rho_{sj} = \frac{2.42 A_b f_{yl}}{p l_s (0.0015 E_{sj})} \leq \frac{2.42 A_b f_{yl}}{p l_s f_{yj}} \qquad \textbf{Equation 5.2}$$

$$\rho_{sj} = \frac{4 t_j}{D_j} \qquad \textbf{Equation 5.3}$$

$$t_j = \frac{0.605 * D_j n A_b f_{yl}}{D' \pi l_s (0.0015 E_{sj})} \leq \frac{0.605 * D_j n A_b f_{yl}}{D' \pi l_s f_{yj}} \qquad \textbf{Equation 5.4}$$

5.2.2 Confinement for Ductility

In Priestley's design, the retrofit technique was intended to increase flexural ductility of poorly confined columns. Doing this requires a certain level of confinement in order to attain the larger plastic rotations. Although in this repair the plastic hinge should not form inside of the steel jacket, damage to

the transverse steel in the plastic hinge would reduce its confinement capacity. As insufficient confinement would be catastrophic should the plastic hinge somehow form inside the repair and large inelastic strains will occur inside the repair due to strain penetration, it is recommended that this be considered. However, even conservatively neglecting any contribution from the spirals of the damaged column, it is unlikely to control the required thickness.

To perform this check, the maximum required compression strain of the column concrete should be found using moment-curvature analysis of the original column cross section and Equation 5.5. Next, the required thickness can be found using Equation 5.6 where f'_{cc} can be taken as $1.5*f'c$ and $\varepsilon_{cm} = 0.15$ is recommended for A36 steel. Following these equations, the column jacket used for the third repair test would have only required a thickness of 0.10 inches.

$$\varepsilon_{cu} = \phi_u c \qquad \textbf{Equation 5.5}$$

$$t_j = \frac{0.18(\varepsilon_{cu} - 0.004)D_j f'_{cc}}{f_{yj}\varepsilon_{cm}} \qquad \textbf{Equation 5.6}$$

5.2.3 Shear Capacity

The final check for thickness of the steel sleeve is for the shear capacity of the repaired section. For a given repair design, an estimate of the overstrength shear demand to the repair can be found using Equation 5.7. The shear capacity of the steel sleeve can then be determined using Equation 5.8 where θ is assumed to be 35°. By ignoring any contribution of shear from the concrete and spirals, Equations 5.7 and 5.8 can be set equal and form Equation 5.9 for the required sleeve thickness for shear. Even with these conservative assumptions, the requirements for shear are expected to be very low, and for Repair #3 of this project the required thickness would only be 0.03 inches.

$$V^o = \frac{M_u}{L_{eff}} \qquad \textbf{Equation 5.7}$$

$$V_{sj} = \frac{\pi}{2} t_j f_{yj} D_j cot\theta \qquad \textbf{Equation 5.8}$$

$$t_j = 0.446 \frac{M_u}{L_{eff} f_{yj} D_j} \qquad \textbf{Equation 5.9}$$

5.3 Bolted Connection Design

During the early steps of designing the bolted connection it was realized that the stress and force demands to the steel sleeve cannot be easily determined. Because of this, a conservative design for the bolted connection was needed to ensure the repair maintains capacity design principles. Since the sleeve thickness design of Section 5.2 is intended to prevent yielding of the sleeve, the triangular stress profile shown in Figure 5.2 was used to prevent failure of the bolts. This design assumes that the sleeve is at its expected yield stress at the top of the repair and has no stress at the base. While this would indicate that this would be an eccentric load to the bolts, the eccentricity was ignored given that: the steel sleeve should not actually yield, and the bolt geometry is relatively square which would reduce the effects of eccentricity.

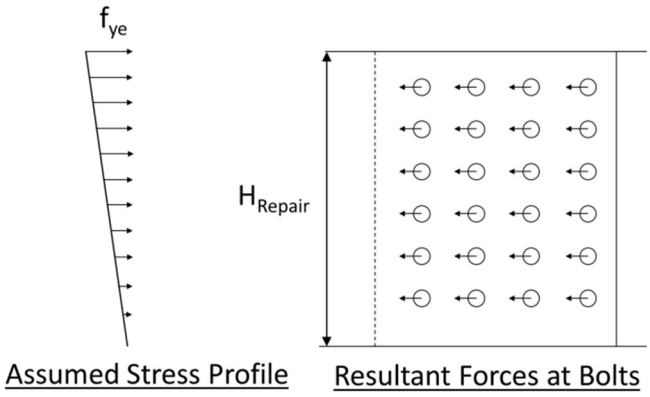

Figure 5.2: Design Assumption for Bolted Connection.

Ignoring eccentricity greatly simplifies the calculation of the bolted connection capacity, which is found by checking bolt bearing, bolt shear, and the base material (steel sleeve) yield and rupture. Since yielding of the steel sleeve is determined by the gross area of the section, which is not affected by the bolt configuration, a design where this controls should prevent a connection failure. However, the results of the experimental tests showed the necessity of preventing slip at the connection. This can be done through pre-tensioning of the bolts and is likely to control the size and quantity of bolts needed for a satisfactory repair.

5.4 Bolt Pre-Tension Design

In order to reliably use the bolted connection for the plastic hinge relocation repair, slip at the connection must be minimized. For the experimental tests in this project, this was done using a calibrated torque wrench to apply a pre-tension to the bolts. This pre-tensioning clamps the two plates together at the connection and prevents slip though friction between the plates.

The design for this pre-tensioned connection follows the slip-critical connection design in Section J3.8 of the AISC Specifications (2016). However, no surface preparation was done to the steel sleeves in the experimental tests. While AISC requires some level of surface preparation for slip-critical connections, the design is based off static equilibrium and the coefficient of friction, μ, would be the only variable affected by surface preparation. A value of $\mu = 0.3$, which is the lower bound value in AISC, was used for the repairs in this project in the absence of any other recommended values. This was deemed acceptable with the understanding that a conservative design should still prevent slip as long as μ is not grossly overestimated.

To determine the size and number of bolts, Equation 5.10 should be used where the frictional force between the plates must be greater than the force applied by the sleeve. The demand from the sleeve (the right-hand side of Equation 5.10) is again determined based off the assumed stress profile of Figure 5.2. The normal force from the pre-tension of the bolts times the coefficient of friction can be used to estimate the frictional force (the left-hand side of Equation 5.10), which if exceeded would cause the plates to slip. For the bolts in this project, the normal force from the bolt pre-tension was taken from Table J3.1 in the AISC Specifications (2016), which gives values for the minimum bolt pretension (T_b) for A325 and A490 bolts.

$$\mu * T_b * n_{bolts} \geq \frac{1}{2} * f_y * H_{Repair} * t_{Sleeve} \qquad \textbf{Equation 5.10}$$

In AISC, T_b is usually increased by a factor of 1.13, which is based off statistical analysis of the ratio of mean installed pre-tension to the table minimums for the calibrated torque wrench, though greater values are allowed. Calibrated torque wrenches are not typically recommended to measure pre-tensioning due to the large variability in the relationship of torque to pretension caused by friction and use of them requires daily pre-instillation verification, whereas other methods like using Direct Tension

Indicators (DTIs) can be more reliable. Since this pretension verification was not done along with no surface preparations, additional conservatism was used in Equation 5.10; however, given that the assumed demand stresses are already conservative, proper surface preparations and pre-tensioning techniques would likely not necessitate this conservatism. Following Equation 5.10 for Repair #3 where pre-tensioned bolts were used for the first time gives 173 kips ≥ 121 kips.

As pre-tension verification was not done for the calibrated torque wrench, Equation 5.11 was used to determine the required torque for each bolt. This is included for clarity, however, use of equations like this are explicitly prohibited by the Research Council on Structural Connections (2009). In Equation 5.11, T is the torque (ft-lbs) needed to apply the pretension, P (lbs), for a given bolt diameter, D (in), and K is a dimensionless coefficient to account for different conditions. In Equation 5.11 K is often takes as 0.2 for bolts that are not oiled and have a plain finish. This led to a required torque of 250 ft-lbs in order to apply 24 kips of pretension to the 5/8" diameter bolts.

$$T = K * D * P / 12 \qquad \textbf{Equation 5.11}$$

5.5 CFRP Design

Using the designs described in the previous sections and improving the bond conditions, the repair will have a stiffened response, resulting in a reduction of displacement capacity. The purpose of the CFRP wrap is to alter the constitutive model of the concrete and increase the curvature capacity of the section. In turn, this will increase the displacement capacity of the repaired column to match that of the original column. The original column curvature capacity can be determined using sectional analysis techniques, considering only the confinement of the concrete core from the transverse steel. To determine the maximum displacement of the original column, the maximum curvature from the sectional analysis can be used in Equation 5.12.

$$\Delta_u = \Delta_y + (\varphi_u - \varphi_y) L_p H \qquad \textbf{Equation 5.12}$$

The same equation can then be used to determine the required ultimate curvature considering the decreased clear height (taken as the total height of the column minus the height of the repair) and the same maximum displacement of the original column. Neglecting the displacement due to rotation of the repaired section with the steel jacket is conservative because it is relatively small compared to the

displacement from bending of the column and will add to the total displacement. So, if the desired displacement can be reached without considering the repair rotation, the repaired column is expected to exceed the displacement capacity of the original column.

The relationship between ultimate curvature and concrete strain is provided in Equation 5.13. For the initial prediction of the number of CFRP wrap layers required the neutral axis depth, c, can be assumed to be equal to the neutral axis depth at the ultimate condition for the original column section. The final design number of CFRP wrap layers required should ultimately be checked with a sectional analysis of the section including the effect of the CFRP wrap. Figure 5.3 shows the calculated concrete in compression constitutive model for the core when both the CFRP wrap and transverse steel reinforcement are considered, according to the model presented by Hu and Seracino (2013). It should be noted that the family of curves shown are a function of the number of layers of CFRP materials and the material and geometric properties of the circular reinforced concrete columns used in this research. The concrete strain calculated using Equation 5.13, used in conjunction with the constitutive models in Figure 5.3, can be used to determine the initial predicted number of CFRP wrap layers.

$$\varepsilon_c = \varphi_u c \qquad \textbf{Equation 0.13}$$

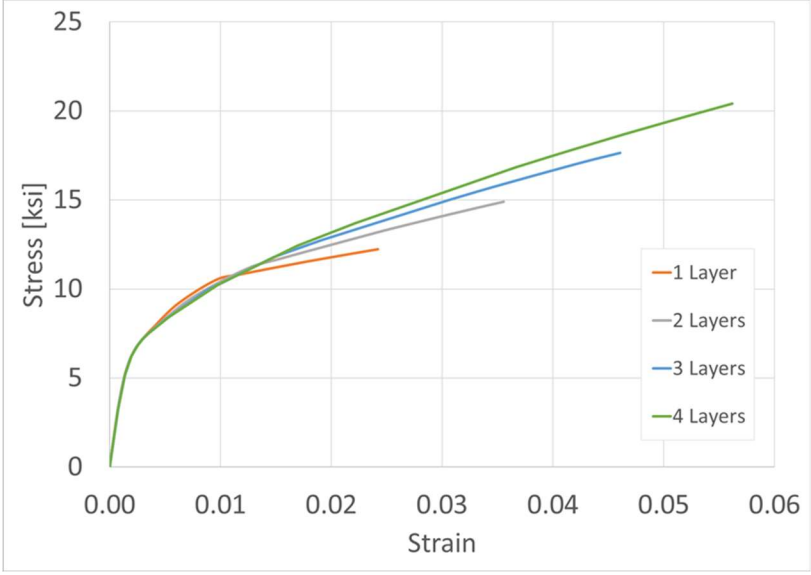

Figure 5.3: Confined concrete in compression stress-strain curve for different numbers of CFRP layers.

Chapter 6: Conclusions

The use of plastic hinge relocation as a repair technique for extreme levels of damage in reinforced concrete bridge columns continues to show promise. Before the development of this repair, if a column was severely damaged (e.g. had fractured longitudinal bars) a complete replacement of the bridge was suggested. Prior studies have already shown the repair's ability to restore a damaged column's load and displacement capacities, and its potential for rapid deployment is favorable. However, the number of studies using this repair technique is limited and two research needs were defined.

Firstly, in previous studies, a CFRP wrap or welded steel sleeve were used as the jacket of the repair. A timely installation of these repairs could be affected by weather and location of the column, as well as the availability of skilled workers to install the weld or CFRP system. An alternative repair without these limitations is desirable to ensure its availability as a rapid repair.

Secondly, past testing has shown that fractured bars in the original plastic hinge tend to debond in the repair tests. This causes the bar to be incapable of sustaining any load and weakens the repaired column. It was hypothesized that preventing this behavior, by improving the anchorage of the bars inside the repair, would improve the repair's behavior. While there are labor-intensive methods that exist which could accomplish this (e.g. splicing and headed studs), they were not used in this project to keep this repair rapid. After improving the anchorage, the repaired column behavior may be further improved, if needed, by using a CFRP wrap in the relocated hinge that may be installed at a later time.

Through the series of experimental tests, the following conclusions can be drawn, presented according to the two research objectives identified in Chapter 1.

Improve Repair Constructability

- The use of a steel sleeve with a pre-tensioned bolted connection is an acceptable alternative to the welded connection or a CFRP wrap for this repair technique. The pretensioned bolts are needed to prevent slip of the plates, which has been shown to weaken the repair.

- While the actual demands to the steel jacket are quite complex, a conservative design method was proposed for both the jacket thickness and bolted connection which is expected to prevent yielding of the sleeve or a connection failure which is acceptable for a rapid repair.
- The use of reinforcing bar couplers pre-embedded in the footing at the time of construction for the repair bars were effective in achieving an elastic, capacity protected repair.
- Equivalent performance was achieved using an epoxy grout, which allows for this repair method to be used in underwater applications, such as many column to footing connections.

Improve Repair Performance

- It was experimentally shown in Repair #3 that the combination of using a thicker steel sleeve to increase confinement and replacing cracked column concrete around fractured bars with fresh repair grout was capable of fully anchoring the bars inside the repair. Experimental tests where only one of these methods were used, without the other, the fractured bars were not able to be fully anchored.
- A method of designing the jacket thickness was proposed that is expected to prevent large cracks from forming inside the repair that would weaken the rebar-concrete bond strength and lead to debonding.
- Increasing the anchorage of fractured bars inside the repair was shown to improve the repaired columns response in terms of energy dissipation and components of deformation. As anchorage is improved, the repaired columns dissipated more energy (evident from a comparison of hysteretic damping) and deformed more like the original column (having more flexural deformation and less strain penetration).
- The repaired column's displacement capacity will inherently be reduced when the bars are fully anchored due to the reduced effective height of the column. When fractured bars debond, the repaired column has more deformation due to strain penetration into the repair and may be capable of maintaining the same displacement capacity as the original column. The tradeoff for this additional displacement is a softened and pinched global response, which would reduce seismic resistance.

- The application of a CFRP wrap on the new relocated hinge can be used to improve the concrete core constitutive response and prevent longitudinal bar buckling in order to increase the displacement capacity of the repaired column. Depending on the environmental conditions and the state of damage, this part of the repair may be installed at a later time.

REFERENCES

ACI Committee 318. (2008). Building Code Requirements for Structural Concrete (ACI 318-08) and Commentary. In *American Concrete Institute, Farmington Hills, Michigan*.

ACI Committee 440. (2008). Guide for the Design and Construction of Externally Bonded FRP Systems for Strengthening Concrete Structures (ACI440.2R-08). *(ACI) American Concrete Institute, Farmington Hills, MI*.

ACI Committee 546. (2014). Guide to Concrete Repair (ACI 546-14). *(ACI) American Concrete Institute, Farmington Hills, MI*.

AISC (American Institute of Steel Construction). (2016). Specification for Structural Steel Buildings, ANSI / AISC 360-16. *American Institute of Steel Construction*, 676.

Barcley, L., & Kowalsky, M. (2020). Seismic Performance of Circular Concrete Columns Reinforced with High-Strength Steel. *Journal of Structural Engineering (United States)*, *146*(2), 1–11. https://doi.org/10.1061/(ASCE)ST.1943-541X.0002452

Burtz, J. L. (2003). *Behavior and Design of Grouted Anchors Loaded in Tension Including Edge and Group Effects and Qualification of Engineered Grout Products* [University of Florida]. http://etd.fcla.edu/UF/UFE0000854/burtz_j.pdf

Chai, Y. H., Priestley, M. J. N., & Seible, F. (1991). Flexural retrofit of circular reinforced concrete bridge columns by steel jacketing: experimental studies. In *Structural Systems Research Project 91/06, University of California, San Diego*.

Desnerck, P., Lees, J. M., & Morley, C. T. (2015). Bond behaviour of reinforcing bars in cracked concrete. *Construction and Building Materials*, *94*, 126–136. https://doi.org/10.1016/j.conbuildmat.2015.06.043

Goodnight, J. C., Kowalsky, M. J., & Nau, J. M. (2017). Seismic Load Path Effects in Reinforced Concrete Bridge Columns and Pier Walls: Volume 1 Strain Limit States for RC Bridge Columns. *AKDOT Report No. 4000(134)*, North Carolina State University.

Hu, H. and Seracino, R. (2013). Analytical Model for FRP-and-Steel-Confined Circular Concrete Columns in Compression. *Journal of Composites for Construction*

Jacobsen, L. S. (1960). Damping in composite structures. *II WCEE, Tokyo*, 1029–1044.

Krish, Z. (2018). *Rapid Repair of Reinforced Concrete Bridge Columns Subjected to Seismic Loading via Plastic Hinge Relocation*. North Carolina State University.

Lehman, D. E., Gookin, S. E., Nacamull, A. M., & Moehle, J. P. (2001). Repair of earthquakedamaged bridge columns. *ACI Structural Journal*, *98*(2), 233–242. https://doi.org/10.14359/10192

Manhard, R. (2019). *Impact of Grade 80 Reinforcing Steel Production Process on the Seismic Behavior of Bridge Columns*. North Carolina State University.

Montejo, L. A., Kowalsky, M. J., & Hassan, T. (2009). Seismic behavior of flexural-dominated reinforced concrete bridge columns at low temperatures. *Journal of Cold Regions Engineering*, *23*(1), 18–42.

Pantelides, C. P., Brown, D. N., & Parks, J. E. (2014). *Seismic Retrofit of Spliced Sleeve Connections for Precast Bridge Piers*. *August*.

Parks, J. E., Brown, D. N., Ameli, M. J., & Pantelides, C. P. (2016). Seismic repair of severely damaged precast reinforced concrete bridge columns connected with grouted splice sleeves. *ACI Structural Journal*, *113*(3), 615–626. https://doi.org/10.14359/51688756

Paulay, T., & Priestley, M. J. N. (1992). Seismic Design of Reinforced Concrete and Masonry Buildings. In *John Wiley & Sons, Inc.* John Wiley & Sons, Inc.

Pellegrino, C., and Modena, C. (2010).“Analytical model for FRP confine-ment of concrete columns with and without internal steel reinforce-ment.”J. Compos. Constr., 10.1061/(ASCE)CC.1943-5614.0000127,693–705.

Priestley, M. J. N., Calvi, G. M., & Kowalsky, M. J. (2007). Displacement-Based Seismic Design of Structures. In *IUSS Press, Pavia, Italy*.

Priestley, M. J. N., Seible, F., & Calvi, G. M. (1996). *Seismic Design and Retrofit of Bridges*. John Wiley & Sons, Inc.

Research Council on Structural Connections. (2009). *Specification for Structural Joints Using High-Strength Bolts*.

Rutledge, S. T., Kowalsky, M. J., Seracino, R., & Nau, J. M. (2014). Repair of reinforced concrete bridge columns containing buckled and fractured reinforcement by plastic hinge relocation. *Journal of Bridge Engineering*, *19*(8), 1–10. https://doi.org/10.1061/(ASCE)BE.1943-5592.0000492

Wu, R. Y., & Pantelides, C. P. (2017). Rapid seismic repair of reinforced concrete bridge columns. *ACI Structural Journal*, *114*(5), 1339–1350. https://doi.org/10.14359/51700789